Materials Advances

ROYAL SOCIETY OF CHEMISTRY

REVIEW

View Article Online
View Journal | View Issue

Cite this: *Mater. Adv.*, 2023, **4**, 4054

Cellulose acetate-based membrane for wastewater treatment—A state-of-the-art review

Md. Didarul Islam, †[a] Foyez Jalal Uddin, †[b] Taslim Ur Rashid *[b] and Mohammad Shahruzzaman *[b]

During the past decades, many conventional technologies of wastewater treatment have been utilized, but they are ineffective in removing recently emerging substances of concern, such as pharmaceuticals, pesticides, personal care products, surfactants, plasticizers, and flame retardants. Membrane technologies have emerged as a great possibility in wastewater treatment since the 18th century, exhibiting high selectivity with high-quality effluent, low sludge production, size reduction of equipment, low energy, low cost, and can replace several treatment processes into a single one. Recently, cellulose acetate-based membranes are widely used for reverse osmosis (RO), ultrafiltration (UF), and nanofiltration (NF) purposes owing to their good toughness, cost-effectiveness, high hydrophilicity, high reflux, high biocompatibility, high salt removal, chlorine resistance, better antifouling properties, and efficient reduction of microorganism content. Moreover, the cellulose acetate membrane can easily be blended with other polymer or incorporated with nanoparticles and easily be functionalized to achieve specific physicochemical properties. Furthermore, as cellulose acetate is a green, energy-saving natural biodegradable polymer, it offers the potential to replace the traditional petrochemical membrane. This review focuses on the synthesis processes and properties of cellulose acetate-based membranes. The removal efficiency of recently modified cellulose acetate-based membranes to separate pollutants from wastewater and approaches to improve these membrane properties are discussed in this review. Future prospects and research directions are also suggested on the basis of the challenges faced during the materialization of these membranes.

Received 20th May 2023,
Accepted 14th August 2023

DOI: 10.1039/d3ma00255a

rsc.li/materials-advances

[a] *Department of Applied Chemistry and Chemical Engineering, National Institute of Textile Engineering and Research, Savar, Dhaka-1350, Bangladesh*
[b] *Department Applied Chemistry and Chemical Engineering, Faculty of Engineering and Technology, University of Dhaka, Dhaka 1000, Bangladesh. E-mail: taslim@du.ac.bd, shahruzzaman@du.ac.bd*
† These authors have equal contribution.

Md. Didarul Islam

Md. Didarul Islam is working as Lecturer in the Department of Applied Chemistry and Chemical Engineering, National Institute of Textile Engineering and Research (NITER). He received his BSc and MSc from the Department of Applied Chemistry and Chemical Engineering, University of Dhaka, Bangladesh. His research interests include biopolymer-based conductive material fabrication, biopolymer, and biocomposite fabrication and their application for ecofriendly smart device application, dye-sensitized solar cell, and waste management.

Foyez Jalal Uddin

Foyez Jalal Uddin is currently pursuing the MS program in the Department of Applied Chemistry and Chemical Engineering at University of Dhaka, Bangladesh. He received his BSc (2020) from the same department. His research interest broadly focuses on industrial process design and control with improved efficiency for the desired product synthesis, clay, or biopolymer (e.g., chitosan and cellulose)-based composites for biomedical application, wastewater treatment, and utilization of biofuel (e.g., biogas, biooil, and biodiesel) for commercial green fuel production.

1. Introduction

Water resources have become increasingly scarce as tons of wastewater is being produced everyday with the increasing number of human populations.[1] Many highly industrialized countries discharge 55% of their sewage without any treatment.[2] In low-income countries, more than 80% of municipal wastewater discharged is untreated.[3–5] According to an infrastructure report titled as SAICE Infrastructure Report Card for South Africa, 2011, 7589 mega liters of wastewater on an average is transported across South Africa.[6] Therefore, this untreated wastewater leads to several environmental and human problems.[7,8] More than 2.6 billion tons drinkable water has become polluted, which may cause life-threatening waterborne diseases.[9] Commonly produced effluents include heavy metals and metalloids, such as arsenic, lead, cadmium, mercury, and chromium, organic contaminants, such as dyes, surfactants, microplastics, humic substances, pesticides, polycyclic aromatic hydrocarbons (PAHs), polychlorinated biphenyls (PCBs), polybrominated diphenyl ethers (PBDEs), plasticizers, phenols, and drug residues, various inorganic salts, acids, and alkalis.[10–13] Recently, identified substances in wastewater, such as diverse group of chemicals and biological agents known as emerging substance of concern (ESOC) are causing growing concern in terms of their health and ecological effects. These groups of ESOC include pharmaceuticals, personal care products, disinfection byproducts, artificial sweeteners, flame-retardants, hormones, steroids, perfluorinated compounds, and nanomaterials. About 10% of disease and 6.3% of death can be controlled worldwide by improving the treatment of wastewater.[9] Traditional treatment technologies, such as trickling filter, activated sludge process, waste stabilization ponds, or innovative modifications of these technologies may become ineffective to treat these substances from wastewater.[12,14,15] Inefficiency, operational difficulties, high energy requirements, lower economic benefit, problems associated with recyclability, and emission of secondary pollutants are some technical limitations that hinder the implementation of these conventional technologies.[16]

In industrialized countries, membrane technology is being increasingly implemented in water treatment processes to reduce pollutants from municipal and industrial wastewater such as ground water, desalination of brackish water and seawater, decontamination of wastewater of diverse nature including urban wastewater, coking, carwash, nuclear power, power engineering steel industry, textile and tannery, pulp and paper, pharmaceutical, and agro-food industries such as dairy, beverage, winery, tomato, and olive oil.[3,12,17,18] It has been proven to be a favorable option in wastewater treatment to bridge the economic and sustainability gap, reduce the chemical usage, and build an environment-friendly process, which has easy accessibility.[6] Membrane-based processes can be applied for different applications such as reverse osmosis, ultrafiltration, nanofiltration, forward osmosis, membrane bioreactor microfiltration, and particle filtration.[19] Generally, membrane materials are classified into organic (polymeric), inorganic (ceramic), and biological materials.[16] Among the commonly used membrane materials, polymeric membranes are the most widespread due to their high mechanical, thermal, chemical, and corrosion resistance.[20] The widespread use of fossil-based polymers in membrane fabrication has led to the continuous improvement of membrane technology in wastewater treatment. However, in recent times, the progressive decline of fossil resources and the negative environmental impact of these fossil-based polymers have made this technology nonsustainable.[16,21] Thus, researchers are now more interested in an environmentally friendlier process of membrane fabrication from organic chemical goods based on renewable natural sources.

Biopolymers have high potential for making the membrane separation process environment-friendly. Biopolymers obtained

Taslim Ur Rashid

Taslim Ur Rashid is Associate Professor in the Department of Applied Chemistry and Chemical Engineering at University of Dhaka, Bangladesh. He received his BSc and MS from the same department. In 2021, he completed his PhD in Fiber and Polymer Science program in the Department of Textile Engineering, Chemistry and Science at North Carolina State University, USA. His broad research interest focuses on separation technology, nanofiber fabrication by electrospinning, industrial waste management, designing polymer nanocomposites with improved properties for separation application, biomedical application, and wastewater treatment.

Mohammad Shahruzzaman

Mohammad Shahruzzaman is working as Assistant Professor in the Department of Applied Chemistry and Chemical Engineering under the faculty of Engineering and Technology, University of Dhaka. He has experience in (i) polymer science, preparation of organic/inorganic hybrids, (ii) organic synthesis and characterization, and (iii) preparation sustainable biocomposites for wastewater treatment He was awarded the highly prestigious Japanese Government (Monbukagakusho: MEXT) scholarship from October 2012 to September 2015.

from natural sources (plants, animals, microorganisms) are now widely used in wastewater treatment to reduce the carbon emission and cost of treatment.[21–23] The natural sources of biobased and renewable polymers are abundant and 5×10^{11} tons are generated annually in the biosphere.[24] Among the biopolymers (hemicellulose, cellulose, pectin, protein, lignin, *etc.*) from agricultural origin, researchers are interested more in cellulose because of its nontoxicity, ease of processability, hydrophilic capabilities, crystallinity, and insolubility in many solvents due to hydrogen bonding.[25] Cellulose is a fibrous, tough, water-insoluble, long linear polysaccharide polymer that consists of β-D-glucopyranose units joined by β-1,4-glycosidic bonds $(C_5H_8O_4)_m$ to form a dimer known as cellobiose, which is the main unit of cellulose. Each monomer of the cellulose chain has three hydroxyl groups.[26] The presence of hydroxyl groups in the cellobiose unit results in crystallized cellulose molecules in a horizontal plane and in parallel chains, forming microfiber packages. The elementary fibers that make up the microfiber packaging are basically organized into high order crystalline parts interspersed by amorphous regions. As a consequence of its structural organization, cellulose presents some properties that limit its application (*e.g.*, lack of antimicrobial properties, high hydrophilicity, and low dimensional stability high melting temperature).[27] The functionalization of cellulose through the hydroxyl group to modify it into derivatives can overcome these drawbacks. Due to its attractive chemical and physical properties, a growing worldwide activity is observed regarding the extensive research on cellulose derivatives for membrane preparation, which can be used for the removal of organic and inorganic pollutants from wastewater and for water purification.[22] The properties of these membranes can be manipulated by several techniques such as the selection of the polymer, solvent and nonsolvent, thickness of polymer solution films at the precipitation of the membrane, and the addition of surfactants at the polymer solution or fillers for composite membrane synthesis.[24]

Among cellulose derivatives, cellulose acetate (CA) is one of the most commonly used with higher hydrophilicity, higher mechanical strength, superior transport characteristics, low protein adsorption, and excellent film forming property during the membrane fabrication process.[28,29] It is repeatedly applied in preparing ultrafiltration and nanofiltration membrane. CA-based reverse osmosis and NF membranes have been used for the desalination of seawater and brackish water, purification of surface water, treatment of food processing wastewater, and the treatment of industrial wastewater, from which a wide variety of compounds such as methanol, ethanol, urea, phenol, neutral endocrine-disrupting chemicals (EDCs), pharmaceutical active compounds (PhACs), pesticides, and viruses are removed. Recent works from scientists on CA membrane shows that it has less tendency for fouling than that of traditionally-used polyacetate (PA) membrane for the wastewater treatment process.[16,21] However, this recent interest in cellulose acetate has also brought about some problems due to the presence of nonreactive functional groups, the poor chemical, thermal, mechanical resistance, and its unsuitability for adsorption separation, which works on the principle of affinity. Moreover, the membrane exhibits low flux during applications because of its dense skin layer and low porosity of the sublayer. Efforts to modify CA membranes to overcome these problems have been continued. Through the modification of the CA membrane, the separation efficiency can be enhanced to obtain high selectivity and high reflux.[28]

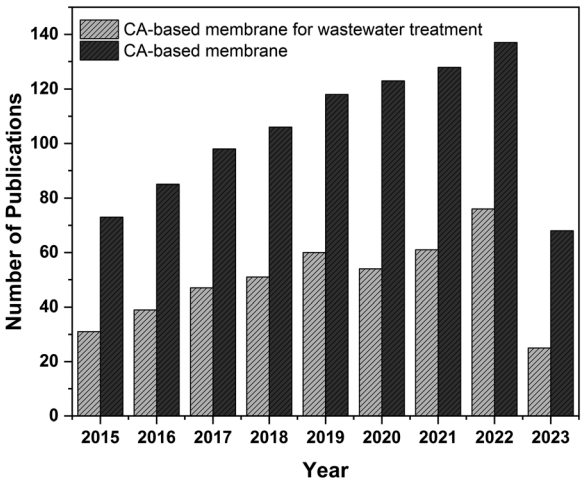

Fig. 1 Publication trend in the field of CA-based membranes published between 2015 and March 2023. The values were obtained from a literature search on Google Scholar using "Cellulose acetate-based membranes for wastewater treatment".

Fig. 1 demonstrates the recent increasing trend in research publications focusing on cellulose acetate-based membranes. Though many works have been done to improve these environmentally-sustainable CA membranes, these works are not yet reviewed exclusively. This review paper summarizes these works on cellulose acetate-based membranes and arranges them into their synthesis, properties, applications, and efficiency in the wastewater treatment process. The future prospects of CA-based membranes on wastewater treatment technology are also discussed in the review.

2. Cellulose acetate

2.1. Synthesis and properties of cellulose acetate

Cellulose acetate (CA) is industrially obtained by the esterification of cellulose molecule in the presence of sulfuric acid with acetic acid and acetic anhydride because of reactant availability, high reactivity, and controllability.[30–32] Wood and cotton linter are the major sources of this cellulose derivative. As these resources are limited, the use of agricultural residues such as corn stalk, rice husk, sugarcane bagasse, and newspaper and environmental synthesis routes have been increasingly reported to replace the use of sulfuric and acetic acids by ecofriendly reagents, such as dialkylcarbodiimide, *N*,*N*-carbonyldiimidazole, aluminium chlorides, *N*-bromosuccinimide (NBS), iodine, phosphotungstic acid as catalyst, room temperature ionic liquid (IL), solid super acid SO_4^{2-}/ZrO_2, and recyclable polymer catalyst.[27,32–37] Agricultural wastes have

become an attractive renewable resource for the synthesis of CA. The agro-industrial residues are mainly composed of cellulose (30–60%), hemicellulose (14–40%), and lignin (7–20%). They can be a sustainable source of biomaterials due to their low cost, availability, and chemical composition. Recently, researchers are emphasizing the acetylation process of cellulose, extracting it from the above lignocellulosic agricultural wastes.[27,38]

Prior to the acetylation step, the pretreatment of this lignocellulosic biomass and wastes is an essential step to isolate the cellulose from noncellulosic component (hemicellulose and lignin), which may negatively affect the cellulose modification and dissolution of cellulose. Pretreatment removes lignin and hemicellulose, reduces cellulose crystallinity, and increases the porosity of the materials. The pretreatment of lignocellulosic materials has been classified as physical, physicochemical, chemical, and biological processes. Pretreatment with dilute acid has become the general method followed for any lignocellulosic biomass substrate. As a chemical pretreatment process, dilute acid hydrolysis has been developed successfully to achieve high reaction rates. Some researchers also carried out pretreatment using alkali. The treated materials are bleached after breaking the intermolecular bond between the lignin and hemicellulose through the solvation and saponification reactions by the alkali. Besides, several methods such as steam explosion, organosolv process, chlorine-free method, combined chemical, and enzymatic extraction have been continuously developed to extract cellulose from biomass. Among these, chemical treatment is used under mild conditions to get relatively complete separation of lignin and hemicellulose.[27,39,40]

Acetic anhydride is typically used in excess during acetylation reactions in solvent-free environments or eventually in stoichiometric levels during acetylation reactions in organic solvents; both techniques require the addition of basic or acid catalysts to facilitate esterification.

The acetylation of cellulose with acetic anhydride is insufficient to weaken the intermolecular action in cellulose. In this step, the hydroxyl groups present in the cellobiose has been replaced with acetyl groups. This substitution is mostly depending on the types of catalyst used, experimental condition, and purity of cellulosic raw materials.[41] During the acetylation step, the degree of substitution (DS) is one of the major parameters indicating replacing the OH groups with acetyl groups per glucose unit. The maximum degree of acetylation is obtained when all OH groups are replaced by acetyl groups, which leads to a DS value of three.[41] On the other hand, DS equal to zero indicates that no substitution occurred during the acetylation stage. Several studies recognized that the DS values of CA greatly affects the mechanical, thermal, chemical and physical properties, and solubility of the fibrous materials.[42–46] For instance, higher DS values lead to an increase in the solubility in solvents such as THF and acetone, while DS values of zero (cellulose) are insoluble in these solvents.[47] Several studies showed that CA with low DS value led to a reduction in the amorphousness. In 2016, Chen *et al.* experimented that on increasing the DS value of the CA, the crystalline diffraction (2θ = 8°, 10°, and 13°) peaks were narrowed, and the peak intensity was also reduced.[32,41,48] In another study, a wide halo at $2\theta = 20^\circ$ known as van der Waals or amorphous was gradually intensified with the increase in the DS value.[48] Freitas and his coauthors investigated the crystalline index as a function of DS. This study showed that increasing the DS values (1.48, 19.8, 2.29, and 2.48) of the CA significantly reduced of crystallinity index (34, 31, 30, and 23%).[41] This property can be explained by increasing disorder when cellulose is acetylated and increasing interlayer distance and break of the microfibrillar structure.[48] From the aforementioned date, it has been concluded that DS is one of the major parameters indicating the degree of acetylation or yield of cellulose acetate (%).

Moreover, researchers are working on finding new effective and environmentally viable pathways to produce cellulose acetate. Depending on the extent of research, the synthesis processes of cellulose acetate have been summarized into heterogeneous and homogeneous acetylation types.[49,50] An overview of the current progresses in the synthesis of cellulose acetate through homogeneous and heterogeneous processes are reviewed and when available, degree of substitution (DS), acetylation yield, and properties of the cellulose acetate produced from different cellulose resources are presented in Table 1. A general flow diagram summarizing the extraction of CA has also been shown in Fig. 2.

2.1.1. Heterogeneous acetylation. Cellulose acetate is generally produced by the reaction of cellulose with an excess of acetic anhydride in the presence of strong mineral acids such as sulfuric acid or perchloric acid. The industrial production of CA is based on this single step heterogeneous modification of cellulose results in cellulose triacetate (DS 3). The heterogeneous acetylation process requires a hydrolysis step afterward to synthesize partially substituted cellulose acetate with DS of about 2.45–2.5, which provides high solubility and good melt properties. This process has some disadvantages such as the necessity of highly pure raw cellulose, economic infeasibility, degradation of cellulose polymer by catalyst H_2SO_4, and formation of complex incorporating sulfuric acid in the CA, resulting in an unstable product. Different investigations have been carried out to overcome these disadvantages.[48,54,71,75]

Cellulose triacetate is a triacetate ester of cellulose with an average degree of substitution 2.8. It is one of the most widely used cellulose esters in pharmaceutical, chemical, and industrial fields due to its low toxicity and low inflammability.[55,59] Hindi *et al.* studied the possibilities of synthesizing cellulose triacetate from cellulose wastes, cotton stalks by heterogeneous acetylation process with glacial acetic acid, concentrated sulfuric acid, and acetic anhydride.[53] A similar heterogeneous acetylation process was used to synthesize cellulose triacetate from the date seeds cellulose with optimum conditions and minimum reagents.[55] The process of acetylation by acetic anhydride inherently leads to the depolymerization of cellulose and is very much corrosive. Instead of acetic anhydride, Chen *et al.* presented an acetylation process using vinyl acetate as a reactant and a reaction medium with 1-ethyl-3-methylimidazolium acetate (EmimAc) as a catalyst for the transesterification of cellulose.[31] Another method to produce cellulose triacetate used *N*-iodosuccinimide as an

Table 1 Properties of cellulose acetate synthesized through different processes

Raw materials	Cellulose percentage	Acetylation type	Degree of substitution	%Yield of cellulose acetate	Product property and major outcome of this study	Ref.
Two bleached pulp	90.1% (BSP)	Heterogeneous type using iodine as a catalyst	—	(54–69%) for BSP	• Degree of crystallinity (%): 82% (BKP), 77% (BSP) • Reduction of DS by 8–10% results in an increase in the crystallinity by 25%	49
	80% (BKP)			(42–45%) for BKP	• Increased Young's modulus by 13–25% • Increased transparency by 1–34%	
Cotton fiber	—	Heterogeneous type using iodine as a catalyst	2.37 (57% of the theoretical yield)	15–24%	• Up to a certain limit, increasing iodine content as the catalyst in the acetylation reaction significantly improves the DS and CA yield (%).	51
Cottonseed hull		Heterogeneous type using iodine as a catalyst	2.03 (22% of the theoretical yield)			
Cotton bur		Heterogeneous type using iodine as a catalyst	2.09 (24% of the theoretical yield)			
Burr fiber		Heterogeneous type using iodine as a catalyst	1.93 (15% of the theoretical yield)			
Waste cotton fabrics	>98%	Acetylation using Brønsted acidic ionic liquid, *N*-methyl-imidazolium bisulfate, [Hmim]HSO_4 as the heterogeneous catalyst	1.25–3.06	124.7–146%	• Pretreatment of cellulose by mechanical milling increases the nanocrystalline fraction, accelerate the acetylation rate, and the yield of CA and DS value • Water soluble CA has also been produced	52
Oil palm empty fruit branch	—	One step heterogeneous acetylation process	2.52	—	• Highly amorphous CA percentage of crystalline region: 6.41% Better mechanical properties than that of commercial CA: (Tensile strength: 21 MPa, Young's modulus: 0.95 MPa)	48
Cotton fibers	97.11%	Heterogeneous acetylation process	2.86	112.18%	• Soluble in chloroform and a mixture of chloroform and methanol (9 : 1 (v/v)) confirms the presence of cellulose triacetate	53
Recycled writing papers	84.76%		2.84	94.43%		
Recycled newspapers	80.97%		2.85	84.37%		
Macerated woody fibers of *Leucaena leucocephala*	67.46%		2.89	72.98%		
Microcrystalline cellulose	—	Heterogeneous process using solid protonic acid (SO_3H-functionalized carbon materials)	1.2–2.94	>70%	• Cellulose diacetate with DS between 2 and 2.7 • Soluble in acetone, CH_2Cl_2, and DMSO • Decomposition temperature (Max): 364 °C • Sulfonated catalyst can be regenerated by simple centrifugal separation from the reaction mixture and can be reused in the next cycle. • No significant reduction in the yield and DS of CA using the recycled catalyst	54
Microfibrillated date seeds cellulose (*Phoenix dactylifera L.*)	23.9% amorphous cellulose	Heterogeneous acetylation	3.02	79% (max)	• Decomposition temperature: 372 °C • Melting temperature: 217 °C	55
Microcrystalline cellulose (Cotto)	—	Acetylation of vinyl acetate by transesterification	2.86	—	• Thermal degradation temperature: 332–397 °C • Almost similar mechanical properties (tensile strength, and elongation at break and elastic modulus) has been achieved by the pyridine-based acetylation process	31

Table 1 (*continued*)

Raw materials	Cellulose percentage	Acetylation type	Degree of substitution	%Yield of cellulose acetate	Product property and major outcome of this study	Ref.
					• Excellent contact angle of 72° has been found • Produced CA limits the depolymerization process	
Bamboo pulp	95% α-cellulose content	Heterogeneous acetylation	2.46	—	• Completely dissolved in acetone with a final concentration of 3%	56
Waste blended fabrics	—	Heterogeneous acetylation using Brønsted ionic liquid as a novel catalyst	1.92–2.62	49.3% (acetone soluble CA	• Glass Transition temperature: 187 °C • Maximum decomposition temperature: 267 °C	57
			2.62 (completely acetone soluble)	51% (DMF- soluble CA)	• *N*-methyl-imidazolium bisulfate to anhydroglucose units from 0 to 0.4 mole rate results in a significant increase of DS of CA	
Waste cotton fabrics	>98%	Acetylation using acidic ionic liquid as quasi-homogeneous catalyst	1.13–2.95	99.6% (cellulose diacetate of DS 2.17)	• Fully substituted CA with 88.8% conversion has been obtained using only 9 mole% of 1-vinyl-3-(3-sulfopropyl)imidazolium hydrogen sulfate as a catalyst • Crystalline index: 54.18%	58
				88.8% (cellulose triacetate of DS 2.92)	• Degree of polymerization: 563	
Cotton cellulose	—	Acetylation using iodine as a Lewis acid catalyst in the presence of acetic anhydride	2.60–3.0	15.39–34.80%	• Specific surface area: 39.63 $m^2 g^{-1}$ (highest) Particle size distribution: 41–897 nm (50% of the samples) Coarse collapsed surface	35
Cotton cellulose	95%	Acetylation using NIS as a catalyst under mild reaction conditions	0.89–2.84	94.32% (optimum condition)	• *N*-Iodosuccinimide has been recommended as a novel and successful catalyst for the acetylation of cotton cellulose. • The reaction time and catalyst concentration can be a major parameter controlling the weight percent gain and DS.	59
Corncob	36.35%	Acetylation using the solvent-free method with iodine catalyst	2.68	60%	• Storage modulus of CA film: 1.89 GPa • Degradation temperature: 350 °C • Improved yield (60%) of CA has been achieved compared to other conventional method.	27
Cajuput twigs (*Melaleuca leucadendron*)	34.71 ± 1.44%	—	1.90	85.4%	• Thermal decomposition temperature: 380–600 °C • Crystallinity Index: 60.2 (CT), 75.6 (SB)	60
Sugarcane bagasse (*Saccharum officinarum*)	43.88 ± 2.91%		1.78	89.5%	• Particle diameter: 10 μm (CT), 20 to 30 μm (SB)	
Pineapple leaves (*Ananas comosus*)	70–82%	—	—	—	• Decomposition temperature: 340 °C • Increasing the acetylation time results in the re-appearance of the OH group, which is due to the deterioration of the overall CA composition.	61
Rice husk	—	—	2.91	66%	• Onset thermal degradation temperature: 326 °C • Overall DS increased as the amount of iodine increased, and the synthesized CA exhibited more thermal stability than the native cellulose.	62

Table 1 (*continued*)

Raw materials	Cellulose percentage	Acetylation type	Degree of substitution	%Yield of cellulose acetate	Product property and major outcome of this study	Ref.
Cellulose sample	—	Heterogeneous acetylation using solid super acid, SO_4^{2-}/ZrO_2	1.8	75.6%	• Initial degrees of polymerization: 403 • Introduction of the milling method as a pretreatment process significantly reduces the degree of polymerization (403 to 324) and crystallinity and increases the DS value (0.43 to 1.80) of CA.	33
Cotton cellulose	> 95%	Heterogeneous acetylation using $ZnCl_2$	2.87 (maximum for cellulose triacetate)	95.83% (cellulose triacetate)	• Completely novel, effective, inexpensive, and low toxicity $ZnCl_2$ catalyst has been proposed in this study. • Degree of polymerization: 438 for DS 2.87	50
			2.69 (maximum for cellulose diacetate)	89.97% (cellulose diacetate)	• Decomposition temperature of CTA of DS −2.87 : 298–375 °C (74.07% decomposition)	
Microcrystalline cellulose	—	Heterogeneous acetylation in *N*-methyl-2-pyrrolidinone (NMP) using acetyl chloride as the acetylation agent and crosslinked polyvinylpyridine (C-PVP) as the catalyst	1.93–2.19	—	• Melting peak in DSC: 1.93–2.19 • Up to 10 h of acetylation reaction time DS and yield of CA gradually increases with the reaction time • Yield and DS of CA also increased with acetyl chloride/hydroxyl functionality under constant reaction time and temperature.	37
Cotton linter pulp	—	Rapid transesterification method	2.90	—	• Tensile strength: 0.29 cN/dtex • Elongation at break: 2.59% • Maximum decomposition temperature: 322 °C	32
Wheat straw pulp			2.83		• Tensile strength: 0.46 cN/dtex • Elongation at break: 3.06%	
Bamboo pulp			2.79		• Tensile strength: 0.55 cN/dtex • Elongation at break: 2.73%	
Bleached softwood sulfite dissolving pulp			2.71		• Tensile strength: 0.58 cN/dtex • Elongation at break: 2.28%	
Bleached hardwood kraft pulp			2.55		• Tensile strength: 0.73 cN/dtex • Elongation at break: 3.86%	
Rice straw	83–85% (after treatment)	Heterogeneous acetylation using phosphotungstic acid	2.2	—	• Acetone soluble CA • Up to 5 h of acetylation reaction time, DS and yield of CA gradually increase with the reaction time while the degree of polymerization decreased	40
Sugarcane straw	90%	Heterogeneous acetylation	2.72	41.05%	• Dense and homogenous CA membrane has been fabricated. • Presence of small particles on the top and bottom surfaces decreased the mechanical resistance of the membrane.	63
Sorghum straw	49.48 wt% cellulose 49.43 wt% α-cellulose	Heterogeneous acetylation	2.6.2.7	—	• Crystallinity degree: 43.73% • Thermal decomposition: 133–450 °C • Viscosity-average molecular weight of 90,833.38 g mol^{-1}	64
Cotton cellulose pulp	—	Homogeneous type reversible reaction with CO_2 in the presence of a super base (DBU) in a solvent DMSO	2.89 (maximum)	—	• No need of external catalysts	65

Table 1 (*continued*)

Raw materials	Cellulose percentage	Acetylation type	Degree of substitution	%Yield of cellulose acetate	Product property and major outcome of this study	Ref.
• Soluble in DMSO, acetone, and $CHCl_3$						
Cornhusk	—	One-step homogeneous acetylation	2.16–2.63	—	• Tensile strength: 30–45 MPa • Elastic tensile modulus: 1–2 GPa • Thermal decomposition temperature: 391.7 °C • Maximum Glass transition temperature: 196 °C • CA was soluble in DMSO, chloroform, and acetone	66
Textile wastes (100% cotton sample)	—	Homogenous acetylation: A solution containing sulfuric acid and glacial acetic acid	2.69 (average)	—	• Average degree of acetylation: 40.69%	67
Recycled newspaper	—	Homogeneous acetylation	1.98 ± 0.02 (from received newspaper) 2.79 ± 0.02 (from delignified newspaper)	—	• 50% degradation at 345 °C (for received newspaper) • Maximum degradation at 360 °C (delignified newspaper) • Prepared the CA membrane exhibited excellent water flux due to the amorphous nature of the membrane.	68
Cellulose powder	—	Homogeneous acetylation: Ionic liquid ([HDBN][OAc with dispersing agent such as acetone, acetonitrile, DBN, or DMSO	—	—	• Dissolve in acetone, chloroform, dichloromethane, and DMSO • Should be careful during the recycling of ionic liquid when using 1,5-diazabicyclo(4.3.0)non-5-ene has been considered as a dispersing agent	69
Waste cotton fibers	>98 wt%	Quasi-homogeneous process using an acidic ionic liquid as catalyst.	1.25	—	• XRD study: Decrease in crystallinity as the diffraction intensity increased and the diffraction peak broadened. • Decomposition temperature: • 251 °C for CA (<original WCFs (350 °C)) • Maximum conversion of water-soluble CA reached to 90.8% • The prepared CA film exhibited 56% transparency at 900 nm • Addition of CNC and CNF to the CA film showed 75 and 91% transparency	70
Prehydrolysis kraft pulp	—	Homogeneous acetylation using organic super base-derived ionic liquids ([DBNH][OAc])	0.25–2.97 (Using Ac_2O and IpeAc) 1.5 (using vinylic reagent)	—	• No need of catalyst • Excellent recovery of the ionic liquid by simple distillation	71
Sugarcane bagasse	—	Homogeneous acetylation using (IpeAc) as an acetyl donor and ([Emim][OAc])	2.5–2.8 (acetylation at 50 °C for 5 h)	—	• Acetone soluble and methanol insoluble CA of 89% purity without any pretreatment and using any corrosive reagents such as strong acid, base, or halogenated chemicals • Reaction temperature and the reaction time are the major parameters controlling the DS and yield of CA.	72

Table 1 (*continued*)

Raw materials	Cellulose percentage	Acetylation type	Degree of substitution	%Yield of cellulose acetate	Product property and major outcome of this study	Ref.
Microcrystalline cellulose powder	—	Homogenous acetylation using (EMIMOAc) in the presence of a chloroorganic cosolvent	1.9 (max)	—	• Maximum DS obtained using 8 wt% dichloromethane • On increasing the DCM content, the DS values also increased gradually.	73
Nordic hardwood (Betula pendula)	—	Homogenous acetylation using an organic super base and an ionic liquid system	2.29 (Solvent: DBN) 2,63(Solvent: [DBNH][OA] (Obtained in presence of catalyst, Pyridine)	—	• Insoluble in DMSO, $CHCl_3$, and acetone (CA obtained using DBN). • Soluble in these solvents (CA obtained from [DBNH][OAc]) • No need of catalyst • Varying the reaction conditions, the desired DS, and degree of polymerized CA can be formed	74
Sugarcane bagasse	85.78% (After Pretreatment)	Homogenous process	2.52	43.50%	• Glass transition temperature: 33 °C • Pyrolytic decomposition temperature: (200–380) °C • CA membrane exhibited porous nature within the range of 13.70–23.70% • High porosity indicating the high-water flux of 8.14×10^{-5} g $s^{-1}.cm^{-2}$	75
Microcrystalline cellulose	—	Homogeneous acetylation with acetyl chloride and acetic anhydride in N_{2228} Cl/acetone	0.60–2.79 (using acetyl chloride) 0.30–0.69 (Using acetic anhydride)	—	• Using acetic anhydride as the acylation agent results in lower DS values than acetyl chloride depending on the solvent applied	76
		Homogeneous acetylation with acetyl chloride and acetic anhydride in N_{2228}Cl/DMAc	0.60–2.72 (using acetyl chloride) 0.04–0.34 (Using acetic anhydride)		• Higher degree of polymerization (128–173) has been found using acetyl anhydride as the acylation agent, while using acetyl chloride produced CA polymer with a lower degree of polymerization (76–140).	
		Homogeneous acetylation with acetyl chloride and acetic anhydride in BMIMCl	2.21–2.81 (using acetyl chloride) 0.27–1.25 (Using acetic anhydride)		• Increasing the acylation agent/anhydroglucose unit led to increased DS value.	
		Homogeneous acetylation with acetyl chloride and acetic anhydride in LiCl/DMAc	2.40–2.83 (using acetyl chloride) 0.15–1.0 (Using acetic anhydride)		• Addition of BMIMCl as a solvent slightly improved the DS value compared to the LiCl/DMAc binary solvent system.	
Royal palm tree agricultural waste	—	Homogenous acetylation	2.08–2.82	89–99.5%	• Crystallinity Index: 8.9% • Water soluble CA also be formed	39
Pulp	—	Homogeneous acetylation using tetrabutylammonium acetate and DMSO solvent system	1.73–2.93	—	• Decomposition temperature: 373.3 °C • Soluble in DMSO, $CHCl_3$, and DMF • The DS of CA can be controlled by changing the reaction time and the concentration of cellulose solution.	77

Note-BKP: bleached kraft pulp; BSP: bleached SEW pulp; DS: degree of substitution; DMSO: dimethyl sulfoxide; DMF: dimethylformamide; NIS: *N*-iodosuccinimide; CT: Cajuput twigs; SB: sugarcane bagasse; CTA: cellulose triacetate; DSC: differential scanning calorimetry; DBU: 1,8-diazabicyclo[5.4.0]undec-7-ene; DBN: 1,5-diazabicyclo(4.3.0)non-5-ene; WCF: waste cotton fibers; ipeAc: isopropenyl acetate; N_{2228}Br: triethyloctylammonium bromide; N_{2228}Cl: triethyloctylammonium chloride.

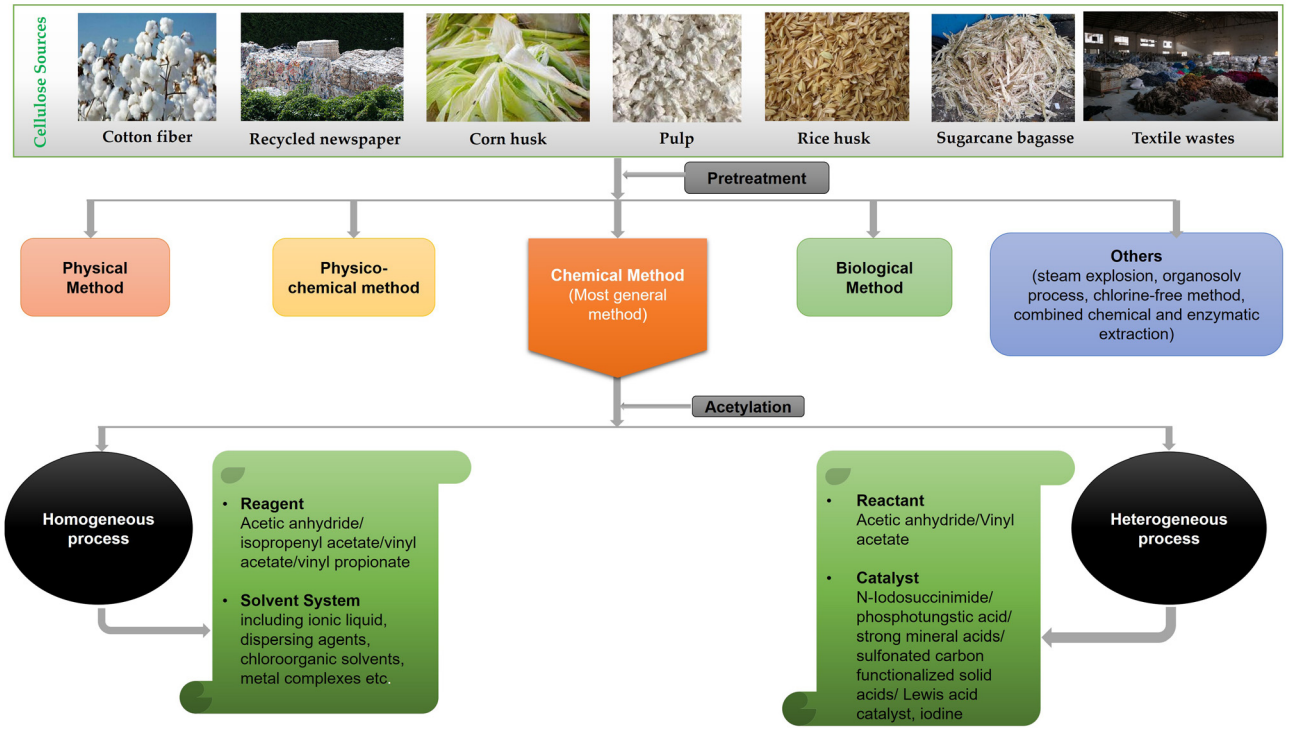

Fig. 2 Schematic diagram of synthesis of cellulose acetate.

effective catalyst in the presence of acetic anhydride in the solvent-free method.[59]

Cellulose triacetate is hydrolyzed to produce secondary cellulose acetate such as cellulose diacetate depending on the final use.[37] The hydrolysis step is necessary in the heterogeneous process to produce the CA of this desired DS.[48] This process can have an economic significance if the hydrolysis step is eliminated. Acetone soluble CA was produced through a one-step heterogeneous acetylation process from oil palm empty fruit branch. To reduce the use of sulfuric acid, a mixture of sodium bisulfate and sulfuric acid was used as a catalyst. In a single-step process, the reaction time and acetic anhydride-to-cellulose ratio were controlled to produce the desired DS of cellulose acetate. Acetone-soluble cellulose diacetate of DS value 2.2–2.7 has a great number of commercial applications[54] and was prepared by Fan *et al.* from rice straw using phosphotungstic acid as the catalyst.[40]

Cellulose acetate was extracted from waste blended fabrics using a Brønsted acidic ionic liquid *N*-methyl-imidazolium bisulfate, [Hmim]HSO_4.[57] Using Brønsted acidic ionic liquid as heterogeneous catalyst, CA can be synthesized from waste cotton fabric. The IL catalyst showed excellent catalytic activity to convert waste cotton fabric into cellulose acetate under solvent-free conditions.[52] IL was used as a novel catalyst for the acetylation of cellulose in an environment-friendly and efficient approach. Instead of wood pulp, bamboo pulp can be used for the acetylation, and cellulose acetate with a better degree of substitution can be prepared though the heterogeneous process.[56] Candido *et al.* and Alves *et al.* utilized the lignocellulosic material, sugarcane straw, to produce and characterize cellulose acetate.[63,64]

Tian *et al.* reported a green, environment-friendly solvent-free method to produce cellulose acetate with acetic anhydride using acidic ionic liquid, 1-vinyl-3-(3-sulfopropyl)imidazolium hydrogen sulfate ([VSim]HSO_4), as the catalyst.[58] The catalyst also provided the dual function of swelling and catalytic activity, which created a quasi-homogeneous state in the synthesis process. A quasi-homogeneous process means that the acidic ionic liquid will act as a catalyst and cause the swelling of cellulose to increase the accessibility to the OH group. Water-soluble cellulose acetate can be synthesized from cost-effective waste cotton fibers through this process.[70] An acidic ionic liquid, 1-methylimidazolium hydrogen sulfate [Hmim][HSO_4], was also used as a catalyst to synthesize CA with controllable DS values. Under optimum reaction conditions, CA with low DS and good water solubility was obtained by this process. As reported, CA with DS in the range of 0.5–1 is water soluble.

Konwar *et al.* developed a green approach for the one-pot synthesis of acetone-soluble cellulose acetate over sulfonated carbon (SO_3H/$PhSO_3H$)-functionalized solid acids or sulfonated carbons as a new, reusable heterogeneous catalyst under mild and solvent-less conditions.[54] Both the cellulose diacetate and cellulose triacetate can be produced in the presence of a nontoxic, cost-efficient solid catalyst, $ZnCl_2$, under the effect of microwave irradiation. In the solvent free system, cellulose acetate with a wide range of DS (2.25–2.87) was successfully produced.[50]

Currently, iodine can be used as a cheap, convenient, and environment-friendly reagent due to its catalytic activity in various organic synthesis; for example, iodine-catalyzed highly stereoselective synthesis of sugar acetylenes, acetylation of

alcohols under solvent-free conditions, acetylation of agricultural byproducts, synthesis of thiiranes from oxiranes, and synthesis of phenanthrimidazole from 9,10-phenanthraquinone. As a Lewis acid catalyst, iodine can make the carbonyl carbon of acetic anhydride more reactive to form acetic acid and subsequently to generate cellulose acetate. Besides, microwave irradiation can increase the swelling of cellulose and diffusion rate of iodine and acetic anhydride. Thus, cellulose triacetates with high DS value can be obtained at reduced time and amount of reagents.[35,78] Cheng *et al.*, Das *et al.*, Araujo *et al.*, Maryana *et al.*, and Egot *et al.* used the solvent-free acetylation method of cellulose, catalyzed with iodine. CA was successfully synthesized from agricultural and lignocellulosic wastes by this green approach.[27,51,60–62]

2.1.2. Homogeneous acetylation. Homogeneous reaction includes many advantages such as creating more options to introduce novel functional group, design new products, control DS, provide good accessibility to the hydroxyl groups, ensure the uniform distribution of functional groups along the polymer backbone, as well as short reaction times and good reproducibility. For this type of functionalization, a suitable solvent is necessary to dissolve cellulose and provide a feasible reaction environment. This solvent must be capable of interacting with the anhydroglucose units and deconstructing the multifaceted interaction network in crystalline cellulose by cleaving inter and intramolecular hydrogen interactions, rendering it soluble since solvent–glucan interactions are dependent on the deconstruction state of cellulose. Due to extreme difficulties in dissolving cellulose, only a limited number of solvent and metal complexes have been reported, for example, *N*,*N*-dimethylacetamide (DMAc)/LiCl, dimethylsulfoxide (DMSO)/tetrabutylammonium fluoride trihydrate (TBAF), dimethylformamide (DMF)/N_2O_4, *N*-methylmorpholine-*N*-oxide monohydrate (NMMO), cuprammonium hydroxide (cuoxam), cadmiumethylenediamine (cadoxen), and molten salt hydrates ($LiClO_4{\cdot}3H_2O$ or $LiSCN{\cdot}2H_2O$). Researchers are focusing on overcoming the limitations such as toxicity, cost, difficulty for solvent recovery, and instability in this process. Besides, these solvent systems require long pretreatment and reaction time, which is undesirable. In recent times, room temperature ILs have earned significant attention due to their several advantages such as enhancement of reaction rates, improvement of selectivity and yields, or ease of recycling catalysts.[32,69,76,79]

A solvent system was based on the derivative dissolution of cellulose with CO_2 through the carbonation reaction in the presence of a strong base, 1,8-diazabicyclo[5.4.0]undec-7-ene (DBU) in DMSO.[65] Cellulose solution (8 wt%) in DMSO was obtained under 0.2 Mpa of CO_2 at 50 °C when the molar ratio of DBU to anhydroglucose unit (AGU) was 3 : 1. The reversible IL system thus synthesized also acted as an efficient media for the acetylation of cellulose to yield CA with high substitution degree from 1.78 to 2.89 under mild conditions using only acetic anhydride as an acetylation reagent. These results also showed that DS can be controlled by varying the stoichiometric ratio of acetic anhydride/AGU, temperature, and reaction time. Cao *et al.* synthesized cellulose acetate through a one-step homogeneous acetylation process using relatively cheap cornhusk as cellulose resources.[66] They successfully acetylated the cornhusk cellulose with acetic anhydride in the absence of the catalyst in the ionic liquid 1-allyl-3-methylimidazolium chloride (AmimCl). Through homogeneous acetylation process, CA can also be produced from recycled newspaper and textile wastes.[67,68] CA of desired DS was synthesized from Nordic hardwood after separating the cellulose-rich fraction using CO_2 and CS_2-based switchable ionic liquids systems.[74] The extracted cellulose was dissolved in an organic super base named 1,5-diazabicyclo[4.3.0]non-5-ene (DBN) and in an IL such as 1,5-diazabicyclo[4.3.0]non-5-ene acetate ([DBNH][OAc]) from where 3 wt% cellulose dissolution was obtained. The acylation of the dissolved cellulose with Ac_2O resulted in CA with a wide range of DS depending on the presence and absence of the catalyst and reaction conditions.

A fast dissolution and homogeneous acetylation process was introduced for cellulose using 1,5-diazabicyclo(4.3.0)non-5-enium acetate [HDBN][OAc], which included the dispersing agent such as acetone, acetonitrile, 1,5-diazabicyclo(4.3.0)non-5-ene (DBN), or (DMSO).[69] Cellulose powder was first dispersed in these agents and then added to the freshly prepared [HDBN][OAc]. Proper dissolution was obtained when it is heated to 70 °C for 0.5 h. When acetic anhydride was added to this ternary cellulose/IL/dispersing agent system, CA with different DS was obtained. Kakko *et al.* synthesized CA of different DS by the homogeneous esterification of cellulose in the IL 1,5-diazabicyclo[4.3.0]non-5-ene acetate ([DBNH][OAc]) as the solvent using some commonly used acylation agents such as acetic anhydride (Ac_2O), isopropenyl acetate (IpeAc), vinyl acetate (VinAc), or vinyl propionate (VinPr).[71]

Transesterification is a relatively mild acetylation method, which uses acetate ester as an innocuous acyl donor, avoiding the formation and introduction of acidic reagents in the acetylation system. According to this process, CA is produced by the transesterification of cellulose with acetic anhydrate or vinyl acetate in DMSO/TBAF.[32] Several studies also proposed *N*-ethyl-pyridinium chloride, *N*,*N*-dimethylacetamide (DMAc)/lithium chloride (LiCl), and 1,3-dimethy-2-imidazolidinone (DMI)/LiCl as the solvent.[42] However, the major drawback of this process is the long pretreatment and reaction time.[42] In a recent study, a simple and rapid transesterification method has been reported where CA fibers were produced from six cellulose raw materials. In this process, the esterification of cellulose was carried out with vinyl acetate under the catalysis of NaOH or KOH in DMSO within 15 min.[32] A similar rapid and direct transesterification method has also been reported in the literature.[80–82]

Highly purified cellulose acetate was produced by controlling the reaction temperature and DS, which does not include any pretreatment. Instead of using bulky chloride of acetyl chloride, a chloroorganic solvent, dichloromethane, can be used as a co-solvent for the homogeneous acetylation of cellulose in the presence of 1-ethyl-3-methylimidazolium acetate (EMIMOAc).[73] This result showed that lower viscosity co-solvent significantly

facilitates the cellulose acetylation process in ILs. Achtel *et al.* used triethyloctylammonium chloride ($N_{2228}Cl$) in combination with the organic solvent *N*,*N*-dimethylacetamide (DMAc) and acetone as a new cellulose solvent.[76] Moreover, for comparison, additional cellulose solvents, namely, LiCl/DMAc and 1-butyl-3-methylimidazolium chloride (BMIMCl), were examined for acetylation at comparable conditions. Their result showed that $N_{2228}Cl$/DMAc and $N_{2228}Cl$/acetone can be used as the reaction media for the homogeneous acetylation of cellulose. In the absence of the catalyst, tetrabutylammonium acetate and dimethylsulfoxide solvent system can synthesize cellulose acetate in this homogeneous approach.[77] Through this approach, CA was synthesized from sugarcane bagasse and from leaf sheath disposed off as agricultural waste during the production of royal palm tree.[39,75]

Different studies confirm that some undesirable problems, such as serious degradation of cellulose, damage to the environment, and high energy consumption of the traditional method of cellulose acetate synthesis poses the necessity for extensive research in this field. Moreover, from the above discussion, it is evident that the DS parameter affects the chemical, physical, mechanical, and morphological characteristics of cellulose. For example, a small change in DS (only by 0.19) can change the mechanical properties of the material as a function of temperature.[45] Thus, different synthesis processes must be explored to introduce an effective way of maintaining the desired DS of CA for commercial applications. Currently, most studies are conducted on the continuous development of green solvent systems, reagents, and catalysts of CA synthesis processes. The green synthesis route of cellulose acetate to get better yield, desired DS, and properties of CA are in the developmental stage to confirm the environmental viability of the methods used.

2.2. Membrane based on cellulose acetate

CA is widely used for its good filtration efficiency but its properties must be improved for application, especially in harsh environments such as high temperature, organic solvents, and corrosive environment. The CA membrane has extremely low flux due to its dense skin layer and low porous sublayer. Besides, CA-based UF membrane has a serious problem of fouling during filtration. Several attempts have been made to increase its thermal stability, mechanical properties, membrane surface hydrophilicity, water permeability, and fouling resistance by blending it with other polymers to introduce reactive functional groups.[28,83]

Ertas *et al.* produced a CA/polybenzoxazine composite nanofibrous membranes through the electrospinning and curing process.[83] Polybenzoxazine is a phenolic type thermoset resin with many attractive properties such as near zero volumetric change upon curing, zero byproducts, no requirement of catalysts during curing, low water absorption, high glass transition temperature, high char yield, and good mechanical and thermal properties, which makes it a suitable membrane material for water filtration. To overcome the solubility problem by achieving effective crosslinking, an additional crosslinking agent, citric acid was used. Due to this crosslinking property, the produced nanofibrous membrane was able to preserve its membrane integrity and fibrous morphology even after overnight immersion in dichloromethane/methane solvent mixture, in which electrospinning was performed. The characterization of this electrospun CA/polybenzoxazine composite nanofibrous membrane proved that this membrane as a very promising membrane material for water purification and wastewater treatment. Ghee *et al.* synthesized the nanofiltration composite membrane by preparing the chitosan/cellulose acetate composite through the phase-inversion technique.[28] Their work resulted in a very porous membrane with channel-like structures and a spongy layer at the top. The substrate membrane with 15 wt% CA concentration provided high mechanical stability to the composite membrane and allowed highest water flux. Chitosan incorporation in this composite membrane improved the membrane's hydrophobicity, regeneration efficiency, water flux, retention, and antifouling property.

Nanodiamond (ND) nanoparticles (NP) as a reinforcement agent can provide excellent thermal and mechanical properties, very high specific surface area, and hydrophilicity on the surface of CA.[84] The impact of NPs on the performance, morphology, hydrophilicity, and the fouling behavior of CA membranes in water treatment was investigated by incorporating the pristine and thermally-functionalized ND, ND-COOH, into CA. The final result showed the highest hydrophilicity, pure water flux, abrasion resistance, and better mechanical properties for the CA/ND-COOH (0.5 wt%) membrane. Despite the many advantages of ND, the presence of carbon impurities and formation of microsized agglomerates may result in poor dispersibility and weak interfacial interactions with the polymer matrix. The CA nanocomposite membrane incorporated with amino (NH_2)-functionalized as well as polyethylene glycol (PEG)-grafted NDs showed that the nanocomposite membrane possessed high hydrophilicity, porosity, and high antibiofouling properties.[85] A flat-sheet nanofiltration membrane with bactericide properties was prepared by incorporating silver into cellulose acetate in two distinct forms: polyvinylpyrrolidone-coated silver nanoparticles (AgNPs) and silver ion exchanged β-zeolite (Ag^+βZ).[86] This work resulted in a composite nanofiltration membrane with enhanced hydrophilic property and high removal coefficient to sulfate salts (Na_2SO_4, $MgSO_4$) compared to chloride salts (NaCl, $MgCl_2$). Besides, the hydraulic permeability of CA/Ag^+βZ was increased by 56.3% in comparison to the CA silver-free membrane. Through the electrospinning method, a core/shell-structured CA/polyimide(PI) electrospun fibrous membrane can be obtained, which is modified with fluorinated benzoxazine (F-PB) in the presence of silicon nanoparticles (SNPs).[87] The resulting nanofibrous membrane possessed the mechanical property of the PI fiber core and the surface roughness of the CA shell. In addition to that, surface modifications with F-PB/SNPs provided superhydrophilicity and superleophilicity to the membrane. CA membrane modified with ZnO showed better hydrophilicity and permeation with consistent UF applications.[88] CA/hydroxyapatite (HA) composite was

prepared through the phase-inversion method for water purification. Hydroxyapatite was used for the removal of harmful substances such as Cr(VI) from aqueous solutions or Ni^{2+}, Cd^{2+}.[89] The incorporation of hydroxyapatite nanoparticles into polymer improves its distribution on the surface of the polymer substrate and overcomes limitations such as low yield of fabrications and slow rate of hydroxyapatite nanoparticles degradation. Hamad *et al.* prepared a hybrid nanofiber composite CA/HA by the electrospinning process, which possessed ultrafine, smooth, homogeneous, and bead-free fibers.[90] The positively charged calcium ions can bind with the negatively-charged carboxylate groups of CA. Besides, the intermolecular/intramolecular interactions can make the composite membrane rich in HA. These characteristics increased the yield and slowed down the degradation rate of HA.

High-performance polymers are blended with CA to improve the membrane properties. A novel ultrafiltration membrane was prepared by blending nanochitosan (NCS), CA, and polyethylene glycol (PEG) in different weight proportions through the phase-inversion process by Vinodhini *et al.*[91] Nanochitosan with a particle size of 100 nm was used to increase the surface area. CA and PEG were used as a membrane matrix material and pore forming agent, respectively. The prepared membrane showed enhanced properties with asymmetric structure, better miscibility, and compatibility. To increase the flux and mechanical stabilities by increasing the concentration of inorganic particles, SiO_2 is a promising compound due to its special properties such as small size, thermal resistance, fine suspension formation in aqueous solution, strong surface energy, and relatively inert material. Ahmad *et al.*[92] prepared a thermomechanically stable membrane CA/PEG/silica to determine the effect of silica on the membrane properties. The mechanical stability was increased as the silica loading increased from 1% to 4% (w/v). According to their study, silica particle incorporation at an optimum level can become an advantage for maximizing the hydrophilicity, fouling resistance, and thermal properties of the membrane. Another study showed that the incorporation of surface-engineered carbon nanotube (CNT) with the polymer matrix yielded CA/PEG, which can effectively improve the thermal stability and mechanical strength of the membrane.[93]

Polyvinyl alcohol (PVA) is a promising membrane material because of its high hydrophilicity, nontoxicity, and polymer biocompatibility with excellent film-forming properties, high mechanical strength, low fouling potential, long-term temperature, and strong pH stability.[94] The presence of polyvinyl pyrrolidone (PVP) in the CA/PVA/PVP membrane provided a denser skin layer and smaller macrovoids. A decrease in the PVP content increased the spongy pores near the bottom surfaces. However, due to the strong hydrophilicity and large swelling capacity of PVA, it is crosslinked with glutaraldehyde, and the improved properties of newly-formed CA/crosslinked PVA(CPVA)/PVP were studied in detail. Glutaraldehyde (GA) will break the hydroxyl group in the PVA, which will result in the reduction of hydrophilicity. In Table 2, the morphology and properties of CA/PVA (90/10)/PVP (3 wt%) and CA/CPVA (80/20)/PVP were summarized.

The advantages of forward osmosis including low energy consumption, low fouling propensity, and high water recovery have made it suitable for wastewater treatment applications.[95] However, its antifouling behavior is not satisfactory. Besides, the osmotic properties of this process are limited by internal concentration polarization in the support layer. A forward osmosis membrane, which is free-standing cellulose triacetate (F-CTO)/graphene oxide (GO), was reported for the first time to overcome these limitations. GO can increase high water permeation by providing strong hydrophilicity. By adding an optimal amount of GO to the polyamide active layer of thin film composite membrane, the water flux can be increased by 52%. The incorporation of GO to the commercial CTA forward osmosis membrane can mitigate the effect of internal concentration polarization and improve the water permeation and antibiofouling behavior.

GO nanosheet has strong hydrophilicity due to its rich oxygen group on atom-thick nanosheets. However, the strong tendency of aggregation of GO nanosheets results in easy stacking, which can reduce the permeation and antifouling properties of GO-blended membranes. To overcome these limitations, metal organic framework (MOF) was introduced as a unique modifier of GO to combine the hydrophilic group of GO and porous structure of MOF.[96] Due to the strong linkages between the metal clusters of MOF and oxygen-containing groups of GO, the interactions between the GO nanosheets decreased, and MOF-GO could effectively inhibit the GO layer's agglomeration. Thus, the UF membrane, CA/MOF-GO, showed better permeability and antifouling performances. Functionalizing membranes with discrete nanomaterials have been actively attempted by the researchers to improve the membrane performances. These types are known as nano-enhanced membranes (NEM). Recently, carbon nanotube (CNT)-based NEM have been reported because of its potentialities to improve water flux and hydrophilicity. Choi *et al.* fabricated a functionalized CNT (f-CNT) blended CA composite membrane, f-CNT (1 wt%)/CA for FO applications through the phase-inversion process.[97] The membrane became hydrophilic after blending with f-CNT, resulting in a 50% increase in water-permeated flux compared to the bare CA membrane. Researchers suggested that this membrane could be pretreated before wastewater treatment to reduce the fouling tendency.

In recent years, it has been studied that the addition of nanoclay can greatly influence the performance and properties of the nanocomposite membrane. Clays as nanoparticle filler have received attention due to their proper dispersion in the polymer matrix, high surface area (up to 750–800 $m^2\ g^{-1}$), low cost, nontoxicity, and availability in nature. Organically-modified montmorillonite (OMMt), such as cloisite 15A, is a promising nanoclay filler in clay polymer nanocomposite membrane.[98] Research on the performance of the CA/OMMT nanocomposite membrane showed that on increasing the amount of OMMt, though the hydrophilicity and porosity increased, the mechanical and thermal properties decreased. Goetz *et al.* changed the surface chemistry of electrospun cellulose acetate by impregnating chitin nanocrystal (ChNC).[99]

Table 2 Morphology and properties of cellulose acetate-based membranes

Membrane type	Production method	Structure and morphological characterization	Properties of membrane	Ref.
CA/polybenzoxazine composite	Electrospinning and thermal curing	Average fiber diameter: 450 ± 160	Maximum degradation temperature: 378 °C Char yield: 24.7% Tensile strength: 8.64 ± 0.63 MPa	83
		Immediately soluble in DCM and methanol Physical appearance: Brownish yellow, flexible film	Ultimate tensile stress: 8.93 ± 0.12% Young's modulus: 213.87 ± 30.79 MPa	
Chitosan/cellulose acetate composite	Phase-inversion technique	Asymmetric sublayer, very porous, spongy structure at the top for the substrate membrane with 15 wt% CA	Contact angle: 48 °C Water flux: 4.37 L m^{-1} h^{-1} Onset of membrane degradation: 207.5 °C Molecular weight cut off: 803.74 Da Mean pore size: 0.78 nm	28
Cellulose acetate/ nanodiamond	Phase-inversion technique	SEM image: Dense layer decreased, number, and length of macrovoids increased compared to CA membrane	Mechanical properties in dry condition: Elongation at break (13.7%), Tensile strength (10.85 MPa) Water contact angle: 54° Water content: 76.1% Porosity: 81.4%	84
		TEM image: Uniform distribution of ND-COOH particles achieved	Pure water flux: 122.5 L m^{-1} h^{-1}	
CA/ND-NH_2	Phase-inversion technique	Porous structure, increased length of macrovoids with decreased size, uniform distribution of the functionalized ND particle	Water contact angle: 53.3° (min) Mean permeate flux: 104.9 L m^{-2} h^{-1} Critical flux: 107 L m^{-2} h^{-1}	85
CA/ND-PEG			Water contact angle: 52.2° (min) Mean permeate flux: 108.5 L m^{-2} h^{-1} Critical flux: 120.3 L m^{-2} h^{-1}	
CA/AgNPs	Phase-inversion technique	—	Removal coefficient: 96.4% (Na_2SO_4), 97.4% ($MgSO_4$) 83.5% (NaCl), 90.4% ($MgCl_2$)	86
CA/Ag + βZ			92.5% (Na_2SO_4), 93.3% ($MgSO_4$) 82.8% (NaCl), 86.5% ($MgCl_2$)	
PI/CA/F-PB/SNP	Electrospinning	Core/shell structured membrane.	Critical tensile strength: 130 MPa Critical tensile strain: 52%	87
		Outer fiber diameter: 200 nm Wall thickness: 5 nm Micro and nanoscale roughness on the surface, highly flexible	water contact angle: 162° Oil contact angle: 0° Water flux: 3106.2 L m^{-1} h^{-1}	
CA/ZnO	Phase inversion	Asymmetric structure	Contact angle: 48°–82.7° Permeability: 1897 LMH/bar (CA (10%)/ZnO (3%))	88
		Average pore radius: 0.0261–0.045 μm Rough surfaces	Zeta potential: +23 mV at pH: 7 and 0.01 M NaCl Mechanical and thermal stability increased with ZnO	
CA/HA	Phase inversion	Average diameter of pores and shape decreases. Emergence of HA crystals with average dimension of 20–30 μm	Water flux: 26.73 L m^{-1} h^{-1}	89
CA/HA	Electrospinning	Homogeneous, ultrafine, smooth, and bed fibers	Nanofiber average diameter: 21.98 nm	90
NCS/CA/PEG	Phase inversion	Asymmetric, porous and rough surface. Crystallinity percentage: 6%	Glass transition temperature: 175 °C Thermal decomposition temperature: 91.44 °C	91
CA/PEG/silica	Phase inversion	Microsized (0.5–1) μm silica particles at top surface	Water flux: 1.28–2.46 L m^{-1} h^{-1} Salt removal: 83–92% Membrane permeability: (3.18–5.32) × 10^{-4} L h^{-1} m^{-2} KPa Lowest contact angle: 24.10° Maximum degradation temperature obtained: 520 °C Glass transition temperature: 80 °C (For 4% silica) Tensile strength: 437.28 MPa (For 4% silica) Elongation at break: 12.23% (For 4% silica)	92

Table 2 (*continued*)

Membrane type	Production method	Structure and morphological characterization	Properties of membrane	Ref.
		Formation of macroscopic defect, which is filled by silica aggregates by increasing the concentration of silica		
CA/PEG/tethered CNT	Phase inversion	Dense, even, and smooth surface. Uniform distribution of CNT but agglomerates formed at high concentration of CNT Root mean square roughness: 22.045 nm (min)	Water content: 92.2% (max) 80% weight loss at 407 °C (max) Hydraulic resistance: 0.0156 bar m^{-2} h^{-1}	93
CA/PVA/PVP	Phase inversion	Dense top layer, porous sublayer, spongy pores near the bottom surface	Porosity: 82.22% Contact angle: 56.2% Flux recovery ratio: 83.5% Viscosity: 15.12 Pa s Pure water flux: 588.1 L m^{-1} h^{-1}	94
CA/CPVA/PVP		Less dense top layer Longer finger-like pores Better vertical interaction with transfixation from top layer to sublayer	Pure water flux: 928.7 L m^{-1} h^{-1} FRR: 86.3%	
F-CTO/GO	Phase inversion	Very thin dense layer at the top and smooth surface Thickness: 1 μm Macrovoids texture turned to bedded rock-like structure as the GO amount increased. Uniform color and become dark as GO increased.	Water flux: 18.43 L m^{-1} h^{-1} Strength: 42.8 MPa Young's modulus: 1.18 GPa	95
CA/MOF-GO	Phase inversion	Asymmetric structure, Dense top layer, Wide pore cannels Smooth surface, Average roughness: 7.2 nm	Thermal degradation: 355 °C (from the DTG curve) Contact angle: 49.5° Water flux: 183.51 L m^{-1} h^{-1} Flux recovery ratio: 88.13%	96
f-CNT/CA	Phase inversion	Asymmetric structure with dense top layer and porous sublayer	Contact angle: 58° Water flux: 14.11 L m^{-1} h^{-1}	97
CA/OMMt	Solution dispersion & phase inversion	Intercalated OMMT within CA matrix Asymmetric structure with dense top layer For 5% OMMt dosage Maximum length of finger-like micropores Porosity: 42.14%	For OMMt loading of 5%, Tensile strength at break: 4.91 MPa Decomposition of OMMt: 290–400 °C Contact angle: 35–40% Pure water flux: 6.6×10^{-5} m^3/m^{-2}	98
Electrospun CA coated with ChNC	Electrospinning	Highly homogeneous coating of chitin nanocrystal Porosity: 85.6% Average pore diameter: 10.07 nm Surface area: 3.709 m^2 g^{-1} (for 5% ChNC)	Tensile strength: 3.31 MPa E-modulus: 1.16 Gpa (for 5% ChNC) Onset of Thermal degradation temperature: 293 °C Water flux: 27 900 L m^{-2} h^{-1} bar^{-1} Contact angle: 0° Zeta potential: −4.7 at pH 7.5	99
CNCs/CDA	Phase inversion	Asymmetric structure with skin layer, finger-like sublayer, sponge-like support layer. Denser, smoother surface, greater interconnectivity, higher porosity, lower resistance of finger-like pores with increasing CNCs.	Water contact angle: 58–60° (min) Water content: 75.5% (max) Tensile strength: 6.28 MPa (max) Elongation at break: 60–70% (max) Pure water flux: 173.77 L m^{-1} h^{-1} (max) Surface roughness: 76.17% (min) Flux recovery ratio: 92.01% (max)	100

Table 2 (*continued*)

Membrane type	Production method	Structure and morphological characterization	Properties of membrane	Ref.
Amine impregnated TiO_2/CA	Phase inversion	Asymmetric structure, less finger-like macrovoid and dense top layer	Water contact angle: 40.9°(min) Pure water flux: 924.7 L m^{-1} h^{-1}	101
PU/CA	—	Homogeneously blended, Asymmetric structure, Spongy surfaces with lots of voids and pores Pore sizes: 0.04–0.1 μm	Contact angle: 34.19° (min) Water content: 83.27% (max) Water flux: 13.93 L m^{-2} h^{-1}	103

Note-ND: nanodiamond; PEG: polyethylene glycol; AgNPs: silver nanoparticles; Ag + βZ: silver-loaded zeolite; PI: polyimide; F-PB: fluorinated polybenzoxazine; SNP: silica nanoparticles; HA: hydroxyapatite; NCS: nanochitosan; CNT: carbon nanotube; PVA: polyvinyl alcohol; PVP: polyvinylpyrrolidone; F-CTO: free-standing cellulose triacetate; GO: graphefe oxide; MOF: metal–organic frameworks; f-CNT: functionalized carbon nanotube; OMMt: organically-modified montmorillonite; ChNC: chitin nanocrystal; CNCs: cellulose nanocrystals; CDA: cellulose diacetate; PU: polyurethane.

Chitin nanocrystal with high surface area and good mechanical properties can provide fungal and bacterial resistance. The membrane showed 87.7% decrease in biofilm formation, 131% increase in strength, and 340% increase in stiffness in comparison with uncoated electrospun cellulose acetate membrane. Thus, the coated membrane obtained for water filtration with biofouling and biofilm resistance characteristics possessed superhydrophilic properties. Cellulose nanocrystals (CNCs) or nanofibrils (CNFs) have intrinsic fibrous nature, hydrophilicity, and high strength, which inherit modifiable surface properties due to abundant hydroxyl groups. CNCs are widely used with polymers to form a nanocomposite with significant characteristics. Cellulose nanocrystals (CNCs)/cellulose diacetate (CDA) blending membrane can overcome the disadvantages of CDA membrane, which has low water flux, poor protein removal, and low biofouling tendency. CNCs as a promising candidate for membrane application showed 20 times higher permeate flux than the CDA membrane and increased the flux recovery ratio to 92.01%.[100] The conventional processes to remove heavy metal from the contaminated water require high energy. Besides, the UF and MF membrane cannot remove the heavy metal because of their larger pore sizes. For that reason, Gebru *et al.* introduced a UF membrane, which is an amine-impregnated TiO_2-modified cellulose acetate. TiO_2 has a stable nature and provides high surface area, porous structure, and antifouling property. TiO_2 nanoparticles are modified with three types of amine, which are tetraethylenepentamine (TEPA), ethylenediamine (EDA), and hexamethylenetetramine (HMTA), as the complex reaction between the heavy metal and the nitrogen atom is important for increasing the effective separation.[101]

Cellulose acetate (CA)/polyethersulfone (PES) membrane was synthesized using DMAc as the solvent can overcome the CA disadvantages and the fouling behavior of PES. PES is a widely-used membrane material due to its mechanical, thermal, and chemical stability as well as membrane-forming properties. The surface morphology of this membrane showed larger finger-like macrovoids and higher porosity. The CA/PES ultrafiltration membrane can be better in hydrophilicity and antifouling properties and was suggested to be used for industrial applications.[102] Riaz *et al.* introduced a cost-effective and sustainable membrane for ultrafiltration by blending polyurethane (PU) with cellulose acetate.[103] PU possesses high thermal, mechanical, and chemical properties. Thus, this PU/CA membrane showed improved hydrophilicity and numerous pores on the blend membrane surfaces and increased the water flux.

Generally, membranes for MF, UF, NF, and RO processes are made from synthetic organic polymer and CA.[6] Among these, NF is an advanced process known as 'loose' RO. NF membranes are made up of cellulose acetate blend in recent times to decrease its hydrolysis over time and sensitivity to pH and increase its selectivity and stability.[104] NF is a pressure-driven process, which can be operated in a relatively low pressure (0.3–1.5 MPa) and has high removal of multivalent ions.[28]

From previous discussion, it is evident that most of the studies based on the CA-based membrane are conducted on

utilizing this NF process. However, the uniform dispersion of NPs, achieving a membrane of asymmetric, smooth, highly porous structure with simultaneously enhanced water flux, hydrophilicity, stability, salt removal percentage, and antifouling behavior is still in the developmental stage according to the previous discussion. Various CA-based membranes, their morphology, and properties are summarized in Table 2.

3. Cellulose acetate-based membrane for wastewater treatment

3.1. Separation of heavy metal

Cellulose acetate (CA) and modified CA-based polymeric materials has been used for long time for the removal of heavy metals from wastewater. Generally, CA is an environment-friendly polysaccharide with extensive source and also possesses excellent hydrophilicity and good film forming ability, which makes its application in different forms of membrane fabrication such as ultrafiltration, nanofiltration, reverse osmosis, and forward osmosis.[105,106] Moreover, CA and its derivatives-based membrane have several advantages including moderate water flux, higher salt or pollutant rejection rate, cost effectiveness, relatively easy manufacturing cost, and also abundant raw material source. All of these properties make them an excellent candidate for membrane synthesis and application. An overview of CA-based membrane used for heavy metal removal from wastewater is summarized in Table 3. However, CA contains β-dehydrated glucose, which is vulnerable to bacterial attack, resulting in serious damage of membrane surface and compact at higher pressure, which limits its industrial application for a long time.[105] For example, a NH_2-functionalized (CA)/silica composite nanofibrous membranes were prepared, which enhance the antibacterial properties with outstanding adsorption capacity (19.46 mg g^{-1}) for Cr^{6+} compared to pure CA (1.28 mg g^{-1}) and CA/silica (3.03 mg g^{-1}) composite.[107] In another study, the blending of electrospun CA membrane with PMAA enhanced the heavy metal removal rate (Hg^{2+}, Cu^{2+}, and Cd^{2+}) as PMAA provide –COOH groups on the surface-increased complexation rate.[108] However, the antibacterial property of CA can also be enhanced with the addition of a polymeric material having antimicrobial properties. Ghaffar *et al.* and his coauthor showed increased antibacterial property along with improved salt removal (89 to 94%).[105] Moreover, CA membrane modified with *N*,*N*-dimethyloctylamine (DMOA) showed improved mechanical and thermal property along with more than 99.9% antibacterial property against both Gram-positive and negative bacteria.[106]

A membrane prepared from modified cellulose acetate, modified chitosan, and TiO_2 can also be used for oil–water separation and the removal of Cu(II) from wastewater.[109] Under optimum operating conditions, the prepared membrane exhibits 97% Cu(II) ion removal efficiency. Gebru *et al.* (2017) prepared an ultrafiltration membrane based on CA polymer blended with polyethylene glycol as an additive and amine-modified TiO_2 (modified with tetraethylenepentamine (TEPA), ethylenediamine (EDA), and hexamethylenetetramine (HMTA)), which offers excellent thermal stability, hydrophilicity, and Cr^{6+} removal efficiency (99.8%).[101] The higher removal efficiency of Cr^{6+} is due to the modification of TiO_2 with amine functional groups in the membrane, resulting in electrostatic attraction between the membrane and Cr^{6+}.

Metal–organic frameworks (MOFs)-based membrane have become more attractive and used widely due to their exceptional characteristics such as flexibility, easily modifiability, higher tunable porosities, larger surface areas, hydrophilicity, fouling resistance, and higher capacities to combine with particular species.[110–112] In 2013, MOF on cellulosic FO membrane was applied to investigate the improvement of the desalination performance and antifouling properties.[113] Generally, polymer and MOFs are bonded by weak interaction such as hydrogen bond, van der Waals forces, and π–π stacking.[114] The addition of MOFs on the membrane surface leads to increased membrane porosity, pore interconnectivity, and hydrophilicity. Moreover, the membrane also showed reduced structural parameter with increased FO water flux (180%) along with excellent organic antifouling properties. Furthermore, MOFs have better affinity for polymeric materials than inorganic materials because of the presence of organic linkers in their structure. Hence, polymer materials such as cellulose and cellulose acetate can easily interact with MOFs by covalent and electrostatic bond. For this reason, a large number of MOFs/polymer-based studies have demonstrated different environmental applications such as adsorption (inorganic and organic contaminants),[115–117] catalysis,[118–121] and membrane (FO,[113,122] RO,[123,124] nanofiltration,[125,126] and ultrafiltration[127,128]). In a recent study, Zn-based MOF-embedded with polyethersulfone, cellulose acetate, and polyvinylidene fluoride were prepared, which exhibited comparatively improved hydrophilicity, porosity, permeation performance, antifouling properties, and higher metal (Cu^{2+} and Co^{2+}) removal rate than neat polymeric membranes.[114]

Zeolites are naturally available silicate framework with three-dimensional cage structure containing permanent negative charges and can be used as an adsorbent for removing heavy metals, which have gained great interest due to its higher ion exchange capacity.[129] However, it is very difficult to separate the zeolite from the solution in the large scale wastewater treatment process because of smaller particle size, and the materials are not suitable for reuse.[130,131] To overcome this drawback, it can be dispersed and embedded in a polymer matrix such as cellulose acetate. In 2012, Ji and his coauthor prepared a CA/zeolite composite membrane, which exhibits excellent adsorption behavior for the removal of Cu(II) (98.5%) and Ni(II) (82.8%) from the aqueous solution than pure CA; after treatment, the membrane can be regenerated and reused without a significant loss of the adsorption performance.[132] The SEM image of CA/zeolite, indicating a larger surface area (16.88 m^2 g^{-1}) along with a smaller pore size (24.6 nm) was formed, which may play an important role in higher adsorption process.

Another important membrane material, polysulfone, has repeating phenylene rings, which contribute to a high degree

Table 3 Application of cellulose acetate-based membranes for the removal of heavy metals

Contaminant name	Name of membrane	Membrane type	Operating condition	Results	Ref.
Cu^{2+} Ni^{2+} Zn^{2+}	CA/PMMA	Ultrafiltration	Initial conc.: 0.1 wt%; pH: 7.2; capacity: 350 mL; rotation speed: 200 rpm; temp.: 22 ± 2 °C pressure: 345 KPa	• Percent removal of Cu(II) ion was found to be higher compared to other metal ions with comparatively lower flux.	136
Cu^{2+} Ni^{2+} Zn^{2+} Cd^{2+}	CA/PSf	Ultrafiltration	Initial conc.: 0.1 wt%; pH: 6.25; temp.: 25 °C pressure: 345 KPa	• Removal of metals were decreased linearly with the addition of PVP and PSf in the following trends $Cu^{2+} > Ni^{2+} > Zn^{2+} > Cd^{2+}$	133
Cu^{2+}	CA/LCD PSf	Ultrafiltration	pH: 6 ± 0.25; pressure: 345 KPa; rotation speed: 200 rpm	• Improved metal ion removal and permeate flux with an increase in the applied pressure (69 to 345 KPa) for each membrane composition was observed.	137
Cu^{2+} Ni^{2+} Zn^{2+} Cd^{2+}	CA/APSf	Ultrafiltration	Initial conc.: 0.1 wt%; pH: 6.5; temp.: 25 °C; pressure: 345 KPa; area: 38.5 cm^2	• Metal removal rate follow the trend $Cu^{2+} > Ni^{2+} > Zn^{2+} > Cd^{2+}$, which was gradually decreased with the addition of PEG and APSf.	138
Cu^{2+} Co^{2+}	CA/MOF-5	Nanofiltration	Initial conc.: 1000 ppm; temp.: 25 °C; pressure: 10 bar; area: 14.6 cm^2	• Porosity and flux were significantly increased with the addition of MOF-5 in the CA membrane. • Enhanced fouling resistant ability, thereby improved recycling of the blend membrane. • Removal of Cu(II) in neat CA and CA/MOF-5 is found to be 50.8% and 53.3%, while 45.3% and 77.0% of Co(II) were removed by neat CA and CA/MOF-5, respectively.	114
Chloride and sulphate salts	CA/Ag	Nanofiltration	—	• 83–93% and 84–97% salt removal rate was attained on treatment with CA/Ag and CA/Ag ion-exchange zeolite-based membrane. • Removal rate of sulfate salts than chloride salts was obtained.	86
	CA/Ag ion-exchange zeolites	Nanofiltration		• Higher permeability fluxes and bactericidal effect erase biofouling in the nanofiltration membrane during water treatment.	
Pb^{2+} Ni^{2+} Zn^{2+} Cd^{2+}	CA/PSf	Ultrafiltration	Initial conc.: 50 mg L^{-1}; pH: 5.00; filtration area: 13.8 cm^2; pressure: 1–3 bar; volume: 50 mL; temp.: 25 ± 2 °C	• Higher molecular weight metals ions were more separated than lower ones and follows the order $Pb^{2+} > Cd^{2+} > Zn^{2+} > Ni^{2+}$ • CA/PSf (80/20) blend membrane exhibits excellent performance among the prepared membranes due to the high heavy metals removal and permeate flux.	139
Cr^{6+}	CA/Ti-TEPA CA/Ti-HMTA CA/Ti-EDA	Ultrafiltration	Initial conc.: 10 mg L^{-1}; pH: 3.5 and 7.0.	• Modification of TiO_2 with TEPA significantly increases the Cr^{6+} removal efficiency from 47.2 to 99.8%.	101
Cu^{2+} Ni^{2+}	CA/Zeolite	—	Initial conc.: 25 mg L^{-1}; pH: 4.5; dose: 4 g L^{-1}; adsorption time: 48 h; temp.: 25 °C	• Adsorption capacity of 98.5 and 82.8% for Cu^{2+} and Ni^{2+} were attained by the treatment with CA/zeolite membrane while only 10% (for both metals) removal efficiency has been achieved by neat CA membrane. • CA/zeolite possess higher regeneration rate with approximately similar adsorption capacity after regeneration.	132
Cu^{2+} Co^{2+}	CA/MOF-5	Nanofiltration	—	• Incorporation of MOF-5 into the polymeric membrane surface improves the hydraulic properties, increases the membrane porosity, pore size, pure water flux, and inhibits microbial growth. • Higher heavy metals removal rate of 77% and 53.3% of Co^{2+} and Cu^{2+} were attained, which was higher than neat CA membrane (removal of 45 and 50.8% for Co^{2+} and Cu^{2+}, respectively).	114
Cu^{2+} Pb^{2+}	Electrospun CA/TiO_2	—	Initial conc.: 50 mg L^{-1}; pH: 6; dose: 100 mg; volume: 50 mL; adsorption time: 300 min; temp.: 35 °C; rotation speed: 150 rpm.	• Surface area was significantly increased from 30.2 to 48.47 m^2 g^{-1} with the addition of TiO_2 in CA. • Under optimum operating condition, 99.7 and 98.9% Pb^{2+} and Cu^{2+} were removed, respectively.	140

Table 3 (*continued*)

Contaminant name	Name of membrane	Membrane type	Operating condition	Results	Ref.
Cr^{6+}	Electrospun NH_2-functionalized CA/silica	Nano filtration	Initial conc.: 100 mg L^{-1}; pH: 1; dose: 50 mg; volume: 100 mL; adsorption time: 60 min; temp.: 30 °C	• Maximum adsorption capacity on the FCA/SiO_2 membrane was 19.46 mg g^{-1}, while CA and CA/SiO_2 possesses only 1.28 and 3.03 mg g^{-1}, respectively. • Membrane can be regenerated by alkalization, and the regenerated membrane possesses similar adsorption capacity.	107
Cu^{2+} Hg^{2+} Cd^{2+}	PMMA-modified Electrospun CA	Nanofiltration	Initial conc.: 50 mg L^{-1}; pH: 5.7; dose: 100 mg; volume: 50 mL; adsorption time: 8 h; temp.: 25 °C	• Membrane has quite high adsorption capacity of ∼5.2, 2.8, and 2.1 mg g^{-1} for Hg^{2+}, Cu^{2+}, and Cd^{2+}, respectively. • Membrane can be regenerated using saturated ethylenedinitrilo tetraacetic acid solution.	108
Cu^{2+}	CS/CA	Nanofiltration	Initial conc.: 150 mg L^{-1}; pH: 5; dose: 1.1 gm; volume: 50 mL; adsorption time: 120 min; rotation speed: 150 rpm; temp.: 25 °C	• Spongy-like and highly porous structures, with specific surface areas in the range of 15.2 m^2 g^{-1}, porosities of 79.7%, pore sizes of 0.22 μm. • Maximum adsorption capacity of Cu^{2+} under optimum operating condition was found to be 48.2 mg g^{-1}. • 99% desorption efficiency was achieved with EDTA solution but only 90% with the HCl solution.	141
Salt (NaCl)	CA modified with *N*,*N*-dimethyloctylamine	Reverse osmosis	Salt conc.: 2000 ppm; effective area: 28.26 cm^2; pressure: 225 psi; pH: 7; temp.: 25 °C	• Higher hydrophobic but more electronegative surface as well as improved thermal and mechanical property. • Higher antibacterial efficiency (for both Gram-positive and Gram-negative bacteria) more than 99.9% along with higher salt removal rate of 96.76%.	106
Salt (NaCl)	CA/Chitosan	Reverse osmosis	Salt conc.: 35 000 ppm; effective area: 14.6 cm^2; pressure: 30–60 bar; temp.: 25 °C	• Addition of 2% chitosan increase the salt removal rate from 89 to 94%. • Presence of chitosan enhances the fouling resistance of the membrane.	105
Se^{4+}	CA	Nanofiltration	Initial conc.: 25 mg L^{-1}; pH: 4 and 8; dose: 250 mg; contact time: 4 h	• Removal efficiency of Se(IV) was improved from 79.5, 84.8, 85.9, and 89.3% at pH 4 reaching 85.8, 91.2, 92.1, and 96% for CA, GO-CA, MNPs-CA, HAP-CA, and GO/MNPs/HAP-CA, respectively.	142
Cr^{6+}	GO-CA MNPs-CA HAP-CA GO/MNPs/HAP-CA			• Cr(VI) removal progressed from 86.7, 86.3, 89.9, 90.6, and 92.9% at pH 4 and 89.8, 90.5, 94.1, 94.7, and 97.3% at pH 8 for CA, GO-CA, MNPs-CA, HAP-CA, and GO/MNPs/HAP-CA, respectively.	

Note-CA: cellulose acetate; PMMA: poly(methyl methacrylate); PSf: polysulfone; LCD PSf: low cyclic dimer polysulfone; APSf: aminated polysulfone; TEPA: tetraethylenepentamine; EDA: ethylenediamine; HMTA: hexamethylenetetramine; GO: graphene oxide; MNPs: magnetic nanoparticles; HAP: hydroxyapatite; CS: chitosan.

of molecular immobility, producing high rigidity, strength, creep resistance, pH resistance, as well as mechanical and dimensional stability, compared to the CA-based membrane.[133,134] Thus, blending polysulfone with an inexpensive polymer such as CA can not only reduce the material cost but also develop a new material possessing the combined properties of polysulfone (PSf) and CA polymers.[135] Sivakumar and his coauthor showed that the pure water flux, water content, molecular weight cut-off, and hydraulic resistance of CA membrane were improved with the addition of PSf up to 25 wt%.[135] Moreover, the removal rate of some selected heavy metals (Cu^{2+}, Ni^{2+}, Zn^{2+}, and Cd^{2+}) (shown in the Fig. 4a) were significantly increased with increasing PSf concentration, which was attributed to the formation of macrovoids and cavities in the membrane surface. In another study, the same authors showed the influence of polyvinylpyrrolidone (PVP) concentrations as an additive.[133] The study reported that pure water fluxes and water content were significantly improved to 115 m^{-2} h^{-1} and 85%, respectively, by the addition of 25% PSf and 7.5% PVP in the CA membrane.

3.2. Separation of textile dyes

CA esters of cellulose can be used for a variety of applications such as films, membranes, composites, or fibers. Most importantly, the CA films or membranes are hydrophobic, biodegradable, have higher mechanical properties, easy processability, and can be modified easily, which make them suitable membranes in the water reclamation process. Sanchuan *et al.* (2010) fabricated a CA nanofiltration membrane and determined the impact of membrane properties on the dye removal rate.[143] Membrane surface charge was found to be one of the most influential properties for dye removal efficiency, which also depends on the solution pH and dye concentration. Moreover, the dye removal rate also varied with changing operating pressure and crossflow velocity. In another study, Yang *et al.* reported a CA ultrafiltration membrane to investigate the surface roughness, permeability, and antifouling properties.[144] The prepared membrane exhibited higher surface roughness, lower water permeability of 98.99 L m^{-2} h^{-1}, lower removal rate of 93.36%, and poorer irreversible antifouling ability with flux recovery ratio of 49.78%. The surface roughness, lower hydrophilicity, and low porosity of the sublayer structure were responsible for the lower antifouling properties of the membrane. Moreover, the organic pollutants were adsorbed in the valleys of the membrane by several strong interactions including hydrophobic interactions, disulfide bond, and electrostatic forces.[144,145] In another study, a novel bacteria-immobilized electrospun CA/PEO nanofibrous membrane was fabricated for the removal of methylene blue (MB) from industrial wastewater.[146] Two completely different methods have been found to be effective for the removal of MB—(a) biodegradation on the surface of immobilized bacteria and (b) adsorption on CA/PEO nanofibers.

Pristine CA membranes are less resistant to microbial corrosion, oxidation, and other organic pollutants, which make them applicable for a long time and also lead to a reduction in the membrane performance over time.[147,148] These limitations can also be improved by chemical modification, blending with fillers, or other polymeric materials.

The main problem of the membrane-based water treatment process is membrane fouling, which blocks the pores on the membrane surface due to the interaction among the foulant (mostly organic molecules) and surface molecules. The addition of photocatalysts, inorganic additives having antibacterial activity, and frequently backwash after the treatment process are the best way for reducing the foulant for a long time. In 2016, Rajeswari and his coauthor developed a nano ZnO-blended cellulose acetate-polyurethane (PU) membrane for the photocatalytic degradation of reactive red (RR 11) and reactive orange (RO 84) using UV light with different parameters.[29] The addition of ZnO as a photocatalyst in the composite membrane displayed increased flexibility, hardness, tensile strength, as well as thermal and chemical stability with outstanding dye degradation capacity (97 and 92% degradation of RR 11 and RO 84, respectively).

The addition of inorganic additives having antibacterial activity such as noble metal and metal oxides including Ag, SiO_2, ZrO_2, Co, and TiO_2 in the surface of membrane support is one of the best options to reduce biofouling along with an increase in the performance.[149–151] Moreover, these inorganic NPs are chemically stable, catalytically active, and also possess antimicrobial properties. For this reason, researchers have been trying to incorporate silver (Ag, Co) nanoparticles into polymeric membranes to reduce bacterial multiplication. However, the drawback of using nanoparticles on the membrane surface leads unintentional metallic leaching. Another challenge in using nanoparticles in practical applications is their photocatalytic activity, which leads to the degradation of the polymeric matrix, resulting in membrane degradation (reducing membrane stability). This problems can be suppressed by the addition of polymeric support to the casting solution such as polyvinylpyrrolidone[86] and graphene oxide.[152] One study showed that CA membranes embedded with graphene oxide-silver nanocomposites exhibit strong bacterial inactivation capacity at a rate of 90% compared to pristine CA membranes.[152] Moreover, the CA membrane containing graphene oxide-silver nanocomposites possess larger surface pores and increased pure water flux compared to pristine membranes, which strongly suggest that the applicability of incorporation of graphene oxide-silver nanocomposites on CA is a promising strategy to produce membranes. On the other side, nanofibrous membranes offer higher permeability due to higher specific surface area, higher fiber aspect ratio, and porosity.[153] In 2016, Wang *et al.* synthesized electrospun CA membrane incorporated with silver nanoparticles for the treatment of dye waste.[149] This electrospun Ag-loaded membrane offers remarkable antimicrobial properties than neat membrane with approximately similar dye removal capacity. Moreover, blending with another polymer as a filler along with the addition of inorganic nanoparticles might suppress almost all limitations arising during membrane filtration, as shown in Fig. 4b. For example, Rajeswari *et al.* prepared CA-based biopolymeric mixed matrix ultrafiltration membranes with various nanoparticles,

which possess higher pure water permeability rate, fouling mitigation effect, porosity, smoother surface, and better removal percentage compared to the bare membrane.[154] In another study, incorporated cobalt nanoparticles (as catalyst) on the PLA/PU/CA nanoporous membrane showed excellent MB and CR removal from wastewater by adsorption and photocatalytic degradation method.[155] Upto 60% of each dye has been removed under UV irradiation with well-described Langmuir isotherms, while the thermodynamic study showed that the adsorption process is mostly dissociative and involves photocatalytic dye degradation. Furthermore, CA-PSf/Al_2O_3 and CA-PSf/nZVI exhibits 91 and 94% dye (MB) removal rate, respectively, while neat CA showed 82% removal capacity. The modification of electrospun CA (electrospinning, followed by deacetylation and carboxymethylation) and then coating with polydopamine (PDA) exhibited improved adsorption capacity against both acidic and basic dye.[156] The enhanced adsorption performance of CA/DCA-COOH might be due to the introduction of –OH, $–NH_2$, and –COOH, which can adsorb both MB (90.77%) and CR (95.03%) comparatively higher than pristine CA (MB: ~42%, CR: ~4%) and DCA-COOH (MB: ~60%, CR: ~80%). Cheng *et al.* fabricated a deacetylated cellulose acetate (DCA)-polydopamine (PDA) nanofiber membrane by electrospinning and surface modification, which demonstrated better removal capacity (88.2 mg g^{-1}) of methylene blue than the unmodified CA (4.9 mg g^{-1}) and DCA (10.2 mg g^{-1}) membrane.[157]

Liu *et al.* fabricated stable hydrophobic metal–organic frameworks (MOFs)-HKUST-1-RGO-PDA nanocomposite membranes incorporating polydopamine (PDA) over a cellulose acetate membrane support layer for the removal of methylene blue and Congo red.[110] Cellulose acetate-supported PDA/RGO/HKUST-1 membrane exhibited outstanding hydrophilic, water flux, removal rate, and antifouling performance. Moreover, at optimum operating condition, 99.8% methylene blue and 89.2% Congo red were removed, while a conventional cellulose acetate membrane exhibited lower removal rate of both the dyes (41% MB and 5% CR removed). Table 4 lists several CA and CA-based membrane treatment processes that have been used to separate/remove dyes from wastewater from different industrial wastewater.

3.3. Separation of polycyclic aromatic hydrocarbons (PAHs)

Polycyclic aromatic hydrocarbons (PAHs) are a major class of environmental organic micropollutants with fused aromatic groups, which are generally produced during the incomplete combustion of fossil fuels.[162] Most PAHs compounds are lipophilic in nature and due to lower solubility in water (~μg L^{-1}), they are present in the contaminated industrial soil site at higher concentrations.[163,164] Approximately 126 compounds have been selected as PAH compounds. Among these, 16 PAH molecules have been selected as the highest priority and highly toxic pollutants by the US Environmental Protection Agency (EPA).[165] Some of the most common PAH compounds are naphthalene, acenaphthylene, acenaphthene, fluorene, phenanthrene, anthracene, fluoranthene, pyrene, benz(*a*)anthracene, chrysene, benzo(*b*)fluoranthene, benz(*a*)pyrene, benzo(*ghi*)-perylene, dibenz(*a*,*h*)anthracene, and indeno(1,2,3-*cd*)pyrene.[166] However, even at a lower concentration of these PAHs (~200 ng L^{-1}) with continuous exposure for long time could cause a detrimental effect to human health, including various cancers such as lung, stomach, skin, chest, kidney, pancreas, esophagus, bladder, prostate, and larynx.[167–169] Therefore, the development of appropriate treatment processes for the removal of these pollutants from the environment are of serious concern.

Over the last few decades, extensive studies have been conducted including chemical oxidation, photodegradation, adsorption, biological treatment process, and membrane separation process for the removal of PAHs from wastewater.[170,171] However, most of these methods have some disadvantages such as high investment and maintenance costs, lower removal efficiency, and complicated operation conditions. Moreover, most PAHs are lipophilic in nature and resistant to biological and chemical degradation processes; more importantly, slight degradation products possess carcinogenic and mutagenic effect than the parent compounds.[172] However, physical treatment processes such as membrane filtration and adsorption process appear to be the best and important sustainable solutions to remove PAHs from contaminated water.[169] Moreover, the presence of lower concentration in water (due to lower solubility) is absent or less possible to the membrane fouling problem.[83,173,174] Nowadays, reverse osmosis (RO), forward osmosis (FO), nanofiltration (NF), and ultrafiltration (UF) are the most commonly used membrane filtration methods for the separation of PAHs.

The cellulose acetate (CA) membrane can be a potential membrane material for the separation of PAHs from wastewater, whereas limited application is available in the literature. This may be due to poor tolerance against temperature, organic solvent, and lower mechanical stability.[83] Several attempts have been made to enhance the filtration efficiency (membrane hydrophilicity, water permeability, fouling resistance, thermal and mechanical resistance, *etc.*) of the CA membrane by blending with other polymers, polymer functionalization, addition of nanofiller, and epoxy resins, as shown in Fig. 4d.[83,174] In 2014, Celebioglu *et al.* synthesized beta-cyclodextrin (β-CD)-functionalized electrospun CA nanofibers by combining electrospinning and click reaction.[175] During this process, the electrospinning of CA provides a uniform nanofibrous membrane with nanoscale porous structure (enhances the surface area to volume ratio and higher density of pores), while the surface modification of CA with crosslinking CD by the click reaction significantly enhances the surface functionalization with higher yields. The filtration capacity of the β-CD–CA nanofiber was investigated by the removal of phenanthrene from its aqueous solution and compared with the pristine CA nanofiber. It was observed that the β-CD–CA membrane removed 95% phenanthrene, while only 83% was found for the pristine CA membrane (Fig. 4d). The higher removal efficiency of the grafted membrane was due to complexation between β-CD and the PAHs molecule; similar results have also been reported in previous studies.[176,177] In another study, the same authors reported the surface modification of polyester

Table 4 Application of cellulose acetate-based membranes for the removal of textile dyes

Contaminant name	Name of membrane	Membrane type	Operating condition	Results	Ref.
Methylene blue Congo red	MOFs-HKUST-1-RGO on CA (MF)	Microfiltration	Initial conc.: 40 mg L^{-1}; pH: 3–11	• 99.8% MB and 89.2% CR were removed. • Outstanding flux, removal rate, hydrophilicity (contact angle 54.5°), and antifouling properties.	110
Reactive red (RR 11) Reactive orange (RO 84)	CA-PU CA-PU/ZnO	—	Initial conc.: 100 mg L^{-1}; pH: 7.00; time: 40 min; volume: 50 mL	• Exhibit higher photocatalytic ability along with good thermal stability and mechanical property. • Improved surface properties (surface roughness, profile valley depth) with the addition of ZnO. • CA-PU/ZnO can degrade 92 and 97% of RO 84 and RR 11, respectively.	29
Reactive black 5	CA	Nanofiltration	Initial conc.: 1000 mg L^{-1}; pH: 6.8; cross flow velocity: 1.1 m s^{-1}; operating pressure: 2.5 MPa	• 99.6% reactive black 5 was removed due to electrostatic repulsive between the dye and membrane surface.	143
Methylene blue	Immobilized bacteria on CA/PEO	Nanofiltration	Initial conc.: 20–200 mg L^{-1}; pH: 7.0; contact time: 48 h; effective area: 4 cm^2	• 93% MB decolorization under optimum operating condition.	146
Methylene blue Congo red	PDA/DCA-COOH	Nanofiltration	Initial conc.: 50–250 mg L^{-1}; volume: 10 mL; dose: 30 mg; rotation speed: 200 rpm; temp.: 25 °C; contact time: 90 min	• Both anionic and cationic dyes were effectively on the nanofiber membrane due to electrostatic attraction and hydrogen bonding. • Excellent membrane stability and recyclability. • 69.89 and 67.31 mg g^{-1} of MB and CR adsorption capacity was achieved by the nanofiber, respectively, which were comparatively higher than the singly used CA membrane.	156
Methylene blue	DA/PDA	Nanofiltration	pH: 6.5; temp.: 25 °C; contact time: 30 h	• DA/PDA nanofiber membrane exhibited 88.2 mg g^{-1} adsorption capacity of MB that was 8.6 times higher than the DA membrane.	157
Methylene blue Congo red	PLA/PU/CA/Co nanoparticle	Nanofiltration	Initial conc.: 25 mg L^{-1}; volume: 50 mL; dose: 0.001 g ml^{-1}; pH: 3, 4 for CR and MB; temp.: 60 °C	• Removal of dyes was anticipated by physisorption into the adsorbent surface, followed by dissociative adsorption *via* a photocatalytic degradation method, then further surface adsorption/diffusion (in case of CR) or favored desorption (in case of MB) along with some adsorption of the catalytic products.	155
Reactive orange 16 Reactive black 5	PPSU/CAP	Ultrafiltration	Initial conc.: 100 mg L^{-1}; pH: 6.8; pressure: 0.1 MPa	• 95.49 and 83.45% of reactive black 5 and reactive orange 16 were removed by the PPSU/CAP membrane, respectively.	158
Methylene blue	p-MWCNTs/CA	Ultrafiltration	Initial conc.: 1–5 mg L^{-1}; pH: 6.5; contact time: 1–4 h; pressure: 200 KPa; rotation speed: 300 rpm; temp.: 25 °C; effective area: 13.4 cm^2	• Addition of CNTs augmented the antifouling properties of membrane. • In FTIR analysis, a clear peak at 1436 cm^{-1} was observed, which is due to the vibration of the C-N bond for MB (adsorption of MB on the membrane surface not retained).	159
Methyl blue Congo red Rhodamine B	Carboxymethylated hydrolyzed CA	Nanofiltration	Initial conc.: 100 mg L^{-1}; pH: 6.8; contact time: 150 min; pressure: 5 bar; temp.: 25 °C; effective area: 32.2 cm^2	• Modified CA hollow membrane exhibit improved anionic dye removal rate (CR: 99.75% and MB: 99.9%) is due to the enhanced charge exclusion, resulting in increased negative charge in membrane surface, while improved (increased two times) water permeability and declined removal rate of the cationic dye Rhodamine B due to the increased pore size.	160
Methylene blue	CA GO-CA MNPs-CA HAP-CA GO/MNPs/HAP-CA	Nanofiltration	Initial conc.: 25 mg L^{-1}; pH: 4 and 8; dose: 250 mg; contact time: 35 min; Visible light radiation	• Surface roughness parameters were increased with addition of GO, MNPs, and HAP. • Addition of HAP induced high cohesiveness of the nanofibers and thus higher elasticity while, incorporation with inorganics (GO and MNPs) inhibited slipping motion, resulting in the development of resistance against creak propagation. • 92.9, 93.3, 93.8, 89.6, and 95.1% of MB was removed by CA, GO-CA, MNPs-CA, HAP-CA, and GO/MNPs/HAP-CA, respectively, after 35 min of continuous exposure to visible light.	142

Table 4 (*continued*)

Contaminant name	Name of membrane	Membrane type	Operating condition	Results	Ref.
Indigo carmine Methylene blue	Activated CA–GO/ TiO_2– NH_2	Nanofiltration	Initial conc.: 10 mg L^{-1}; pH: 2; contact time: 250 min; UV irradiation: 40 W.	• Both dyes were initially adsorbed on the membrane surface due to electrostatic interaction, followed by photodegradation.	161

Note-CA: cellulose acetate; MOFs: metal–organic frameworks; RGO: reduced graphene oxide; PU: polyurethane; PEO: polyethylene oxide; PDA: polydopamine; DCA: deacetylated cellulose acetate; PLA: polylactic acid; PPSU: polyphenylsulfone; CAP: cellulose acetate phthalate; p-MWCNTs: pristine multiwalled carbon nanotubes; GO: graphene oxide; MNPs: magnetic nanoparticles; HAP: hydroxyapatite; CNT: carbon nanotube.

with CD (α, β, γ) polymer in the presence of citric acid as a crosslinker.[178] The surface-modified membrane also exhibited better filtration performance over the pristine polyester nanofiber membrane.

The modification or crosslinking of CA with other polymers (such as benzoxazine) is another alternative way to improve the membrane performances summarized in Table 5.[83] Ertas and his coauthors crosslinked electrospun CA nanofiber with benzoxazine (BA-a) in the presence of citric acid (CTR) (to obtain uniform membrane surface) by following the simple thermal curing process.[83] Themodified CA/PolyBA-a/CTR membrane exhibits a slight improvement in the thermal property along with a significant enhancement in the mechanical properties (260%, 150%, and 130% increased tensile strength, ultimate stress, and Young's modulus, respectively, compared to pristine CA membrane). Furthermore, the modified membrane showed excellent phenanthrene removal efficiency of 78% and 98.5% within 10 and 150 min, respectively.

The molecular imprinting technique (MIT) is considered one of the most successful and effective techniques for functionalized polymer synthesis. More importantly, the membrane prepared in MIT can separate/remove the targeted pollutants from a mixed solution.[179,180] Shafy *et al.* reported a molecularly-imprinted membrane (An-MIM) by hybridizing anthracene molecularly-imprinted nanoparticles polymer (An-MINP) with cellulose acetate (CA) for the separation of targeted PAHs (anthracene, naphthalene, pyrene, benzo(a)pyrene, phenanthrene, and acenaphthylene).[174] The removal rate of the An-MIM toward anthracene, naphthalene, pyrene, benzo(a)pyrene, phenanthrene, and acenaphthylene was 96%, 80%, 54%, 40%, 25%, and 69%, respectively, while $<5\%$ of individual PAHs were rejected by cellulose acetate and nonimprinted membranes. The higher removal rate of PAHs by An-MIM was due to the higher binding capacities toward selected PAHs.

3.4. Separation of pharmaceuticals

Pharmaceutical products and intermediates have been used worldwide; today, more than 4000 pharmaceutical compounds are available.[181] These compounds can contaminate the environment coming from many sources including manufacturing processes, livestock, disposal of expired and unused products, and effluents from hospitals and sewer systems in households.[182] Its continuous input into the environment even in lower concentration (<1 μg L^{-1}) may constitute in the long term a potential risk for aquatic and terrestrial organisms.[183–185] For this reason, the search for novel materials serving in the removal or reduction of pharmaceutical contaminants from pharmaceutically-rich sewage system is a major concern.

CA and modified CA-based microfiltration, ultrafiltration, nanofiltration, forward osmosis, and reverse osmosis membrane has been used for the removal of pharmaceutical and personal care products for a long time.[181,186–188] Most of the membrane-based treatment processes follow three different methods for the removal of pharmaceuticals: (a) adsorption, (b) repulsive mechanism, and (c) sieving, as shown in Fig. 3. The removal of contaminants by adsorption occurs when the

Table 5 Application of cellulose acetate-based membranes for the removal of polyaromatic hydrocarbons (PAHs)

Contaminant name	Name of membrane	Membrane type	Operating condition	Results	Ref.
Phenanthrene	CA CA-propargyl β-CD-modified CA	Nanofiltration	—	• β-CD-modified CA nanofibrous membrane removes 95% phenanthrene from the solution after 8 h, while pristine CA can do only 85%.	175
Anthracene Naphthalene Pyrene Benzo(*a*)pyrene Phenanthrene Acenaphthylene	CA An–MINP An–MIM (An–MINP + CA	—	Conc.: 100 μg L^{-1}; volume: 500 mL; pressure: 35 bar; flow rate: 1.8 L min^{-1}; effective area: 25 cm^2; temp.: 25 °C	• Hybridized anthracene molecularly-imprinted nanoparticles polymer (An-MINP) embedded in the CA membrane exhibited the selective removal of anthracene from the aqueous solution.	174
Phenanthrene	Pristine CA CA/PolyBA-a/CTR	Nanofiltration	Conc.: 1 mg L^{-1}; volume: 30 mL; flow rate: 1.8 L min^{-1}; effective area: 36 cm^2; temp.: 25 °C	• Thermal, mechanical, and adsorption performance were significantly improved due to the incorporation of polybenzoxazine (PolyBA) and citric acid (CTR) in the CA membrane.	83
Acenaphthene Fluorene Fluoranthene Phenanthrene Pyrene	Poly-CD	Nanofiltration	Conc.: 400 μg L^{-1}; volume: 50 mL; time: 60 min; effective area: 14.6 cm^2; temp.: room temp; pressure: 10^4 Pa	• Excellent recyclability with almost similar performance of the membrane. • Outstanding permeability (237 L m^{-2} h^{-1} KPa^{-1}), water flux (3090 L m^{-2} h^{-1}), PAHs removal efficiency (92.6% within 40 s).	166

Note-An-MINP: anthracene molecularly-imprinted nanoparticles polymer; CA: cellulose acetate; An-MIM: hybridizing anthracene molecularly-imprinted nanoparticles polymer (An-MINP) with cellulose acetate (CA); polyBA: polybenzoxazine; CTR: citric acid; poly-CD: polycyclodextrin.

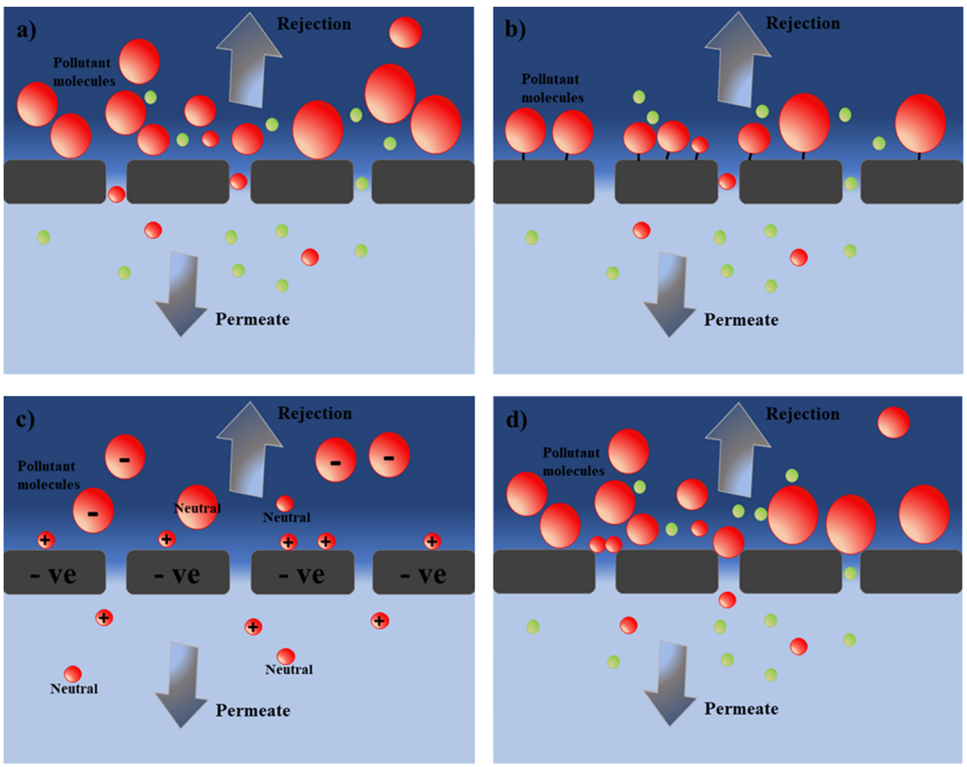

Fig. 3 Schematic illustration of the proposed mechanism for the CA-based membrane during the desalination process. Modified with permission from ref. 193. Copyright (2020) Elsevier. (a) Size exclusion by which pollutants of larger size than the membrane pore is rejected; (b) hydrophobic interaction by which the hydrophobic organic pollutant molecules are adsorbed on the membrane surface; (c) electrostatic repulsion, negatively-charged pollutants are rejected by the negatively-charged CA-based membrane; and (d) membrane fouling layer formation due to the adsorption, deposition, and redeposition of the pollutant on the membrane surface.

contaminants contain opposite charge of the adsorbent site. In case of CA-based membrane, negative functional groups such as hydroxyl and carboxylic groups are predominant, which can adsorb positively-charged pharmaceuticals.[189,190] Removal by the charge repulsion mechanism arises when the charge of the membrane surface and the ions of the electrolyte in pharmaceutical and personal care products (PPCPs) are similar and prevent the ion from contacting the membrane.[187] In the sieving mechanism, pollutants are separated by molecular size if molecules are larger than the membrane pores that cannot pass through the membrane.[191,192] The incorporation of a photocatalyst (metal, metal oxide nanoparticles, and metal organic frameworks) on the surface of CA also follows the photodegradation mechanism.[29,181] Emam and his coauthor established a highly porous photoactive cellulose acetate-Ti-MIL-MOF film, which exhibited both adsorption and photodegradation capacity of paracetamol in the presence of visible light.[181] The adsorption and photodegradation capacity of pure Ti-MIL-MOF were 72.6 and 270.5 mg g^{-1}, respectively, indicating that the removal rate follows the degradation mechanism. However, the incorporation of Ti-MIL-MOF in the porous CA membrane significantly enhanced the removal capacity from 82.7 mg g^{-1} to 519.1 mg g^{-1} as it follows both the adsorption (presence of CA) and degradation mechanism (presence of Ti-MIL-MOF).

Etemadi *et al.* studied the effect of aeration rate (specific aeration demand per membrane area (SADm) of 0.5, 1, 1.5, and 2 m^3 m^{-2} h^{-1}) on the antifouling properties of the cellulose acetate nanocomposite membranes (CA/ND-NH_2) in a membrane bioreactor system for the treatment of pharmaceutical wastewater.[194] Operating at a high aeration rate condition leads to membrane blockage by sludge flocs and extracellular polymer substrates (EPS), thereby significantly affecting irreversible fouling generation and reduced long time membrane application. On the other hand, a lower aeration rate leads to the lowering of the pollutant removal efficiency. For this reason, an optimum aeration rate should be maintained.

The major drawback of pure CA membranes is that pharmaceuticals and EDCs are not effectively removed because of the presence of smaller pores compared to commercially-used membranes.[188] Membrane performance can be improved by surface modification and/or blending with another polymer.[188,191] Fig. 4c summarizes several CA and modified CA-based membranes that exhibit that only <60% pharmaceuticals can be separated by neat CA membrane, while after modification, the CA membrane exhibited better results.[181,188,191,192,195–198] Rana *et al.* (2012) synthesized a novel CA membrane containing surface modifying macromolecules to remove pharmaceuticals from wastewater.[191] The modification was done in two different tailor-made polymeric additives, (a) charged surface modifying macromolecule (CSMM) additive synthesized by reactive diisocyanate and dihydroxy naphthalene disulfonate and (b) incorporating poly(ethylene glycol) as the end groups (LSMM). The removal of pharmaceuticals by CA/CSMM CA/LSMM followed the order Smz > Carb > Ib as the molecular weight and radii increased in same direction, but the removal rate was found to be slightly lower than that of the neat CA membrane. Narbaitz *et al.* also found similar results.[188]

Although neat CA and modified CA membranes are common polymers employed for the fabrication of porous polymeric membranes, they possess several disadvantages such as lower mechanical and thermal stability and lower susceptibility to chemical and microbial attack.[195] To solve these issues, researchers have been trying to introduce new CA membranes blended with other miscible polymers (polyvinylchloride, polysulfone, polyurethane, and polyethylene oxide)[103,199,200] or the addition of nanofillers such as hydroxyapatite, layered clays, andlayered double hydroxides (LDHs)[201,202] shown in Table 6. Laura *et al.* fabricated a cellulose acetate-based membrane modified with block co-polymer poly(4-vinylpyridine-*b*-ethylene oxide) (P4VP-*b*-PEO) for the adsorption of several electron-deficient EDPs.[189] This study showed that the adsorption behavior of the membrane is directly relevant to the electron deficiency and spatial orientation of the contaminants. Moreover, the incorporation of 1% P4VP-*b*-PEO into the CA membrane significantly enhances the adsorption efficacy by at least 2-fold. In addition, the adsorbed EDPs may possibly be eluted from the membrane surface by treatment with an organic solvent such as ethanol.[203] The addition of an inorganic nanofiller such as SiO_2 also improves the hydrophobic and mechanical properties of the CA membrane. Mahdavi *et al.* reported the CA/SiO_2 nanofiltration membrane, which exhibited impressive ceftriaxone sodium removal rate (90%) than the neat CA membrane.[196] Silica was functionalized with (3-aminopropyl)triethoxysilane to fabricate the CA/SiO_2-poly (2-acrylamido-2-methylpropane sulfonic acid) membrane, which exhibited 96% removal rate with comparatively improved mechanical properties. The incorporation of layered double hydroxides (LDHs) as the nanofiller in the CA membrane is another approach to achieve the desired mechanical properties along with enhanced membrane performance. For instance, CA/Mg-Al LDH membrane was fabricated *via* the phase-inversion method to increase their permeability and adsorption capacity for two pharmaceutical contaminants diclofenac sodium (DS) and tetracycline (TC).[195] The investigation showed that the addition of nanofiller (Mg-Al LDH) leads to a considerable increase in the porosity, hydrophilicity, water permeability, and mechanical properties. Moreover, a significant improvement of the removal rate of DS from 2.7 to 17% with the addition of 4% filler was achieved, while an approximately similar result was obtained in the case of TC removal. In another study, Das *et al.* investigated the efficiency of electrospun montmorillonite-impregnated cellulose acetate nanofiber membranes (MMT-CA-NFM) for the removal of ciprofloxacin (CIP).[197] At optimum conditions of contact time, pH, dose, and CIP concentration of 60 min, 6.0, 4 g L^{-1}, and 10 mg L^{-1}, the reaction equilibrium was reached with 76% removal rate.

The CA-based membrane was synthesized through the phase-inversion method using mixed metal oxides nanoparticles-polymer composite (Fe-Al-Mn-chitosan) as the nanofiller.[204] At optimum process parameter of pH 6–9 and transmembrane pressure 6–8, the 8% filler-loaded membrane exhibits significantly higher fluoride-contaminated water treatment capacity

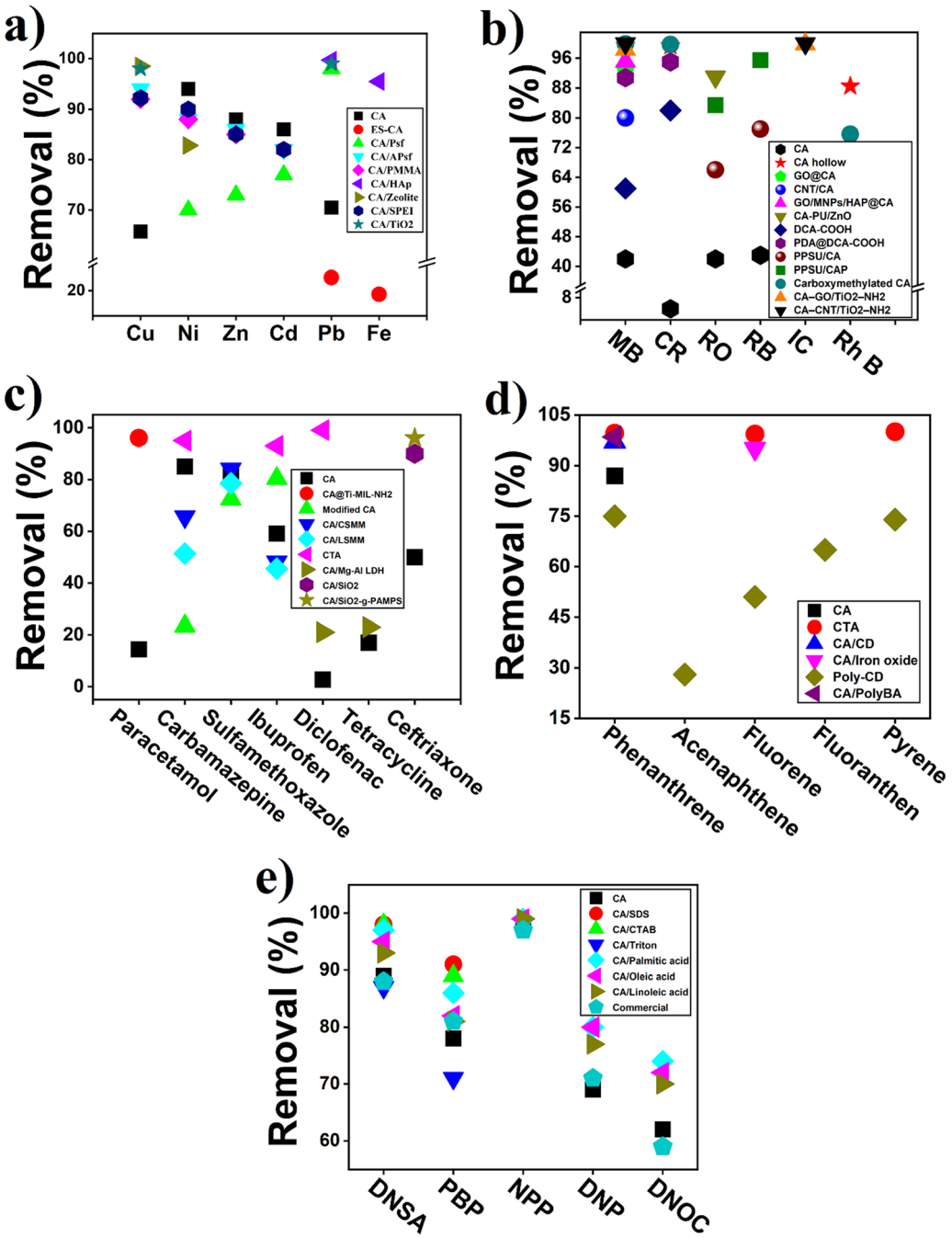

Fig. 4 Evidence for CA and CA-based membrane removal performance: (a) several heavy metals (Cu^{2+}, Ni^{2+}, Zn^{2+}, Cd^{2+}, Pb^{2+}, and Fe^{3+});[90,132,136,138–140,241] (b) several industrial dyes including methylene blue (MB), Congo red (CR), reactive orange (RO), Reactive black (RB), indigo carmine (IC), and Rhodamine B;[29,142,143,156,158–161,242] (c) pharmaceuticals;[181,188,191,192,195–198] (d) several selective polycyclic aromatic hydrocarbons (PAHs);[83,166,175,243–245] and (e) pesticides including *p*-nitrophenol (PNP), 2,4-dinitrophenol (DNP), 3,5-dinitrosalicylic acid (DNSA), 2-methyl-4,6-dinitrophenol (DNOC), and 4-nitrophenyl phosphate disodium salt hexahydrate (NPP).[217,221,222]

than other membranes. Emam *et al.* (2021) fabricated a highly porous photoactive CA-metal organic framework (Ti-MIL-NH_2) film to investigate the removal efficiency of paracetamol, one of the most widely used pharmaceutical intermediates.[181] The synthesized films were applied in the adsorption and photodegradation of paracetamol separately and together to find out which mechanism was suitable to explain the removal process. This study confirmed that the presence of higher photocatalytic activity of MOF (Ti-MIL-NH_2) in the film increases the removal rate of paracetamol by the photodegradation process (k_1 = 760.0 m^{-1}) compared to the adsorption (k_1 = 160.0 m^{-1}). Moreover, the removal efficiency was significantly increased from 82.7 mg g^{-1} for CA film to 519.1 mg g^{-1} for the porous CA-Ti-MIL-NH_2 film.

Table 6 Application of cellulose acetate-based membranes for the removal of pharmaceuticals, reuse, and recovery

Contaminant name	Name of membrane	Membrane type	Operating condition	Results	Ref.
Carbamazepine Ibuprofen Sulfamethazine	Modified CA	Nanofiltration	Initial conc.: 0.666 ppm; pH: 5.9; pressure: 345 & 690 Kpa; area: 21 cm^2; capacity: 6.9 L min^{-1}; flow rate: 0.8 L min^{-1}.	• 23.4, 72.4, and 80.4% of carbamazepine, ibuprofen, and sulfamethazine, respectively, were removed at high feed concentration; the results were comparable with the NF-270 filtration unit. • At high pressure, the removal rate was gradually decreased.	188
Mixed Pharmaceuticals (COD of 2300 mg L^{-1})	CA/ND-NH_2	Nanofiltration	Initial COD: 2300 ppm; SRT: 24 h; HRT: 25 days; pH: 5.9; pressure: 0.15 bar; DO: 0.7 mg O^2 L^{-1}; area: 14.7 cm^2; effective volume: 50 mL; flow rate: 0.8 L min^{-1}.	• Better membrane performance (both neat CA and CA/ND-NH_2) in terms of antifouling properties (FRR, RFR, TFR, and IFR) were achieved at specific aeration demand per membrane area (SADm) of 1 m^3 m^{-2} h^{-1}. • High aeration rate more than 1 m^3 m^{-2} h^{-1}, the COD removal rate increased but leads to the breakage of sludge flocs, and promoted the release of soluble EPS from the microbial flocs to the bioreactor. • Approximately 90% COD removal efficiency was achieved by CA and CA/ND-NH_2 membrane.	194
Diclofenac sodium Tetracycline	CA/Mg-Al LDH	Nanofiltration	Initial conc.: 0.01 g L^{-1}; pH: 7; pressure: 2 bar; area: 21 cm^2; volume: 60 mL.	Sixfold (2.7 & 17%) increase in the DS adsorption capacity with the addition of filler, conversely similar capacity (21 & 23%) was attained.	195
Carbamazepine Ibuprofen Sulfamethazine	CA/CSMM CA/LSMM	Nanofiltration	—	• Removal rate of the CA/CSMM membrane can be used for long time performance for the removal of ibuprofen 48.4 to 65% for 1 h and 10 h, respectively. • The order of removal by CA/LSMM was Smz > Carb > Ib as the molecular weight and radii increased in the same direction.	191
Ciprofloxacin	Electrospun montmorillonite-impregnated CA	Nanofiltration	Initial conc.: 10 mg L^{-1}; pH: 6.00; time: 60 min; dose: 4 g L^{-1}; temp.: 30 °C; agitation speed: 100 rpm.	• Increase in temperature results in more CIP removal from 1.843 mg g^{-1} to 13.8 mg g^{-1}. • Both Langmuir and Freundlich isotherm models were comparable, while the sorption kinetics can be described by the Elovich kinetics model. • The membrane can be regenerated and can be reused by treatment with NaOH.	197
Catechol Paranitrophenol Phenol Orthochloro phenol Metanitrophenol	CAP-Al_2O_3	—	Initial conc.: 100 mg L^{-1}; pH: 5.7–8.2; time: 24 h; effective area: 36.3 cm^2; agitation speed: 150 rpm; pressure: 690 KPa	• Addition of nanoparticles increased the porosity and permeability of the membrane. • Maximum adsorption capacity of CC, PNP, OCP, phenol, and MNP were 66, 62, 57, 55, and 51 mg g^{-1}, respectively.	205
Paracetamol	CA Porous CA Ti-MIL-NH_2 CA-Ti-MIL-NH_2	—	Initial conc.: 30 mg L^{-1}; pH: 5; time: 30 min; temp.: 30 °C; visible light chamber: 12 W	• The total removal of paracetamol from aqueous medium followed the order: porous CA-Ti-MIL-NH_2 film (517.1 mg g^{-1}) > Ti-MIL-NH_2 (428.4 mg g^{-1}) > porous CA film (168.7 mg g^{-1}) > CA film (77.5 mg g^{-1}).	181
Amoxicillin Metoprolol Naproxen Phenacetin	CA	Ultrafiltration Nanofiltration	—	• The removal rate with the UF membranes followed the sequence naproxen > metoprolol > amoxicillin > phenacetin, while the NF membranes followed the trend amoxicillin > naproxen > metoprolol > phenacetin due to the role of other mechanisms such as size exclusion and electrostatic repulsion.	187

Table 6 (*continued*)

Contaminant name	Name of membrane	Membrane type	Operating condition	Results	Ref.
Carbamazepine Diclofenac Ibuprofen Naproxen	Cellulose triacetate	Forward osmosis	Initial conc.: 250 μg L^{-1}; pH: 8; time: 24 h; effective area: 42 cm^2; Crossflow velocity: 23.2 cm s^{-1}; temp.: 24 ± 0.5 °C; pressure: 60–200 psi	• Under alkaline condition (pH 8), the removal rate followed the order carbamazepine (96%) > diclofenac (99%) > ibuprofen (83%) > naproxen (73%), which was related with the hydrophobicity of each compound. Both adsorption capacity and size exclusion contributed to the removal rate.	192
Bisphenol A	CA	Nanofiltration Reverse osmosis	Initial conc.: 50 mg L^{-1}; volume: 15 L; pH: 5–6.5; time: 24 h; effective area: 140 cm^2; concentrate flow rate: 1.6 L min^{-1}; temp.: 25 °C; pressure: 10 bar	• CA based CE BWRO membrane offered a low (10–40%) removal for BPA.	190
Estrone	CA	Nanofiltration Reverse osmosis	Initial conc.: 100 ng L^{-1}; pH: 7; time: 24 h; effective area: 169 cm^2; concentrate flow rate: 20 L min^{-1}; temp.: 22 ± 0.1 °C; pressure: 1379 kPa for NF and 2758 kPa for RO membrane	• Presence of organic matters significantly enhanced the removal efficiency with the maximum removal of 21.6 and 11.6% for NF and RO membrane, respectively.	206
Phenacetin Primidone Bisphenol A Isopropylantipyrine Carbamazepine Sulfamethoxazole 17 β -Estradiol	CA	Reverse osmosis	Initial conc.: 100 μg L^{-1}; pH: 7; time: 24 h; effective area: 32 cm^2; concentrate flow rate: 0.35 mL min^{-1}; temp.: 20 °C; pressure: 0.5 MPa	• The removal rate with membranes followed the sequence: primidone ≈ carbamazepine > sulfamethoxazole > isopropylantipyrine > 17 β-estradiol > bisphenol A > phenacetin	198
Ceftriaxone sodium	CA CA/SiO_2 CA/SiO_2-poly(2-acrylamido-2-methylpropane sulfonic acid)	Nanofiltration	Initial conc.: 40 mg L^{-1}; pH: 8; time: 24 h; temp.: 25 °C; pressure: 500 KPa	• Ceftriaxone sodium removal rate was about 50, 90, and 96% for CA, CA/SiO_2, and CA/SiO_2-poly(2-acrylamido-2-methylpropane sulfonic acid), respectively.	196

Note-CA: cellulose acetate; ND-NH_2: amino-functionalized nanodiamond; LDH: layered double hydroxides; CSMM: charged surface modifying macromolecules; LSMM: hydrophilic surface modifying macromolecules; CAP: cellulose acetate phthalate.

In another study, the removal efficiency of four pharmaceuticals by a cellulose triacetate (CTA)-based forward osmosis membrane was investigated.[192] Hydroxyl and carboxylic groups (negatively charged) are the predominant functional groups in the CTA-based membrane, which leads to the removal of negatively-charged pharmaceuticals by the electrostatic repulsive force. Moreover, the removal performance of the CTA membrane can also depend on the adsorption capacity and size exclusion. Hydrophobic and larger molecular-weighted molecules are rejected more; a similar phenomenon was also observed by Emam *et al.*[181]

3.5. Separation of pesticides

Any substance or mixture of substances preventing, destroying, or controlling the unwanted species of plants and animals during the production, processing, storage, transport, or marketing of agricultural products are known as pesticides.[207] Due to their direct influence on production, they have been used exclusively. The widespread use of pesticides for agricultural and nonagricultural purposes results in the presence of their residues in various environmental components including surface groundwater, which is one of the major sources of drinking water.[208] Even though their contamination level in wastewater is very low (concentration level pg L^{-1} to ng L^{-1}), they may result in potentially adverse health effects including cancer, genetic malformations, neurodevelopmental disorders, and damage to the immune system.[209,210] For that reason, the Drinking Water Directive sets a maximum permeable limit of 0.1 μg L^{-1} for a single active ingredient, and 0.5 μg L^{-1} for the sum of all individual active ingredients.[211] Moreover, World Health Organization (WHO) and the U.S. Environmental Protection Agency (USEPA) set individual risk assessment toxicity data-based guidelines for individual active substances.[212,213]

CA and CA-based membranes have been used since the late 60s for the treatment of organic hydrophilic and hydrophobic pesticides from wastewater. Hindin *et al.* reported an asymmetric cellulose acetate (CA) membrane for the removal of a few chlorinated pesticides including dichloro-diphenyl-trichloroethane (DDT), 1,1-dichloro-2,2-bis(4-chlorophenyl) ethane (TDE), benzene hexachloride (BHC), and lindane by the reverse osmosis process.[214] The reduction of each pesticide after RO filtration, employing a CA membrane, represents the promising membrane-based treatment process for the removal of low concentrations of organic pollutants including pesticides. In another study, the RO-CA membrane showed excellent performance (over 80%) in removing a variety of pesticides, including chlorinated hydrocarbons, organophosphorus, and miscellaneous pesticides (Fig. 4e).[215] However, the removal rate of pesticides is comparatively lower than other polymeric membranes such as polyamide and polyester-based membranes. This behavior has been attributed to the higher polarity of CA membranes, resulting in higher hydrophilic interaction with polar pesticides and leading to poor removal.[208] On the other hand, neat CA membrane produces a highly dense skin layer and a low porous sublayer, which leads to a lower flux and removal ratio.[216,217] The incorporation of polymeric and inorganic additives into the CA casting solution has been applied to improve the membrane characteristics and pesticide removal capacity. The presence of polymeric/organic additives including pluronic F127,[216] PEG 600,[218,219] polyvinylpyrrolidone (PVP),[133,220–222] polyetherimide (PEI), and poly(vinyl chloride) (PVC) and their concentration plays a critical role in controlling the membrane porosity, pore size, pore shape, and also producing well-interconnected pores on the membrane surface, which influences the overall membrane performance.[219,223] On the other hand, the addition of inorganic additives such as monovalent (LiCl[224,225]), divalent ($CaCl_2$[224]), or trivalent salts in the casting solution also improve the membrane permeability and selectivity. The presence of organic/inorganic additives in the casting solution increases the solution viscosity, which accelerate the coagulation rate and result in excellent interconnectivity between the membrane pores; however, the reduced mechanical strength of such a membrane has been observed.[223,226,227] For example, Fontananova *et al.*[228] showed that the addition of LiCl in the casting solution doping increases the flux of the casted membranes at a low LiCl concentration of 2.5 wt%, but it also suppressed the macrovoid formation at a high concentration of 7.5% LiCl and resulted in a decrease in the membrane permeation flux. Moreover, the addition of some nanoparticles such as SiO_2,[107,196,229,230] Al_2O_3,[231] ZnO,[232] and TiO_2[231–233] as additives not only increases the membrane stability and reduces the membrane hydrophilicity but also degrades the bacteria and some organic micropollutants and mitigates the membrane fouling problem.[234] Ghaemi in his study reported the effect of the surfactant on the characteristics and separation of nitrophenols (*p*-nitrophenol (PNP) and 3,5-dinitrosalicylic acid (DNSA)) by the CA/PVP nanofiltration membrane.[221,222] The addition of surfactants as additives resulted in membranes with superior pure water flux, permeation, and removal in comparison to the CA membrane. Moreover, a small amount of (0.25%) anionic surfactant (sodium dodecyl sulphate (SDS)) and cationic surfactant (cetyltrimethylammonium bromide (CTAB)) resulted in significant increments in both PNP and DNSA removal ability, while the addition of nonionic surfactant (Triton X-100) followed the opposite direction. Recently, several studies have been conducted to investigate the influence of fatty acids on the membrane structure and its performance.[217,235,236] Ghaemi and his coauthors showed that the addition of amphiphilic fatty acids (palmitic, oleic, and linoleic acids) on the CA membrane leads to improved membrane porosity and hydrophilicity, which results in the removal of hydrophobic organic pesticides, including nitroaromatic pesticides (*i.e.*, nitrophenols as one of the most important pollutants). *p*-Nitrophenol (PNP), 2,4-dinitrophenol (DNP), 3,5-dinitrosalicylic acid (DNSA), 2-methyl-4,6-dinitrophenol (DNOC), and 4-nitrophenyl phosphate disodium salt hexahydrate (NPP).[217] The addition of fatty acids in the casting solution leads to the formation of complexes between fatty acids and polymer molecules, which results in a reduction in the membrane pore size and improves the membrane porosity. Moreover, the addition of amphiphilic additives influences the penetration rate of the coagulation

solution and increases the demixing rate, which also enhances the membrane structural properties.[217,235,236] CA and CA-based membranes that have been used for the treatment of pesticides are shown in Table 7.

4. Factor affecting membrane performances

4.1. Membrane properties

The selection of an appropriate membrane and composition along with the addition of additives is one of the most critical steps in the design and operation of the membrane-based treatment process. The most important parameters affecting the membrane performances include the crystallinity of the membrane-based polymer, porosity/pore size, hydrophobicity/hydrophilicity (contact angle), surface charge/surface charge density (zeta potential), and surface roughness, as summarized in Table 8.

4.1.1. Crystallinity of the polymer. The crystallinity of the membrane polymer is a prime factor that affects the mechanical properties and pollutant permeability on the polymeric membranes. The crystallinity of a polymer can be determined by the glass transition temperature (T_g), which is directly related to chain flexibility, chain interactions, and molecular weight of the polymer.[253] In most cases, cellulose acetate-based membranes are a mixture of amorphous and crystalline phases known as semicrystalline membranes. In the crystalline phase, polymer chains are compacted regularly due to intermolecular interactions such as hydrogen bonds. Moreover, the crystallites of the polymer that are connected in randomly-oriented molecular chains are known as the amorphous phase. It has been found from the literature that the polymer packed with the crystalline phase cannot permeate the solute pollutants while the transport of solute takes place through the amorphous phase.[246] On the other hand, a higher packed polymer structure (crystalline nature) results in thermal, mechanical, and solvent resistivity, which are the most important parameters for long-time membrane application. The higher T_g values of polymeric materials represent higher amorphous nature and produced frequently brittle membranes. In general, CA possesses higher T_g, roughly 180 °C, and represents more amorphous polymer in the matrix, which can be significantly improved or reduced by the addition of plasticizers[254] or functionalization of the CA membrane.[107,160,247,255] For example, carboxymethyl cellulose acetate butyrate is an ester with larger groups having T_g value between 135 and 141 °C, representing higher crystallinity, possessing higher thermal and mechanical properties and long-time desalination application.[256] In 2020, Salah and his coauthor compared the most commonly used three RO membranes cellulose acetate, cellulose acetate propionate, and cellulose acetate butyrate for water desalination application.[257] This study showed that functionalization with larger polymer molecules results in more hydrophobicity (contact angle, 56, 71, and 74° for CA, CAP, and CAB, respectively) along with higher salt removal and pure water permeability of the membrane.

Rearrangement and recrystallization of the polymer chain is another way to improve the membrane properties. In this process, there is almost no effect on the overall crystallinity but the formation of smaller crystallites is induced, which enhances the interfacing surface area between the amorphous and crystalline regions shown in Fig. 5. This increased interfacial area could facilitate the fixation of the amorphous loops in the crystalline lattice, thereby reducing the number of nonselective pathways for mass transport, which also significantly improves the desalination efficiency.[258,259] Lu *et al.* modified the cellulose triacetate membrane with the treatment with a plasticizer (*p*-nitrophenol) solution, followed by water rinsing, which resulted in the reduction of the crystalline size of the polymer matrix, consequently improving the mass transport properties (water flux and water salt selectivity).[254] In another study, Minelli *et al.* reported the effect of plasticization (glycerol as plasticizer) of microfibrillated cellulose on the water sorption, diffusion coefficient, and structure of the polymer films.[260] The addition of plasticizers generally increases the mobility of the polymer chains in the polymer matrix, which results in an improvement of water molecule diffusion and also the membrane performances. The incorporation of inorganic nanoparticles such as SiO_2, Al_2O_3, TiO_2, Mg-Al LDH, and MOF[107,181,195,197,261] is another approach that improves the polymer crystalline properties. For example, Yu *et al.* reported that the incorporation of a higher concentration of SiO_2 in the PVDF hollow fiber membranes resulted in a transition from the α-phase to the β-phase crystal structure and restricted the movement of PVDF. This led to the deterioration of transport properties of the membrane and improved the antifouling, mechanical, and thermal properties compared to the neat PVDF membrane.[229]

4.1.2. Membrane molecular weight cut-off, Donnan effect, and dielectric effect. The performance or removal rate of the CA membrane is often quantified by the membrane molecular weight cut-off (MWCO). It can be defined as the lowest M_W (in Daltons) of a solute that can be separated at 90%, although this definition is not clear and can vary between 60 and 90% depending upon the protocols used by manufacturers. This variation of percentile separation can be described by solute characteristics, solute concentration, solvent characteristics, as well as flow conditions.[262] There is a close relation among the membrane molecular cut-off, pore size, and separation process shown in Fig. 6. According to the MWCO concept, molecules become larger as their mass increases, while as the molecules become larger, the sieving effects due to steric hindrance increase, and the molecule is rejected by the membrane more often than a smaller molecule.[208] It should be noted that MWCO can also be associated with diffusion because larger molecules will diffuse more slowly compared to smaller molecules. In general, reverse osmosis (RO) membrane and some nanofiltration (NF) membranes restrict the solute molecules following the diffusion method while ultrafiltration (UF), microfiltration (MF), and conventional filtration process follow the sieving mechanism.[263] Zhang *et al.* studied the correlation between the MWCO of four NF membranes and the removal of

Table 7 Application of cellulose acetate-based membranes for the removal of agricultural pesticides and herbicides

Contaminant name	Name of membrane	Membrane type	Operating condition	Results	Ref.
p-nitrophenol	CA/PVP in SDS as surfactant	Nanofiltration	Conc.: 0.1 mM;	• Addition of SDS in CA membrane resulted in higher pure water flux with reduced pore size compared to the pristine CA membrane.	221
3,5-dinitrosalicylic acid			pressure: 4.5 × 10^5 Pa; pH: 8.0; time: 9 h; agitation speed: 300 rpm; effective area: 11.94 cm^2; temp.: 25 ± 2 °C	• Surface roughness also increased due to the addition of SDS, resulting in a superior removal rate compared to the neat CA membrane.	
p-nitrophenol	CA/PVP in various surfactants CTAB	Nanofiltration	Conc.: 0.1 mM;	• Addition of surfactants as additives resulted in membranes with superior pure water flux, permeation, and removal in comparison to the CA membrane.	222
3,5-dinitrosalicylic acid	and Triton		Additives: 0.25%; pressure: 4.5 × 10^5 Pa; pH: 8.0; time: 9 h; agitation speed: 300 rpm; effective area: 11.94 cm^2; temp.: 25 ± 2 °C	• Addition of ionic surfactant as an additive (CTAB) resulted in a higher removal rate compared to nonionic surfactant (DNSA).	
p-Nitrophenol 2,4-dinitrophenol 3,5-dinitrosalicylic acid 2-methyl-4,6-dinitrophenol 4-nitrophenyl phosphate disodium salt hexahydrate	CA/PVP	Nanofiltration	Conc.: 0.1 mM; Additives (palmitic acid, oleic acid, and Linoleic acid): (0–2)%; pressure: 4.6 × 10^5 Pa; pH: 4.5, 7.0, and 8.0; time: 10 h; agitation speed: 300 rpm; effective area: 11.94 cm^2; temp.: 25 ± 2 °C	• Membrane properties have been improved including pure water flux, mean pore size, surface roughness, contact angle, and zeta potential with the addition of amphiphilic fatty acids. • Removal of PNP molecules increased with the increment in the concentration of additives similar to other nitrophenols; PNP molecules revealed different behavior by an alteration in the solution pH.	217
Atrazine	SiO_2/CA	Nanofiltration	Conc.: 0.1–10 mg L^{-1}; pressure: 10 bar; time: 1 h; effective area: 0.002 m^2; temp.: 23 °C	• Removal rate was increased (96 to 98.3%) with increasing transmembrane pressure from 10 to 20 bars.	230
Propazine Prometryn	CA Cu-MOF-CA			• Increased feed concentration from 0.1 to 10 ppm results in higher removal rate for each individual pesticide.	
Dimethoate		—	Initial conc.: 20 ppm; volume: 50 mL;	• The surface area was significantly increased from 78.4 m^2 g^{-1} to 965.8 m^2 g^{-1} with the incorporation of 40% Cu-MOF in the porous CA membrane.	237
			Dose: 20–60 mg; pH: 3–11; temp.: 25–55 °C; time: 6 h	• The adsorption capacity was enhanced from 207.8 mg g^{-1} to 321.9 mg g^{-1} for the Cu-MOF-CA membrane. Moreover, it showed excellent recyclability with reduced adsorption capacity of 249.5 mg g^{-1} after 5 cycles.	
γ-HCH β-HCH Aldrin Heptachlor epoxide p,p′-DDE Endrin	CA CAB CTA	—	Initial conc.: 500 ng L^{-1}; volume: 1 L; effective area: 24 cm^2;	• CTA membrane exhibited comparatively higher chemical and mechanical stability than the other three membranes.	238
	CA-CTA		Temp: 25 °C; time: 1 h; rotation speed: 150 rpm	• Among the four membranes, the CTA membrane showed maximum accumulation capacity.	
γ-HCH β-HCH Aldrin Heptachlor epoxide p,p′-DDE Endrin	TECAM TECAB TECTA	—	Initial conc.: 500 ng L^{-1}; volume: 1 L; effective area: 24 cm^2;	• All triolein-embedded membranes exhibited better removal efficiency compared to their corresponding neat membrane.	238
	TECA-CTA		Temp: 25 °C; time: 1 h; rotation speed: 150 rpm	• TECTA showed the highest uptake rates, and TECAB showed the poorest accumulation.	
Methyl parathion Ethoprophos Sulfotepp	CA CA-GO	Nanofiltration	Initial conc.: 0.1 mg L^{-1}; volume: 10 mL; adsorbent dose: 15 mg; pH: 12; temp.: room temperature; time: 15 min	• Addition of graphene oxide (0–10%) significantly increases the hydrophilicity of the nanofabric membrane.	239

Table 7 (*continued*)

Contaminant name	Name of membrane	Membrane type	Operating condition	Results	Ref.
Chlorpyrifos				• The removal of organophosphorus pesticides (OPPs) by the nanofiltration membrane followed the adsorption process, which was due to π–π interaction, electrostatic interactions, and hydrogen bonding between the membrane and OPPs. • Addition of GO on the CA membrane increases the adsorption capacity for each OPPs molecule.	
Chlorpyrifos	CA (20–60%) MIL-53-NH_2-CA	Microfiltration	Initial conc.: 20 mg L^{-1}; volume: 50 mL; adsorbent dose: 40 mg; temp.: 30 °C; time: 4 h	• The maximum capacities for the chlorpyrifos adsorptive removal were 160.36 mg g^{-1} and 356.34 mg g^{-1} for CA and 60% MIL-53-NH_2-CA, respectively.	240

Note:-CA: cellulose acetate; PVP: polyvinylpirrolidone; SDS: sodium dodecyl sulfate; CTAB: cetylethreemethylammonium bromide; γ-HCH: γ-hexachlorocy-clohexane; β-HCH: β-hexachlorocyclohexane; p,p′-DDE: 1,1-bis(p-chlorophenyl)-2,2-dichloroethylene; MOF: metal organic framework; CAB: cellulose acetate butyrate; CTA: cellulose triacetate; CA/CTA: cellulose acetate-cellulose triacetate blend; TFCAM: triolein-embedded CA; TFCAB: triolein-embedded CAB; TFCTA: triolein-embedded CTA; TFCA-CTA: triolein-embedded CA-CTA.

two triazine herbicides (atrazine and simazine).[264] This study concluded that the membrane with smaller MWCO possesses higher pollutant removal efficiency than the larger MWCO, which was in agreement with previous research work.[265] For instance, in a recent study, Cheng[160] and Ciobanu[236] reported CA membranes with an MWCO of 369 and 2591 Da, where the fomer MWCO CA membrane exhibited 90.4% salt removal efficiency while only 56% salt was rejected by latter. In another study, Zhang *et al.* demonstrated that the MWCO of the membrane only poorly correlated with the removal of the studied compounds and is only capable of providing a rough estimate of the sieving effect.[264]

However, the MWCO or size exclusion mechanism cannot explain the nanofiltration-based membrane separation process. for a better understanding of the membrane separation process, ionic pollutants separation, and selectivity of the nanofiltration membrane, three different effects have been proposed: charge repulsion, Donnan effect, and dielectric effects.[267,268] The charge repulsion effect is caused by the charged nature of the membrane and the feed solution. The Donnan theory described the charged ion distribution near the semipermeable membrane at equilibrium condition when one of the charged ions cannot pass through the membrane, while dielectric effects can arise when ions (pollutants) are in direct contact at the interface between the materials of different dielectric constant, in this case, the polymer matrix and the solvent.[269,270] Several studies has been conducted to investigate the influence of Donnan factor on the membrane separation process.[267,270–272] In 2008, Yannick and his coauthor investigated the influence of the ion size and Donnan factor on the membrane performance for both neutral and electrically-charged membranes.[271] They conclude that the dielectric exclusion and Donnan effect have almost no impact on the membrane performance through the neutral membrane surface. On the other hand, for larger charged membranes (fixed value), dielectric effects and Donnan effect increase the membrane potential at a particular concentration. Similar results have also been reported by Szymczyk *et al.*[270] In another study, it has been estimated that the dielectric constant inside the membrane pores also depends on the physicochemical behavior of the membrane and pollutant-dependent solution properties including pH, concentration, and chemical nature of pollutants.[271] Finally, it can be concluded that during the nanofiltration membrane selection and performance evaluation, three of the abovementioned parameters should be considered.

4.1.3. Membrane pore size and pore structure. Porosity is expressed as pore density, pore size distribution (PSD), or effective number of pores (N) in the membrane top layer and other related quantities such as nominal pore size of a membrane, which usually refers to the smallest pore size in the membrane matrix and have been regarded as representative parameters for predicting the removal of different organic compounds or particles.[273–275] All of these parameters are generally attributed to the pore geometry of the membranes. Moreover, the pore geometry of the individual membranes can

Table 8 Major parameters and their effect on the membrane separation process

Parameter	Affect	Ref.
Membrane properties		
Crystallinity	Crystalline membranes exhibit higher physiochemical properties including thermally, mechanically, and solvent resistivity along with lower solute diffusion rate (higher removal).	246
Molecular weight cut-off (MWCO)	Solute molecules with larger size than the membrane MWCO cannot pass through the membrane and are easily be removed.	208
Surface charge	Increasing the surface charge increases the electrostatic repulsive force, resulting in enhanced solute removal efficacy.	191 and 247
Surface roughness	Rough surface increases the total surface area to which the foulants can be attached, and the ridge-valley structure favors the accumulation of the foulants.	248
Pollutant properties		
Solute molecular weight (M_W)/size/geometry	Solute with a higher molecular weight is prone to separate due to the molecular sieving mechanism than a lower one.	6
Hydrophobicity/hydrophilicity and polarity	Hydrophobic molecules are adsorbed on the membrane surface due to hydrophobic interaction or hydrogen bond formation.	249 and 250
Operating parameter		
pH	Change in the membrane surface charge and surface structure	192 and 251
Presence of organic matter	Formation of negatively charged complexation leading to augmented electrostatic repulsion between the membrane and complexion, and also leading to removal by following the sieving mechanism	192 and 251
Temperature	Increases the mass transfer and diffusion rate of the feed	252
Transmembrane pressure (TMP) and flow rate	The higher the TMP and flow rate, the higher the diffusion rate (driving force)	252

be controlled by selecting proper fabrication methods, polymer concentration, and fabrication parameters (coagulation bath temperature, humidity, and annealing temperature), precipitation time, solvents, nonsolvents, and addition of additives.[253,276] For example, increasing the polymer concentration in the casting solution produces a lower porous and small pore-sized membrane. In this case, the macrovoid formation is suppressed, and the tendency to form sponge-like structures is enhanced. In one study, the 12–20% polymer concentration in the casting solution has been used for the fabrication of the UF membrane, while polymer concentration $\geq$20% produces the RO membrane.[277] The selection of the solvent/nonsolvent system also influences the membrane morphology. The higher miscibility of the polymer in a solvent results in the formation of a highly porous membrane, while the lower miscibility or nonsolvent leads to the fabrication of a nonporous membrane.

Membrane pore size and pore density can also be improved by controlling the coagulating bath temperature. It was commonly known that the lower coagulation bath temperature results in a lower coagulation rate, which promotes the formation of a sponge-like denser layer, while higher temperature promotes faster coagulation rate, resulting in the formation of a loose finger-like membrane.[253] Guoliang and his coauthors fabricated PET-enhanced CA membranes using the phase-inversion technique and investigated the effect of membrane fabrication parameters, including the concentration and temperature of the casting polymer solution, temperature, and time of evaporation, coagulation, and annealing processes in the membrane pore size along with the performance.[278] The optimum key parameters for fabricating a forward osmosis (FO) membrane required 18% CA casting solution with an evaporation temperature of 25 °C for 60 s, coagulating in a water bath at 5 °C for 24 h, and annealing at 70 °C for 1 h, which produces a grille-like dense top surface and a porous bottom membrane (both larger finger-like and sponge-like structure present in the sublayer). Moreover, the blending of two different polymers offers attractive alternatives for the membrane surface modification and showed a synergistic effect in membrane performance. In addition, the addition of inorganic (such as LiCl, TiO_2, GO, CNTs, Al_2O_3) and organic additives (polyvinylpyrrolidone (PVP), polyethylene glycol 600 (PEG-600), polyethylene terephthalate (PET), poly(styrene-*co*-maleic anhydride) (PSMA), sulfonated poly(ether ether ketone) (SPEEK), Pluronic F127) as the third component to the blend polymers has been one of the important procedures used in membrane preparation to control the surface morphology (especially pore size and percentile porosity) and performance of the membranes.[148,231,278–280] The addition of additives can function as a pore former, increasing the solution viscosity of the casting solution, which leads to the thermodynamic instability of the casting solution, accelerating the precipitation rate in the coagulation bath, and also leading to a reduction in the pore size along with a significant increase in the surface roughness, which significantly increases the removal rate or membrane performance. Han *et al.* fabricated the CA/CMCA blend UF membrane *via* the phase inversion method to investigate the influence of blending composition in the presence and absence of additives (PEG 600).[281] The study revealed that increasing the concentration of CMCA in the presence of additives in the blending solution leads to an increase in the surface roughness and produces more pores in the top and sublayer (porous structure in the cross-section) of the membrane compared to a neat CA membrane without additives.[281] In a recent study, Baniasadi fabricated a CA FO membrane containing TiO_2 and Al_2O_3 nanoparticles as additives.[231] The addition of metallic oxide nanofillers made the membrane denser with finger-like voids extended from top to bottom of the membrane structure. These longer finger-like macrovoids lead to a higher porous membrane, resulting in higher removal efficiency. Moreover, membrane porosity (microvoids) was significantly enhanced with increasing nanofiller

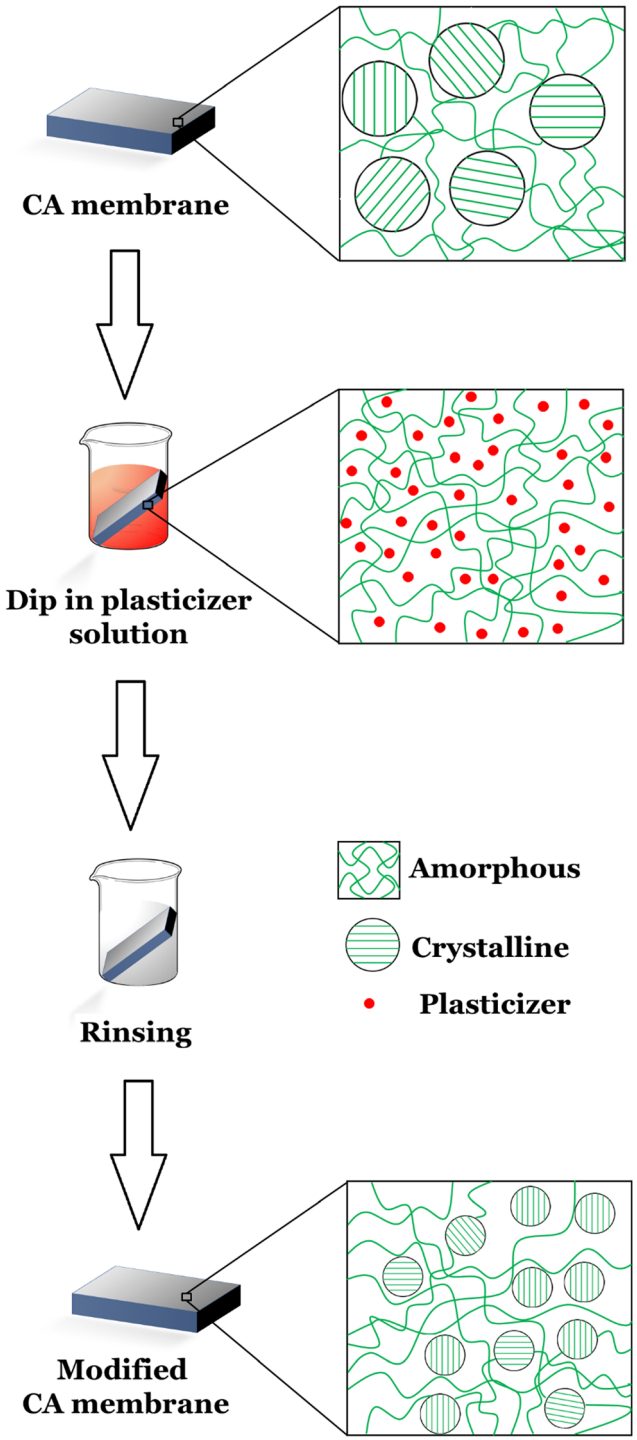

Fig. 5 Schematic illustration of a proposed mechanism for the role of plasticizer on the crystalline structure of the cellulose acetate (CA) membrane.[254] The pristine CA membrane consists large crystallites embedded in amorphous regions. Soaking of the membrane in plasticizer solutions leads to the swelling of both the crystalline and amorphous regions. Plasticizer is gradually released by water rinsing, resulting in the rearrangement and recrystallization of the polymer chains.

concentration up to a certain limit (TiO_2 < 1.0% and Al_2O_3 < 0.1%) and was then suppressed at higher additive dosages. The reduction of the %porosity of the membrane at higher nanofiller concentration was because of the higher viscosity of the polymeric solution, which prevents the increment of finger-like pores in the phase inversion process and leads to the agglomeration of nanofillers.[282,283]

4.1.4. Membrane charge. Electrostatic interaction or repulsion between the solutes and the porous membrane surface have been reported to be an important contaminant removal mechanism. These interactions or repulsion is mostly dependent on the membrane surface charge, which is generally measured by the zeta potential value.[262] The zeta potentials and the acidity of the membrane surface can be determined using electrophoresis and potentiometric titration methods.[284,285] Negative zeta potential values (value depends on solution pH) of cellulose acetate and cellulose acetate-based membranes represent the overall negative surface charge.[217,221,222] The majority of the used RO, NF, and UF cellulose acetate membranes in the wastewater treatment process or desalination application are negatively charged, which tends to minimize the adsorption of negatively-charged foulants and microorganisms present in the feed water, enhance the removal of dissolved salts, and also the membrane shelf-life with consistent performances.[253] Hu *et al.*[286] and Schafer *et al.*[287] showed that charged lower molecular weight organic acids exhibited higher removal efficiency by RO and UF membranes than larger neutral organics due to electrostatic repulsion. However, the presence of –OH and acetyl groups in the CA membrane surface make it a hydrophilic nature; also, the increasing swelling properties lead to the suppression of the long-term membrane application.[191] These drawbacks can be solved by physiochemically modified crosslinking, grafting, sulfonation, amination, *etc.*[191,247]

In several studies, it has been reported that the heavy metal removal rate remarkably enhanced after the adsorbents have been modified by the functional groups including $–NH_2$, –SH, –COOH, and $–HSO_3$.[85] The presence of –OH groups in the CA membrane and negatively-charged functional groups in modified CA membrane preferentially combine with water molecules and form a hydration layer, which reduces the absorption of negatively-charged protein molecules on the membrane surface and enhances the antifouling properties.[246] In addition, the negative charge of the membrane surface may be deprotonated in the feed solution. Yoon *et al.* in their study investigated the removal mechanism of perchlorate ions by a series of negatively-charged membranes.[288] This study showed that increasing the surface charge of the membrane results in higher removal efficiency. More interestingly, the removal rate by the individual membrane was greater than the theoretical results based on only the size exclusion mechanism, which confirmed that the removal mechanism followed both size exclusion and electrostatic interaction. In several investigated cases of negatively-charged membrane surfaces, the performance can be improved by increasing the feed solution pH, which is because increasing the pH of the solution increases the deprotonation (negative zeta potential) of the membrane surface, resulting in electrostatic repulsion between the membrane and negatively-charged solute molecules.[288–290]

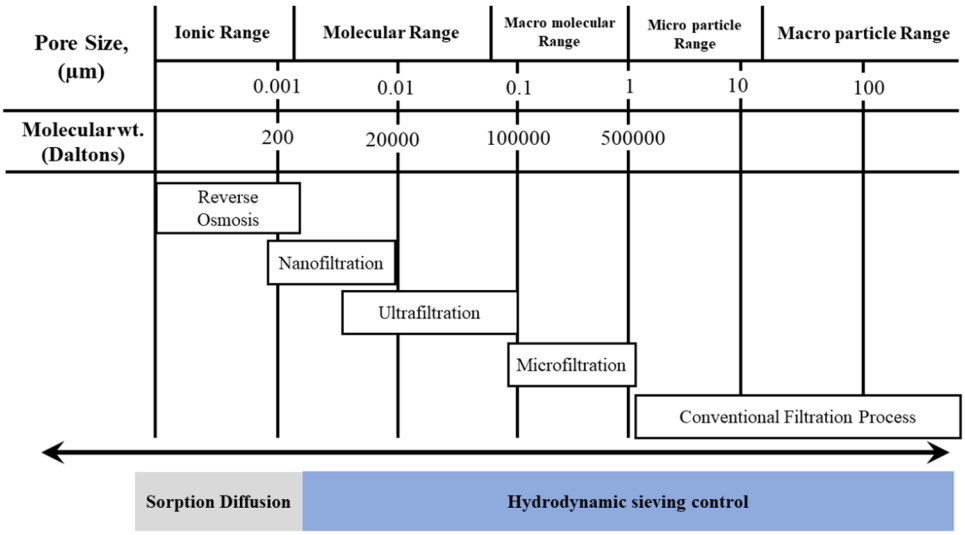

Fig. 6 Membrane molecular weight cut-off (MWCO)/pore size ranges used in the different membrane treatment processes. Modified with permission from ref. 266. Copyright (2011) Taylor & Francis.

Surface charge is a particularly important parameter for the determination of antifouling properties (especially when foulants are charged such as bacteria, protein, or colloidal particles).[291] In general, foulants having negatively-charged, electrostatic repulsion between CA membrane and foulants prevent foulant deposition on the membrane surface (antifouling property). Moreover, the CA membrane surface charge can be improved by the increasing pH of the feed solution or by surface modification (increasing acidic functional groups). Although most CA-based membranes are mainly negatively charged, however, several positively-charged CA membranes have been developed that can be used for the removal of cations and cationic macromolecules such as dyes and positively-charged proteins.[253,292–294] In a recent study, Liu and his coauthor modified a base membrane made of cellulose acetate/chitosan (CA/CS) blend with heparin (H), quaternary ammonium (Q), or immobilized with silver ions (Ag) to investigate the influence of pH on the membrane surface.[290] This study confirmed that CA/CS and CA/CS-Ag membranes possess relatively small zeta potential, while modification with heparin (CA/CS-H membrane) exhibited −10 mV and +12 mV in case of modification with quaternary ammonium (CA/CS-H membrane). The negative charge of the CA/CS-H membrane is expected due to the presence of $-CH_2SO_3^-$, $-COO^-$, or $-NHSO_3^-$ groups in heparin, while the positive electric charges can be attributed to the many $-N^+R_3$ groups in the quaternary ammonium. More interestingly, the zeta potential of each membrane changed from more positive (or less negative) at a lower pH to more negative (or less positive) at a higher pH, which were in agreement with previous studies.[106]

4.1.5. Surface roughness. There is a strong positive correlation between the membrane fouling and the surface roughness for CA-based membranes. In general, membranes with smooth surface are less prone to colloidal fouling compared to rougher surfaced polymer membrane. This may be because greater roughness increases the total surface area to which foulants can be attached, and the ridge-valley structure favors the accumulation of foulants at the rough surface. As a result, membranes with rougher surface exhibited faster fouling rate, which resulted in a significant reduction of membrane performance with time. Chung *et al.* fabricated UF hollow fiber membranes and reported that the pure water flux of the membranes was nearly proportional to the mean roughness, while higher mean roughness was correlated with a lower removal of organic macromolecules.[295] However, contradictory findings have also been reported on the effect of surface roughness on membrane flux: higher surface roughness can mean higher flux, lower flux, or no effect on flux.[142,222,231,296,297]

In 2013, Ramon *et al.* investigated the correlation between the surface roughness of coating films and the underlying porous support membrane.[248] From this simulation, they pointed out two hypothesis: (i) permeability increases with increasing surface roughness that produces thin regions in the coating film and reduces the base film thickness, but if the roughness is formed on top of the unvarying base film thickness, the permeability of the film decreases with increased roughness; and (ii) when the surface roughness comes at the expense of base film thickness, the thinner regions (''valleys'') present locally higher flux (''hot spots'') than the thicker regions (''peaks''); hence, these hot spots may be points of initiation for colloidal and organic deposition as well as mineral scale formation.

Surface roughness properties mostly depends on the membrane fabrication process and fabrication parameters. For example, membranes fabricated by phase inversion, track-etching interfacial polymerization, and electrospinning method exhibited comparatively smooth surface (antifouling properties), while the stretching method produced a rougher surface.[253] Moreover, the fabrication parameters such as in case of electrospinning-based membrane synthesis process, for

example, viscosity, conductivity, tip-to-collector distance, feed rate, composition in polymer blend, and voltage applied, affect the surface roughness properties.[107,156,298] In another study, Elkony *et al.* experimented that the addition of a small amount of crosslinker and/or grafting monomer also improved the surface morphology, thus also enhancing the antifouling properties.[299,300]

With the addition of a small amount of nanofiller such as GO, MOF, HKUST-1, ZnO, gC_3N_4, and Al_2O_3 in the CA membrane, an obvious decease in the surface roughness was observed.[144] With the AFM technique, Yang *et al.* showed the impact of addition of GO, MOF, and combination of GO and MOF in the CA membrane.[144] This study revealed that the addition of a filler at a certain amount produces a smoother surface, while further addition leads to the agglomeration of the nanofiller, resulting in an increase in the surface roughness of composite membranes. On the other hand, the addition of inorganic nanofiller improves the hydrophilic nature of the membrane surface, which leads to more water permeability (increasing water flux) and also limits the interaction between the hydrophobic contaminants and the membrane (increasing repulsive force).[127,301] In another study, Ghaseminezhad *et al.* investigated the influence (surface roughness and salt removal capacity) of graphene oxide (GO) NPs in the CA membrane.[302] This study showed that the addition of GO up to 1% reduced the surface roughness from 6 to 4.3 nm, which also significantly improved salt removal from 50 to 90%. Further addition of GO results in agglomeration, which increases the roughness (9.0 nm) along with the reduction of salt removal. Yang in his study showed that the antifouling properties (higher reversible foulant and lower irreversible foulant) also significantly increased with the addition of GO and MOF as the filler, as shown in Fig. 7b.[144] With the addition of GO on the CA membrane surface up to a certain limit, the surface roughness was significantly reduced, which improved the antifouling properties of the membrane at the same time as the water flux ratio as expected, as shown in Fig. 7a.

4.2. Pollutant properties

The physiochemical properties including molecular weight, size, geometry charge, and hydrophobicity of pollutant molecules are the most important parameter determining the membrane performances. In recent studies, several research groups have systematically studied the role of the aforementioned parameters on membrane removal, and their results are discussed.

4.2.1. Solute molecular weight (M_W) and size. Overall polymeric membrane-based separation depends on three basic parameters including adsorption, sieving, and electrostatic interaction (Fig. 3). Among them, nonionic and negatively charged pollutants (mostly) are removed from the feed solution by following the sieving mechanism as most cellulose acetate-based membranes are negatively charged. Moreover, the pore size of the selected membranes is also critical for the removal of solute molecules. In the molecular sieving process, pollutant molecules with higher molecular weight or MWCO than the membrane pore size cannot pass through (lower diffusion) the membrane and lead to more removal efficiency.[6] One recent study showed that in case of glassy polymeric membrane, the diffusion coefficient is decreased with an increase in the molecular weight, which reduces the permeability of solute molecules. On the other hand, in case of rubbery polymers, two different scenarios have been observed. Permeability increased with increasing molecular weight (upto 100), while opposite results has been found for the molecular weight above 100.[6]

As cellulose acetate-based membranes are in general negatively charged, it can separate negatively charged due to electrostatic repulsion while the uncharged pollutant can be separated by the simple sieving mechanism (Fig. 3a). Several studies showed that there is a positive correlation between the removal rate and molecular weight of pollutants.[133,139,191,208] In a pilot plant, a series of nitroaromatic pesticides including *p*-nitrophenol (PNP; M_W: 371.14), 2,4-dinitrophenol (DNP; M_W: 184.1), 3,5-dinitrosalicylic acid (DNSA; M_W: 228.1), 2-methyl-

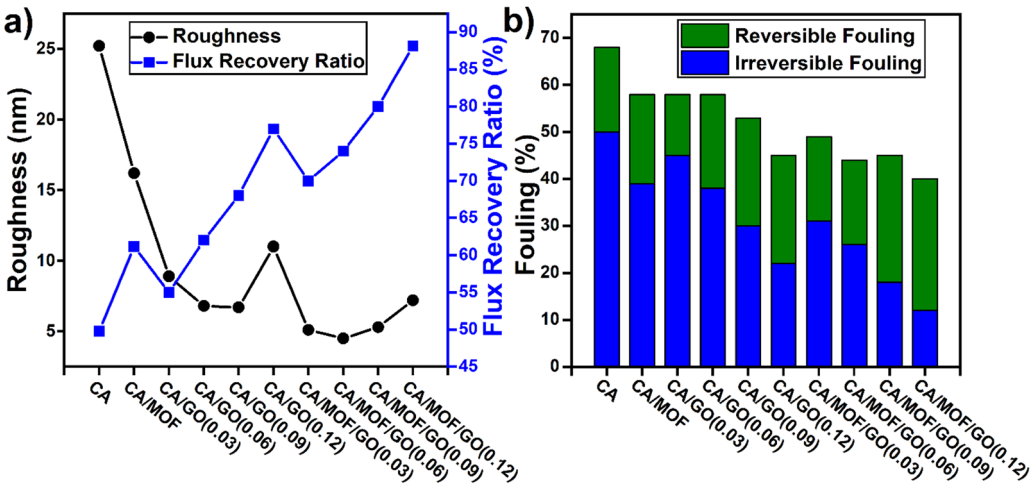

Fig. 7 (a) Influence of MOF and GO dosing on cellulose acetate membrane on surface roughness and flux recovery ratio; (b) effect of MOF and GO dosing on cellulose acetate membrane on the antifouling performance (reversible and irreversible fouling).[144]

4,6-dinitrophenol (DNOC; M_W: 198), and 4-nitrophenyl phosphate disodium salt hexahydrate (NPP; M_W: 139.1) were treated to investigate the influence of molecular weight in membrane performance.[217] Membrane performance was found to be significantly increased with increasing molecular weight as follows: NPP (97.5%) > DNSA (89%) > DNOC (85%) > DNP (80%) > PNP (76). In 2013, Alturki *et al.* investigated the removal of charged and neutral pharmaceuticals with various molecular weights by the cellulose acetate membrane.[303] This study revealed a positive correlation between the molecular weight of pollutants and CA-based membrane performance, as shown in Fig. 8. The removal efficiency of both hydrophilic and hydrophobic neutral organic pollutants increased with increasing molecular weight due to the simple sieving mechanism, but their efficiency can be significantly influenced by the feed and draw solution temperature and flow rate while other parameters such as temperature and transmembrane temperature exhibited little influence on the removal efficiency.[304] On the other hand, the removal of charged pollutants is dominated by electrostatic repulsion than size exclusion (sieving), and the removal efficiency is comparatively much higher than the same molecular weight neutral pollutant. Moreover, the removal efficiency is also dependent on the membrane surface charge and pH of the solution. At higher pH, the feed solution has a more negative of zeta potential, which represents more negative sites on the membrane surface, thus enhancing electrostatic repulsion.

In recent studies, researchers confirmed that other than the solute molecular weight, several parameters including molecular width and length, Stokes radii, and molecular mean size are useful parameters for the estimation of the removal mechanism.[305–307] In case of inorganic ions separation, all ions are spherical shape, and their removal efficiency can be better described by the Stokes radius of individual ions.[308] In the case of organic pollutants, the removal model is extremely critical and depends on the molecular structure, size, shape, length, and width.[308] However, molecular Stokes radius cannot be used to explain the solute diffusivity as the Stokes radius is based on the assumption that molecules are spherical in shape and rigid, which is not true for organic molecules.[262] Among them, molecular length and molecular width are the most critical shape parameters; in this approach, a molecule is approximated by a rectangular parallelepiped, a cylinder, or an ellipsoid. For example, Kiso and his coauthor showed that the removal efficiency of organic molecules depends mostly on molecular length and/or molecular width rather than molecular weight (Fig. 9).[308] In their investigation, they selected organic molecules of similar molecular weight with different molecular length and width and correlated it with their removal efficiency. This study showed that the removal rate displayed a linear positive relation with molecular width but opposite to the molecular length with some exception. In 2014, Doederer *et al.* also found a positive correlation between the molecular width and removal rate rather than the molecular weight.[309] These results indicated the significance of solute molecular shape parameter on removal, and the solute transport predictions through the membrane should not be based only the solute's molecular weight.

4.2.2. Hydrophobicity, hydrophilicity, and polarity. In case of organic pollutants, removal by adsorption or electrostatic repulsion is the most important mechanism. These parameters mostly depend on the hydrophobic/hydrophilic nature of the pollutants. Several studies claimed that the interaction between the nonpolar hydrocarbon segments of the solute molecule and that of the membrane surface is due to hydrophobic bonding.[208,265,273,310,311] Moreover, some study also revealed that in addition to the hydrophobic interaction, adsorption might also take place through hydrogen bonding. The hydrophobic

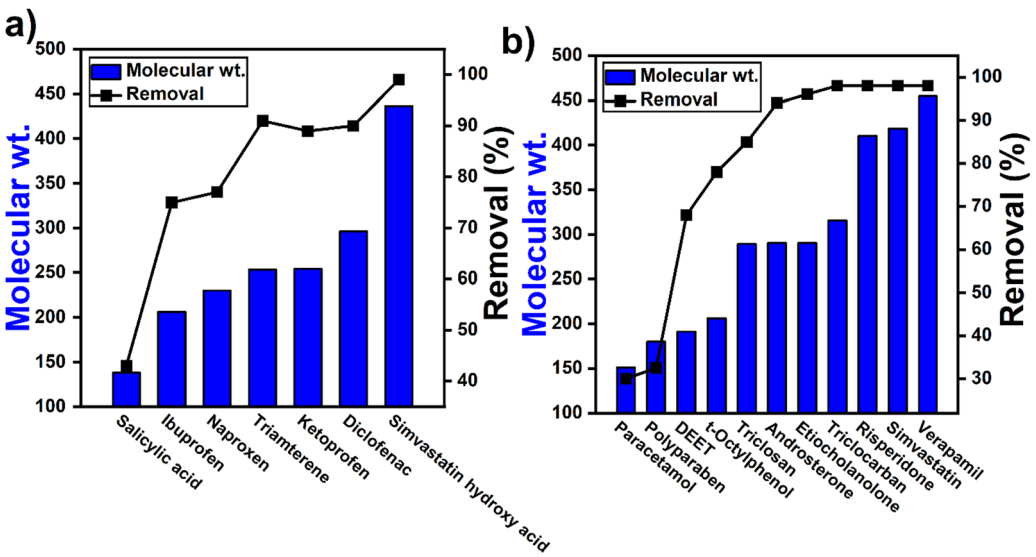

Fig. 8 Correlation of molecular weight of (a) negatively charged, and (b) neutral pharmaceuticals and personal care product *vs.* cellulose acetate membrane.[303]

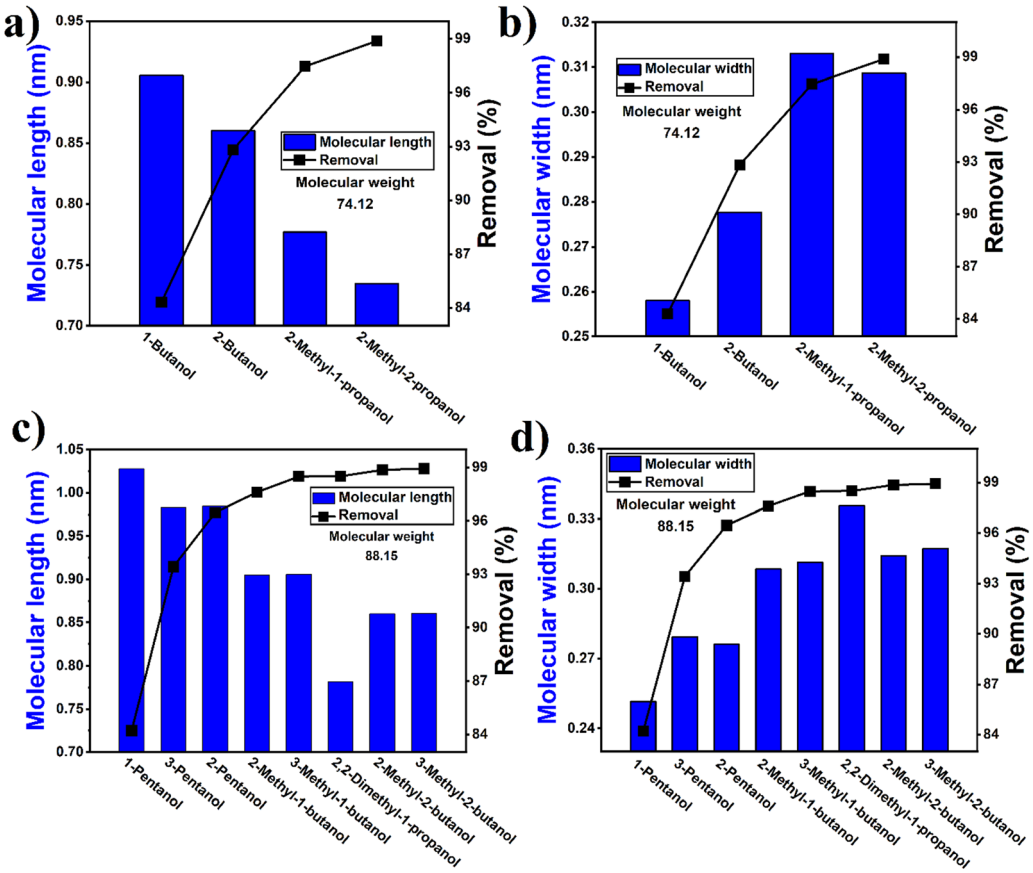

Fig. 9 Correlation of molecular size parameter of (a) and (c) molecular length, and (b) and (d) molecular width of organic pollutant *vs.* removal rate (%) of reverse osmosis membrane.[308]

interaction and hydrogen bonding can apparently act either independently or together. Several studies suggested that hydrophobic interaction is the predominant one to explain the removal mechanism.[249,250] The hydrophobicity/hydrophilicity of the solute is measured by estimating the partitioning coefficient ($\log K_{ow}$) and apparent partitioning coefficient ($\log D$). In general, the $\log K_{ow}$ values of trace organic molecules vary between −3 and 7, with a higher value of more than 2 representing the hydrophobic nature of the organic compounds. Kiso *et al.* studied a sequence of studies to set up a correlation among $\log K_{ow}$, retention, and adsorption of a number of aromatic and nonphenolic organic pollutants on the membrane surface.[312–315] These studies confirmed that there is almost no correlation between the removal rate and $\log K_{ow}$, while a strong correlation exists between adsorption and $\log K_{ow}$. In another study, Rakhshan *et al.* showed lower removal of several organic pesticides with increasing hydrophobicity ($\log K_{ow}$), which can be better explained by considering the dipole moments (Debye value) and molecular structure of the solutes.[230] In a systematic study on the effect of pharmaceuticals on removal,[192] a competition was identified between the partitioning coefficient ($\log K_{ow}$) and the pH-dependent partitioning coefficient ($\log D$). The removal rate was better explained by logD than $\log K_{ow}$. Furthermore, molecules containing negatively-charged polar groups including –C(O)O–, –OH–, –CO–, HCON, CH_3CON, and –O– are rejected due to electrostatic repulsion force.[192] The removal of some organic compounds such as alcohols, phenols, and carboxylic acids by the membrane was due to hydrogen bond formation, which increased with the reduction of solution pH, which was due to the increase in the H-bond forming ability at a lower pH.[316,317] The increase in the hydrogen bond formation ability results in lowering the diffusion across the membrane, which results in a lower removal rate due to subsequent flux decline. It was also expected that if polar molecules have similar sizes of membrane pore, it would block the membrane pore due to hydrogen bond formation, resulting in foulant formation and also a decline water in flux, thus significantly reducing the membrane performance.

4.3. Effect of operating parameter

The operating parameters play an important role in controlling the membrane performance or removal rate. The basic operating parameters includes crossflow velocity, transmembrane pressure, temperature, and pH. Although the effect of these parameters on the membrane performance is not always linear, these parameters greatly change the removal rate. The respective literature studies are discussed below.

4.3.1. pH of the feed solution. The role of pH on organic pollutant removal is a crucial factor and is related mainly to the

change in the membrane surface charge and surface structure. This surface change can be estimated by the zeta potential value. It has been found from previous literatures that increasing the pH of the feed solution leads to increasingly negative zeta potential, which represents the deprotonation of surface functional groups and also leads to electrostatic interaction or repulsion force with negatively charged pollutants.[142,192,208,221,251,318] Moreover, pore elongation or shrinkage can occur depending upon the electrostatic interactions between the dissociated functional groups of the membrane. Jin *et al.* investigated the variation in the zeta potential value of cellulose triacetate (CTA) FO membrane at various pH values ranging from 3 to 9 at room temperature.[192] This investigation showed that the active layer of membranes was negatively charged, with the zeta potential becoming more negative at a higher pH, which was due to the presence of hydroxyl groups in CTA the membrane. Therefore, it was obvious that increasing the pH of the feed solution significantly enhanced the removal rate of negatively charged organic pollutants (such as naproxen/ibuprofen) due to electrostatic repulsion; similar results were also observed by Chang.[319] Addition or blending with polymer containing functional groups such as –COOH, –OH, –CO–, and –O– significantly enhanced the negative zeta potential value.[192,251] Furthermore, during the removal of heavy metals from wastewater, the addition of some negatively charged organic materials such as humic acid (containing –COOH, –OH) create a HA-metal complex due to electrostatic interaction.[251,318] At higher pH, the zeta potential of the HA-metal complex increased causing electrostatic repulsion between the complex and negatively charge membrane, which increases the removal rate, as shown in Fig. 10.[251] But, in case of heavy metal removal from feed solution without organic materials, changing the pH of the solution resulted in different ionic forms of that individual ion, resulting in a variation of the removal and adsorption rates. For instance, at acidic pH range, the hexavalent chromium was present in the form of chromic acid (H_2CrO_4) and as the pH increases, it converts to acid chromates ($HCrO_4^-$) and with further increase in alkaline pH, it gets transformed to chromates (CrO_4^{2-}).[320] Thus, under alkaline condition, the adsorption of chromium ion is less favorable than that under acidic condition.

4.3.2. Presence of natural organic matter (NOM). A number of studies has been conducted to investigate the influence of presence of organic matters in the pollutant removal rate.[251,318,319,321] During wastewater treatment process, in most of the cases, pollutants are present in surface and ground water together with natural organic matters (NOM). In general, the concentration of NOM usually ranges from mg L^{-1} to few hundred mg L^{-1} in the form of autochthonous organic matter (*i.e.*, proteins (bovine serum albumin), lipids, nucleic acids, and polysaccharides produced by aquatic organisms) and allochthonous matter (*i.e.*, humic and fulvic acid, alcohols, amino acids, and carboxylic acids generated from the decomposition of plant residue).[208,322] Among these NOM humic substances, proteins (bovine serum albumin) and polysaccharides are the major organic foulant-creating substances.[323,324] Humic substance (HS) is considered to be the major fraction of universal

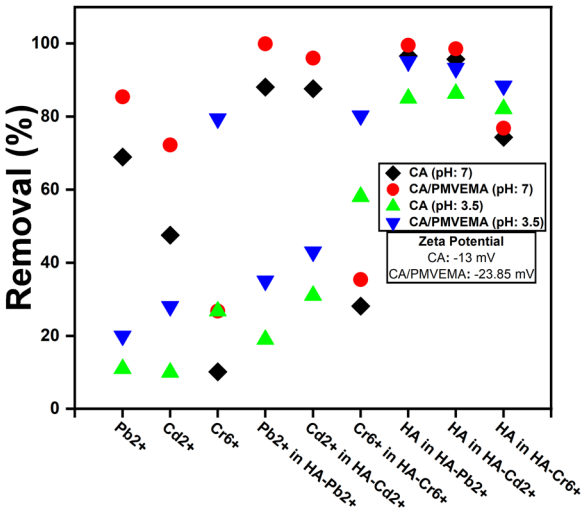

Fig. 10 Influence of pH, polymer composition, and addition of negatively-charged organic compound on removal rate of three heavy metals (Pb^{2+}, Cd^{2+}, and Cr^{6+}).[251] (Metal ion concentration = 10 ppm, Humic acid = 20 ppm, pressure = 4 bar, contact time = 2 h, rotation speed = 300 rpm, and Temperature = 25 °C).

component of natural organic matters (NOM) and structurally, they are low molecular weight refractory anionic macromolecules.[325] Moreover, HS are may be both aromatic and aliphatic substances that consist of carboxylic and phenolic functional groups and are mostly negatively charged in natural aquatic environment.[325–327] The presence of HS in the feed solution significantly influences the membrane performance and also the membrane fouling-properties.[328] A low pH of the feed solution leads to the reduction of macromolecular configuration of HS due to the reduction of electrostatic repulsion. This smaller-sized macromolecular-structured HS increased adsorption on the membrane surface. Moreover, at low pH near 4, a more thick and dense fouling layer may be formed due to electrostatic repulsion between HS and the membrane surface.[329] As the fouling rate increases at lower pH of the feed solution, it is obvious that the membrane performance also gradually reduces with time. In 1997, Hong and his coauthors demonstrated that membrane fouling increases with decreasing solution pH, thus increasing the electrolyte concentration.[326] Bovine serum albumin (BSA), another important NOM, which is a polypeptide molecule, consists of 583 amino acid residues. It can bind with metals including Ca^{2+}, Na^+, and K^+ cations present in the aqueous media due to electrostatic interaction, thus affecting the membrane performance. Another study reveals that the presence of Ca^{2+} ion in the feed solution may bind with BSA molecules and create an intermolecular bridging of the NOM molecules and enhance the membrane-fouling rate.[330] Moreover, the hydrophobic side groups present in the exterior of the BAS molecule can be improved by changing the pH of the solution.[330,331] It has been found that at low pH near the isoelectric point, BSA molecules may contain positively-charged cations, which may interact with the negatively-charged CA membrane due to electrostatic interaction, which can block the membrane pores, significantly reduce the membrane

performance, and increase the membrane fouling nature.[330] A recent study showed that in the presence of calcium ion and pH value at the isoelectric point of the feed solution, fouling due to BSA was maximized.[330] At a pH value lower and higher than the isoelectric point, the water flux was found to be almost similar, which is an indication of low membrane foulant formation. Moreover, the presence of alginate (a polysaccharide) as the co-foulant also enhanced BSA fouling on the RO membrane. The gradual increase in fouling can be due to hydrophobic interactions between BSA and alginate, known as foulant/co-foulant adhesion force.

Previous literature also suggests that there is a dependence of HS on both organic and inorganic pollutant removal, which mostly depends on the complexation or electrostatic interaction between the pollutants and HS molecules. Inorganic pollutant-containing positive charge such as all heavy metals may form a comple due to electrostatic interaction with –COOH and –OH groups of HS molecules and form a larger complex compound and cannot pass through the membrane surface (higher removal rate). Moreover, the electrostatic repulsion between the negatively-charged complex and negatively-charged CA membrane also enhanced the removal rate. Furthermore, in case of organic pollutants, organic compounds may be agglomerated and be easily separated by the membrane. For that reason, a majority of published articles agree on the fact that the retention of organic and inorganic pollutants in the CA-based membrane system tends to increase in the presence of organic matters.[251,318] In 2019, Lavanya *et al.* investigated the influence of humic acid (HA as organic matters) on the removal of three heavy metals Pb^{2+}, Cd^{2+}, and Cr^{6+} and HA (as organic pollutants).[251] This study showed that the addition of organic matters significantly improved the metal removal rate from 68.9, 47.57, and 10.12% to 88.12, 87.67, and 28.10% of Pb^{2+}, Cd^{2+}, and Cr^{6+}, respectively. Although the addition of negatively or neutral charged organic matters exhibited improved removal rate, they may block the membrane pore, which reduces the membrane performance over time.[319]

4.3.3. Transmembrane pressure and pure water flux. According to the solution-diffusion theory,[208,332] the solute removal rate is increased at higher water flux, whereas the smaller removal took place at lower flux. But, with the increment of a certain amount of pressure, the removal rate significantly reduced due to significant internal concentration polarization (ICP).[333] Ahmad *et al.*[334] found linear correlation among applied pressure, permeate flux, and removal of two pesticide (dimethoate and atrazine). In this study, two times permeate flux increment was observed when the operating pressure was doubled from 6 to 12 $\times$ 10^5 Pa, which also enhanced the removal rate. Meanwhile, pesticide concentration in the feed solution exhibited no or little impact on the permeation flux. In another study, the effect of pressure on pesticide separation was negligible in the case of a high desalting membrane, but for polar pesticides, the removal rate was significantly increased with pressure.[208] Arthanareeswaran *et al.* systematically investigated the influence of addition of polymerasic additive (PEG 600) and various transmembrane pressure (69, 138, 207, 276, 345, and 414 kPa) on membrane pure water flux.[219] The similar correlation between pressure and water flux was observed while water flux was increased with the addition of PEG 600 concentration up to 6.25%, after which the flux value was significantly declined. The reduction of water flux was due to the aggregation of the polymer blend, resulting in lower membrane pore percentile.

Similar to organic pollutant removal, heavy metals removal rate also showed similar relation with transmembrane pressure, but the removal mechanism is completely different.[320] This finding was in agreement with the study performed by Boricha *et al.*,[320] where the removal of chromium and copper ions were increased (increased linearly) by $\sim$23 and $\sim$15% respectively, from 0.4 to 1 MPa. The linear increment was due to negligible ionic concentration polarization in the membrane cell in this pressure range. Increasing both transmembrane pressure and feed flow rate significantly increased the removal efficiency of both chromium and copper ion. Under optimum operating conditions of 1 MPa transmembrane pressure and 16 LPM feed flow rate, 83.40% chromium and 72.60% copper were removed.[320]

4.3.4. Temperature. Among all other operating parameters, the temperature of the draw solution and feed solution plays an important role in influencing the membrane performances as it has direct influence on the thermodynamic properties such as diffusion coefficient and viscosity.[335] In general, increasing the operating temperature is likely to increase the solute diffusivity, thereby positively influencing the water flux, while the solute removal efficiency is significantly reduced (more solute can pass through the membrane).[335] Moreover, increasing the feed temperature led to a decrease in the solution viscosity, which significantly enhanced the mass-transfer coefficient. Furthermore, increased temperature may also lead to an increment in the membrane pore size and molecular cut-off (MWCO), which also explains the reduction in the removal efficiency and the increase in the fluxes.[336] In 2010, Boricha *et al.* fabricated N,O-carboxymethyl chitosan/cellulose acetate blend nanofiltration membrane and investigated the effect of feed temperature in the range of 30–80 °C on the removal of chromium and copper.[320] Increasing the temperature of the feed solution, a linear decrease in the percentage removal of both chromium and copper ions was obtained. Shibuya *et al.* showed the temperature dependence on osmotic-driven membrane performance of cellulose triacetate toward osmosis hollow fiber membrane and found 1.7 times increase of pure water flux at 35 °C than that measured at 15 °C owing to the higher osmotic pressure, salt diffusion coefficient, and lower water viscosity.[337]

In recent study, Xu and his coauthors investigated the influence of temperature on the retention of charged and neutral pharmaceuticals and personal care products on the nanofiltration membrane.[338] They showed that the removal rates of positively and neutrally charged micropollutants decreased with temperature increased, which was mainly due to the steric hindrance effect. In the case of negatively charged micropollutants, temperature had a negligible effect, which was possibly facilitated by the co-function of both electrostatic

repulsion and steric hindrance effect. Similar phenomena were also reported by Zhou *et al.*[336] and Hawari *et al.*[339]

5. Future prospects

The demand for ecofriendly and cost-efficient membranes to remove various organic and inorganic pollutants from wastewater has significantly increased. We have covered the current research that suggested CA-based membranes are an efficient option for removing contaminants. However, there are obstacles inhibiting the widespread industrial deployment of this unique technology because of the problems and difficulties it encounters. We recommend the following next research directions to maintain the commercial viability of the developed CA-based membranes for water treatment and to enhance environmental sustainability and safety.

• The previously reported studies have focused on the extraction of cellulose from agricultural residues. Here, pretreatment is a necessary step to separate cellulose in the purest form. All the research works applied chemical pretreatment as a general process. According to Table 1, the extracted cellulose percentage using the same chemical pretreatment process is not high enough for every lignocellulosic raw material. Hence, other options for pretreatment must be investigated to get the optimum separation of pure cellulose. Besides, for the acetylation purpose, different green synthesis routes have been approached by recent works using ecofriendly reagents. But the performance efficiency obtained in laboratory experiments may not be the same as in industrial setups. Many complications that can arise under industrial conditions must be studied to implement the green approach of CA synthesis realistically.

• Attention must also be given to developing CA-based membranes with improved thermal, mechanical, and chemical stability. From Table 2, it is evident that the phase-inversion technique has been used in maximum cases, whereas the electrospinning method can be a potential alternative with a better outcome. Moreover, for industrial applications, precautions must be taken in designing the membrane fabrication process because the performance efficiency can be altered under different industrial conditions.

• As previously discussed, one of the greatest problems of using CA membrane is their lower mechanical properties (tensile strength and elongation), gradual decrease of membrane performance (lower stability), and higher degradation rate compared to other synthetic polymer such as PAN, PVDF, PES, and PSF. The addition of inorganic nanoparticles (titanium oxide (TiO_2), zinc oxide (ZnO), copper oxide (CuO), graphene oxide (GO), silver (Ag), MXene, or graphitic carbon nitride (g-C_3N_4)) into the cellulose acetate (CA) membrane surface may lead to an increase in the mechanical, thermal, and chemical stability of the membrane.[340–344] The incorporation of nanoparticles or nanofillers up to a certain limit in the matrix leads to photocatalytic activity, which enhances the self-cleaning abilities and endows the membrane with powerful cycle stability and reusability. The simple photodegradation of organic pollutants on the nanoparticle surface (g-C_3N_4) is shown in Fig. 11d. For better photodegradation performance, nanoparticle doping with metal or

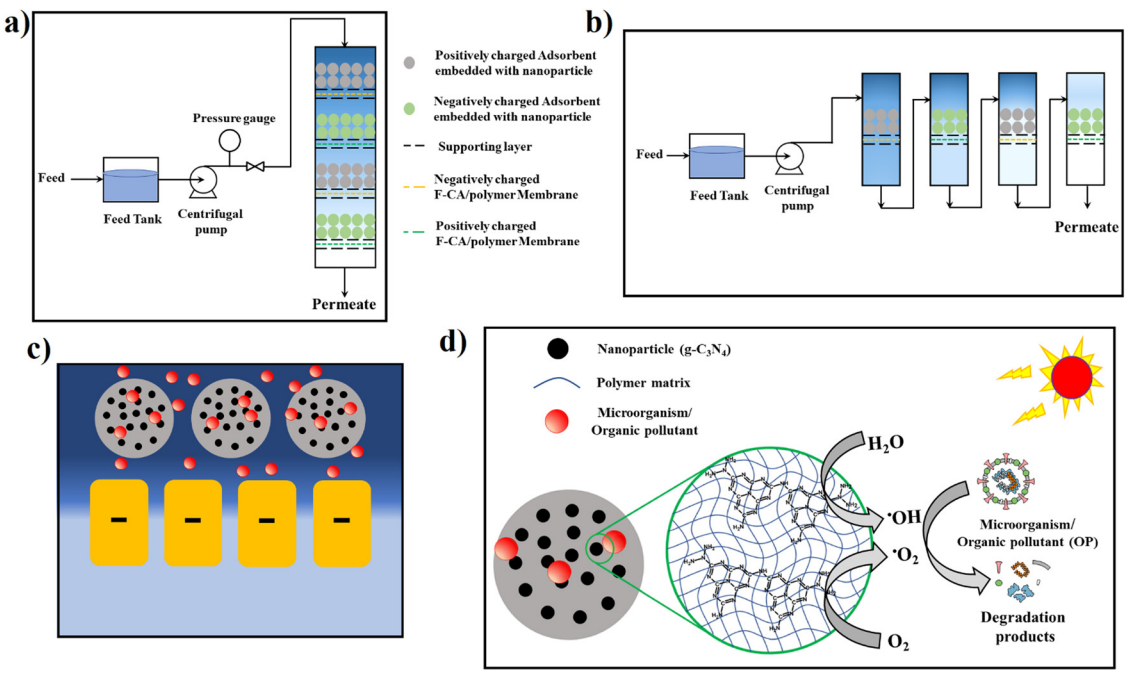

Fig. 11 A scheme proposed diagram of functionalized CA membrane-based wastewater treatment process; (a) single column with multiple compartment; each compartment composed of a F-CA/polymer with oppositely-charged adsorbent, (b) series of columns with single compartment composed of a F-CA/polymer with oppositely-charged adsorbent; (c) simple representation of pollutant removal from wastewater; and (d) proposed photodegradation mechanism of organic pollutant on the adsorbent surface embedded with nanoparticles (g-C_3N_4).

nonmetals is another approach that enhances the self-cleaning ability by lowering the band gap energy, thus leading to absorption of visible wavelength of solar radiation (act as visible-light photocatalyst). Moreover, the addition of nanoparticles or nanofillers such as MXene or g-C_3N_4 may create an interlayer-free space, which significantly increases water flux and water permeability. More interestingly, to the best of our knowledge, no available report has been published ondoped nanoparticle-based CA membrane used for wastewater reclamation system. Moreover, in the literature, a few studies have been done on membrane stability, which is a major requirement for long-time practical application. This stability also depends on the proper dispersion of nanoparticles. Inappropriate incorporation may result in the leaching of inorganic nanoparticles, which can impact our environment. For this reason, much attention should be given in the area. However, one of the major concerns during membrane modification with nanoparticles is the possible leaching of this nanoparticles and thus contaminating the source water. In these cases, these leached nanoparticles may create secondary pollution, and some cases pose health risk to the aquatic environment.[340,345] For this reason, during selection, the nanoparticle leaching rate and their cytotoxicity effect on the local environment should be carefully analyzed. A recent study showed that introducing a polishing step before membrane (nanoparticle incorporated) application for water reclamation can remove potentially leached nanoparticles.[340]

• As we know from several literatures, lower surface charge (lower zeta potential value) and lower mechanical properties of pristine CA membrane make them unsuitable for practical applications (due to lower removal efficacy). Surface modification (functionalization) and/or blending with polymer/polymers are the best options for their practical applications. In the literature, most researchers focused their attention on any one of them, but blending functionalized CA with another polymeric matrix (having excellent mechanical properties) may be another research window. In this review, we proposed two column types of functionalized electrospun CA (F-CA) coupled with other polymer (enhance mechanical properties) membranes termed as F-CA/polymer for wastewater treatment.

a. Single column with a series of compartments. Each compartment should have a functionalized CA membrane with oppositely charged adsorbents, as shown in Fig. 11a. For example, if the first compartment contains a negatively-charged F-CA/polymer membrane, in that case, the adsorbent must be positively charged. Negatively-charged pollutants (*e.g.* proteins, colloids, and foulants) are separated due to electrostatic repulsion by the negatively-charged F-CA/polymer membrane, and separated pollutants are absorbed on the positively-charged adsorbent. Similarly, positively-charged pollutants (metallic ions, positively-charged proteins) can be removed in the compartment of positively-charged F-CA/polymer membrane and negatively-charged adsorbent.

b. Series of columns with single compartment. Each column should have a functionalized CA membrane with oppositely-charged adsorbents, as shown in Fig. 11b. In this system, the feed solution initially passes through the first column, where a F-CA/polymer membrane with an oppositely-charged adsorbent removes the pollutant having the same charge of the membrane. Oppositely-charged pollutants can be removed in the second column. A series of columns can be used for better performance.

Moreover, the addition of several nanoparticles (g-C_3N_4, MXene, and GO) on the surface of the adsorbent under solar radiation results in the photodegradation of organic pollutants; thus, adsorbents can be used for a long time. However, it should be noted that the presence of nanoparticles could degrade the membrane surface, leading to a gradual decrease in membrane performance.

6. Conclusion

One of the imposing challenges to be overcome in modern society is to secure adequate water resources of desirable quality for various designated uses. To address this challenge, membrane water treatment is expected to play an increasingly important role in areas such as drinking water treatment, brackish and seawater desalination, and wastewater treatment and reuse. For satisfying these requirements, several highly efficient advanced treatment technologies have been developed. Among them, membrane technologies have achieved much more attention from researchers and technologists due to their outstanding performance, easier operation, longevity, and reusability after a simple back flush/wash (simple washing process). Moreover, the use of developed green, biodegradable, environment-friendly biopolymer-based membranes is also another imperative criterion that can mitigate environmental pollution. In this review, we briefly retrospect the development of natural biopolymer cellulose acetate-based membranes and their application in wastewater treatment, including the state-of-the-art of other commercial polymeric membranes. The greatest advantages of using CA membranes can be justified by the abundant naturally available raw materials, easy synthesis procedure, easy modifiability, and minimum impact on the environment (complete biodegradability), which are limited in the case of synthetic polymers such as polysulfone, polyether imides, and polyvinylidene fluoride. However, in the context of life-cycle, mechanical stability, and performance (lower water flux, higher antifouling properties, *etc.*), the biobased polymers are not suitable for long-term practical application. Those drawbacks can be easily solved by any four of the followings: (a) blending with another polymer; (b) functionalization; (c) incorporation of nanoparticles or nanofillers; and (d) cross-linking. After compaction with any of these, mixed matrix membranes offer the synergistic effect of the individuals: enhanced separation performance, fouling resistance, and mechanical stability for filtration applications. But it should be noted that most of these studies were based on laboratory-based, but very few reports exist on large-scale production and industrial application. More research is needed to evaluate the cost-effectiveness of large-scale industrial applications. Moreover, to date, there is almost no study based on the compaction

of all four solutions (as mentioned above) in a single membrane system. Although each of the above solutions possess several limitations, extensive research should be done in these directions to find the optimum composition and operating conditions to improve the performance as well as the longevity of the membrane.

Author contributions

Md. Didarul Islam: data curation; formal analysis; investigation; methodology; software; visualization; writing – original draft; writing - review & editing. Foyez Jalal Uddin: data curation; formal analysis; investigation; methodology; software; visualization; writing – original draft; writing - review & editing. Taslim Ur Rashid: conceptualization; investigation; project administration; resources; supervision; software; visualization; writing – original draft; writing – review & editing. Mohammad Shahruzzaman: conceptualization; investigation; project administration; resources; supervision; writing – original draft; writing – review & editing.

Conflicts of interest

The authors declare no competing financial interest.

References

1 T. U. Rashid, S. M. F. Kabir, M. C. Biswas and M. A. R. Bhuiyan, *Ind. Eng. Chem. Res.*, 2020, **59**, 9719–9745.
2 M. D. Islam, M. M. Hasan, A. Rahaman, P. Haque and M. M. Rahman, *SN Appl. Sci.*, 2020, **2**, 1–11.
3 R. P. Schwarzenbach, T. Egli, T. B. Hofstetter, U. Von Gunten and B. Wehrli, *Annu. Rev. Environ. Resour.*, 2010, **35**, 109–136.
4 M. Uddin, M. Hasan, M. Islam, A. Rahaman and S. M. Shamsuddin, *Text. Leather Rev.*, 2020, **3**, 64–77.
5 M. N. Hossain, M. D. Islam, A. Rahaman, N. Khatun and M. A. Matin, *Appl. Water Sci.*, 2023, **13**, 73.
6 E. O. Ezugbe and S. Rathilal, *Membranes*, 2020, **10**, 89.
7 S. Biswas, T. U. Rashid, T. Debnath, P. Haque and M. M. Rahman, *J. Compos. Sci.*, 2020, **4**, 16.
8 N. Khatun, M. N. Hossain, M. D. Islam and A. Rahaman, *Pollution*, 2023, **9**, 531–544.
9 R. S. Dongre, K. K. Sadasivuni, K. Deshmukh, A. Mehta, S. Basu, J. S. Meshram, M. A. A. Al-Maadeed and A. Karim, *Polym.-Plast. Technol. Mater.*, 2019, **58**, 1295–1310.
10 S. Biswas, J. Fatema, T. Debnath and T. U. Rashid, *ACS ES&T Water*, 2021, **1**, 1055–1085.
11 T. Saha, Z. Uddin, M. N. Islam, M. Shamsuzzaman, A. Al Tahsin and M. D. Islam, *Text. Leather Rev.*, 2022, **5**, 103–119.
12 R. A. Hamza, O. T. Iorhemen and J. H. Tay, *Environ. Technol. Innovation*, 2016, **5**, 161–175.
13 M. M. Mahdi, M. D. Islam and M. A. Hossain, *Current Developments in Biotechnology and Bioengineering*, 2023, pp. 139–152.
14 M. D. Islam and M. M. Mahdi, *Biodegrad. Detoxif. Micropollutants Ind. Wastewater*, 2022, pp. 1–26.
15 M. D. Islam, M. M. Mahdi, M. A. Hossain and M. M. Abedin, *Wastewater Treat.*, 2022, pp. 139–156.
16 S. Mansoori, R. Davarnejad, T. Matsuura and A. F. Ismail, *Polym. Test.*, 2020, **84**, 106381.
17 J. M. O. Pulido, *Sci. Total Environ.*, 2016, **563**, 664–675.
18 M. Islam, A. Rahaman, M. M. Mahdi and M. Hossain, *Environ. Degrad. Monit. Assess. Treat. Technol.*, 2022, pp. 1–13.
19 Z. Pan, C. Song, L. Li, H. Wang, Y. Pan, C. Wang, J. Li, T. Wang and X. Feng, *Chem. Eng. J.*, 2019, **376**, 120909.
20 J. R. Werber, C. O. Osuji and M. Elimelech, *Nat. Rev. Mater.*, 2016, **1**, 16018.
21 F. Galiano, K. Briceño, T. Marino, A. Molino, K. V. Christensen and A. Figoli, *J. Membr. Sci.*, 2018, **564**, 562–586.
22 B. Peng, Z. Yao, X. Wang, M. Crombeen, D. G. Sweeney and K. C. Tam, *Green Energy Environ.*, 2020, **5**, 37–49.
23 M. M. Hasan, M. D. Islam and T. U. Rashid, *Energy Fuels*, 2020, **34**, 15634–15671.
24 V. K. Thakur and S. I. Voicu, *Carbohydr. Polym.*, 2016, **146**, 148–165.
25 N. S. A. Rahman, M. F. Yhaya, B. Azahari and W. R. Ismail, *Cellulose*, 2018, **25**, 4887–4903.
26 M. A. Mohamed, M. Abd Mutalib, Z. A. Mohd Hir, M. F. M. Zain, A. B. Mohamad, L. Jeffery Minggu, N. A. Awang and W. N. W. Salleh, *Int. J. Biol. Macromol.*, 2017, **103**, 1232–1256.
27 D. Araújo, M. C. R. Castro, A. Figueiredo, M. Vilarinho and A. Machado, *J. Cleaner Prod.*, 2020, **260**, 120865.
28 A. Ghaee, M. Shariaty-Niassar, J. Barzin, T. Matsuura and A. Fauzi Ismail, *Desalin. Water Treat.*, 2016, **57**, 14453–14460.
29 A. Rajeswari, S. Vismaiya and A. Pius, *Chem. Eng. J.*, 2017, **313**, 928–937.
30 N. Cândido, M. Teresa and P. Amorim, *Mater. Today: Proc.*, 2020, **21**, 315–317.
31 M. Chen, R.-M. Li, T. Runge, J. Feng, J. Feng, S. Hu and Q.-S. Shi, *ACS Sustainable Chem. Eng.*, 2019, **7**, 16971–16978.
32 J. Chen, J. Xu, K. Wang, X. Cao and R. Sun, *Carbohydr. Polym.*, 2016, **137**, 685–692.
33 L. Yan, W. Li, Z. Qi and S. Liu, *J. Polym. Res.*, 2006, **13**, 375–378.
34 J. S. Jo, J. Young Jung, J. H. Byun, B. K. Lim and J. K. Yang, *J. Korean Wood Sci. Technol.*, 2016, **44**, 241–252.
35 A. El Nemr, S. Ragab and A. El Sikaily, *Iran. Polym. J.*, 2017, **26**, 261–272.
36 G. B. Nagarajappa, K. K. Pandey, A. S. Shinde and H. M. Vagdevi, *Holzforschung*, 2016, **70**, 421–427.
37 J. Luo and Y. Sun, *J. Appl. Polym. Sci.*, 2006, **100**, 3288–3296.
38 Y. Sun and J. Cheng, *Bioresour. Technol.*, 2002, **83**, 1–11.
39 R. Battisti, E. Hafemann, C. A. Claumann, R. A. F. Machado and C. Marangoni, *Polym. Eng. Sci.*, 2019, **59**, 891–898.
40 G. Fan, M. Wang, C. Liao, T. Fang, J. Li and R. Zhou, *Carbohydr. Polym.*, 2013, **94**, 71–76.
41 R. R. M. De Freitas, A. M. Senna and V. R. Botaro, *Ind. Crops Prod.*, 2017, **109**, 452–458.

42 J. Chen, J. Xu, K. Wang, X. Cao and R. Sun, *Carbohydr. Polym.*, 2016, **137**, 685–692.
43 K. Kamide and M. Saito, *Polym. J.*, 1985, **17**, 919–928.
44 S. Fischer, K. Thümmler, B. Volkert, K. Hettrich, I. Schmidt and K. Fischer, *Macromol. Symp.*, 2008, **262**, 89–96.
45 R. R. M. de Freitas, A. M. Senna and V. R. Botaro, *Ind. Crops Prod.*, 2017, **109**, 452–458.
46 P. Fei, L. Liao, B. Cheng and J. Song, *Anal. Methods*, 2017, **9**, 6194–6201.
47 H. Kono, H. Hashimoto and Y. Shimizu, *Carbohydr. Polym.*, 2015, **118**, 91–100.
48 W. R. W. Daud and F. M. Djuned, *Carbohydr. Polym.*, 2015, **132**, 252–260.
49 R. Yadollahi, M. Dehghani Firouzabadi, H. Mahdavi, A. Saraeyan, H. Resalati, K. S. Mikkonen and H. Sixta, *Cellulose*, 2019, **26**, 6119–6132.
50 A. El Nemr, S. Ragab and A. El Sikaily, *Carbohydr. Polym.*, 2016, **151**, 1058–1067.
51 H. N. Cheng, M. K. Dowd, G. W. Selling and A. Biswas, *Carbohydr. Polym.*, 2010, **80**, 449–452.
52 X. Zhang, W. Zhang, D. Tian, Z. Zhou and C. Lu, *RSC Adv.*, 2013, **3**, 7722.
53 S. S. Z. Hindi and R. A. Abohassan, *BioResources*, 2015, **10**, 5030–5048.
54 L. J. Konwar, P. Mäki-Arvela, A. J. Thakur, N. Kumar and J.-P. Mikkola, *RSC Adv.*, 2016, **6**, 8829–8837.
55 A. Nabili, A. Fattoum, M.-C. Brochier-Salon, J. Bras and E. Elaloui, *Iran. Polym. J.*, 2017, **26**, 137–147.
56 Z. Yang, S. Xu, X. Ma and S. Wang, *Wood Sci. Technol.*, 2008, **42**, 621–632.
57 X. Sun, C. Lu, W. Zhang, D. Tian and X. Zhang, *Carbohydr. Polym.*, 2013, **98**, 405–411.
58 D. Tian, Y. Han, C. Lu, X. Zhang and G. Yuan, *Carbohydr. Polym.*, 2014, **113**, 83–90.
59 A. El Nemr, S. Ragab, A. El Sikaily and A. Khaled, *Carbohydr. Polym.*, 2015, **130**, 41–48.
60 R. Maryana, E. T. Muryanto, O. Oktaviani, H. Prasetia, A. K. Das and Y. Sudiyani, *Waste and Biomass Valorization*, 2022, **13**, 1535–1545.
61 M. P. Egot and A. C. Alguno, *Key Eng. Mater.*, 2018, **772**, 8–12.
62 A. M. Das, A. A. Ali and M. P. Hazarika, *Carbohydr. Polym.*, 2014, **112**, 342–349.
63 R. G. Candido and A. R. Gonçalves, *Carbohydr. Polym.*, 2016, **152**, 679–686.
64 J. A. A. Alves, M. D. L. dos Santos, C. C. Morais, J. L. R. Ascheri, R. Signini, D. M. dos Santos, S. M. C. Bastos and D. P. R. Ascheri, *Int. J. Biol. Macromol.*, 2019, **135**, 877–886.
65 Y. Yang, L. Song, C. Peng, E. Liu and H. Xie, *Green Chem.*, 2015, **17**, 2758–2763.
66 Y. Cao, J. Wu, T. Meng, J. Zhang, J. He, H. Li and Y. Zhang, *Carbohydr. Polym.*, 2007, **69**, 665–672.
67 N. C. Homem and M. T. P. Amorim, *Mater. Today: Proc.*, 2020, **31**, 315–317.
68 G. R. Filho, D. S. Monteiro, C. da Silva Meireles, R. M. N. De Assunção, D. A. Cerqueira, H. S. Barud, S. J. L. Ribeiro and Y. Messadeq, *Carbohydr. Polym.*, 2008, **73**, 74–82.
69 O. Jogunola, V. Eta, M. Hedenström, O. Sundman, T. Salmi and J.-P. Mikkola, *Carbohydr. Polym.*, 2016, **135**, 341–348.
70 J. Cao, X. Sun, C. Lu, Z. Zhou, X. Zhang and G. Yuan, *Carbohydr. Polym.*, 2016, **149**, 60–67.
71 T. Kakko, A. W. T. King and I. Kilpeläinen, *Cellulose*, 2017, **24**, 5341–5354.
72 S. Suzuki, R. Yada, Y. Hamano, N. Wada and K. Takahashi, *ACS Sustainable Chem. Eng.*, 2020, **8**, 9002–9008.
73 G. Alfassi, D. M. Rein and Y. Cohen, *J. Polym. Sci., Part A: Polym. Chem.*, 2018, **56**, 2458–2462.
74 V. Eta and J.-P. Mikkola, *Carbohydr. Polym.*, 2016, **136**, 459–465.
75 R. G. Candido, G. G. Godoy and A. R. Gonçalves, *Carbohydr. Polym.*, 2017, **167**, 280–289.
76 C. Achtel and T. Heinze, *Macromol. Chem. Phys.*, 2016, **217**, 2041–2048.
77 Y. Yu, J. Miao, Z. Jiang, H. Sun and L. Zhang, *Appl. Phys. A: Mater. Sci. Process.*, 2016, **122**, 656.
78 J. Li, L.-P. Zhang, F. Peng, J. Bian, T.-Q. Yuan, F. Xu and R.-C. Sun, *Molecules*, 2009, **14**, 3551–3566.
79 J. Wu, J. Zhang, H. Zhang, J. He, Q. Ren and M. Guo, *Biomacromolecules*, 2004, **5**, 266–268.
80 X. Cao, X. Peng, L. Zhong, S. Sun, D. Yang, X. Zhang and R. Sun, *Cellulose*, 2014, **21**, 581–594.
81 X. Cao, S. Sun, X. Peng, L. Zhong, R. Sun and D. Jiang, *J. Agric. Food Chem.*, 2013, **61**, 2489–2495.
82 X. Gao, H. Liu, J. Shuai, J. Zhao, G. Zhou, Q. Huang, H. Ling, W. Ge and X. Wang, *Int. J. Biol. Macromol.*, 2023, **242**, 125133.
83 Y. Ertas and T. Uyar, *Carbohydr. Polym.*, 2017, **177**, 378–387.
84 H. Etemadi, R. Yegani and V. Babaeipour, *J. Appl. Polym. Sci.*, 2017, **134**, 1–14.
85 H. Etemadi, R. Yegani and M. Seyfollahi, *Sep. Purif. Technol.*, 2017, **177**, 350–362.
86 S. Beisl, S. Monteiro, R. Santos, A. S. Figueiredo, M. G. Sánchez-Loredo, M. A. Lemos, F. Lemos, M. Minhalma and M. N. de Pinho, *Water Res.*, 2019, **149**, 225–231.
87 W. Ma, Z. Guo, J. Zhao, Q. Yu, F. Wang, J. Han, H. Pan, J. Yao, Q. Zhang, S. K. Samal, S. C. De Smedt and C. Huang, *Sep. Purif. Technol.*, 2017, **177**, 71–85.
88 A. M. Asiri, F. Petrosino, V. Pugliese, S. B. Khan, K. A. Alamry, S. Y. Alfifi, H. M. Marwani, M. M. Alotaibi, C. Algieri and S. Chakraborty, *Polymers (Basel).*, 2021, **14**, 4.
89 A. M. Pandele, F. E. Comanici, C. A. Carp, F. Miculescu, S. I. Voicu, V. K. Thakur and B. C. Serban, *Vacuum*, 2017, **146**, 599–605.
90 A. A. Hamad, M. S. Hassouna, T. I. Shalaby, M. F. Elkady, M. A. A. Elkawi and H. A. Hamad, *Int. J. Biol. Macromol.*, 2020, **151**, 1299–1313.
91 P. A. Vinodhini, K. Sangeetha, G. Thandapani, P. N. Sudha, V. Jayachandran and A. Sukumaran, *Int. J. Biol. Macromol.*, 2017, **104**, 1721–1729.
92 A. Ahmad, S. Waheed, S. M. Khan, S. E-Gul, M. Shafiq, M. Farooq, K. Sanaullah and T. Jamil, *Desalination*, 2015, **355**, 1–10.

93 A. Sabir, M. Shafiq, A. Islam, A. Sarwar, M. R. Dilshad, A. Shafeeq, M. T. Zahid Butt and T. Jamil, *Carbohydr. Polym.*, 2015, **132**, 589–597.
94 J. Yin, H. Fan and J. Zhou, *Desalin. Water Treat.*, 2016, **57**, 10572–10584.
95 X. Wang, X. Wang, P. Xiao, J. Li, E. Tian, Y. Zhao and Y. Ren, *Colloids Surf., A*, 2016, **508**, 327–335.
96 S. Yang, Q. Zou, T. Wang and L. Zhang, *J. Membr. Sci.*, 2019, **569**, 48–59.
97 H. Choi, M. Son, S. Yoon, E. Celik, S. Kang, H. Park, C. H. Park and H. Choi, *Chemosphere*, 2015, **136**, 204–210.
98 F. Sabeti Dehkordi, M. Pakizeh and M. Namvar-Mahboub, *Appl. Clay Sci.*, 2015, **105–106**, 178–185.
99 L. A. Goetz, B. Jalvo, R. Rosal and P. Aji, *J. Membr. Sci.*, 2016, **510**, 238–248.
100 J. Lv, G. Zhang, H. Zhang and F. Yang, *Carbohydr. Polym.*, 2017, **174**, 190–199.
101 K. A. Gebru and C. Das, *Chemosphere*, 2018, **191**, 673–684.
102 Z. Sun and F. Chen, *Int. J. Biol. Macromol.*, 2016, **91**, 143–150.
103 T. Riaz, A. Ahmad, S. Saleemi, M. Adrees, F. Jamshed, A. M. Hai and T. Jamil, *Carbohydr. Polym.*, 2016, **153**, 582–591.
104 A. Sagle and B. Freeman, *Futur. Desalin. Texas*, 2004, 1–17.
105 M. A. A. El-Ghaffar, M. M. Elawady, A. M. Rabie and A. E. Abdelhamid, *J. Polym. Res.*, 2020, **27**, 1–12.
106 F. Li, P. Fei, B. Cheng, J. Meng and L. Liao, *Carbohydr. Polym.*, 2019, **216**, 312–321.
107 A. A. Taha, Y. Wu, H. Wang and F. Li, *J. Environ. Manage.*, 2012, **112**, 10–16.
108 Y. Tian, M. Wu, R. Liu, Y. Li, D. Wang, J. Tan, R. Wu and Y. Huang, *Carbohydr. Polym.*, 2011, **83**, 743–748.
109 H. Yu, H. Liu, X. Yuan, W. Ding, Y. Li and J. Wang, *Chemophere*, 2019, **235**, 239–247.
110 Y. Liu, M. Zhu, M. Chen, L. Ma, B. Yang, L. Li and W. Tu, *Chem. Eng. J.*, 2019, **359**, 47–57.
111 W. Lu, Z. Wei, Z. Gu, T. Liu and J. Park, *Chem. Soc. Rev.*, 2014, **43**, 5561–5593.
112 J. D. Evans, C. J. Sumby and C. J. Doonan, *Chem. Soc. Rev.*, 2014, **43**, 5933–5951.
113 A. Zirehpour, A. Rahimpour, S. Khoshhal, M. D. Firouzjaei and A. A. Ghoreyshi, *RSC Adv.*, 2016, **6**, 70174–70185.
114 G. Gnanasekaran, S. Balaguru and D. B. Das, *Sep. Sci. Technol.*, 2019, **54**, 434–446.
115 L. Joseph, B. M. Jun, M. Jang, C. M. Park, J. C. Muñoz-Senmache, A. J. Hernández-Maldonado, A. Heyden, M. Yu and Y. Yoon, *Chem. Eng. J.*, 2019, **369**, 928–946.
116 B. Jun, S. Kim, Y. Kim, N. Her, J. Heo, J. Han, M. Jang, C. M. Park and Y. Yoon, *Chemosphere*, 2019, **231**, 82–92.
117 B. M. Jun, J. Heo, C. M. Park and Y. Yoon, *Chemosphere*, 2019, **235**, 527–537.
118 B. M. Jun, S. Kim, J. Heo, N. Her, M. Jang, C. M. Park and Y. Yoon, *Ultrason. Sonochem.*, 2019, **56**, 174–182.
119 S. L. Hou, J. Dong, X. L. Jiang, Z. H. Jiao and B. Zhao, *Angew. Chem., Int. Ed.*, 2019, **58**, 577–581.
120 Y. S. Wei, M. Zhang, R. Zou and Q. Xu, *Chem. Rev.*, 2020, **120**, 12089–12174.
121 K. Z. Rui Li and W. Zhang, *Adv. Mater.*, 2018, **30**, 1705512.
122 M. U. Alireza Zirehpour and A. Rahimpour, *J. Membr. Sci.*, 2017, **531**, 59–67.
123 Q. Lyu, X. Deng, S. Hu, L. C. Lin and W. W. Ho, *J. Phys. Chem. C*, 2019, **123**, 16118–16126.
124 H. M. Park, K. Y. Jee and Y. T. Lee, *J. Membr. Sci.*, 2017, **541**, 510–518.
125 H. Liu, M. Zhang, H. Zhao, Y. Jiang, G. Liu and J. Gao, *RSC Adv.*, 2020, **10**, 4045–4057.
126 Y. Xiao, W. Zhang, Y. Jiao, Y. Xu and H. Lin, *J. Membr. Sci.*, 2021, **624**, 119101.
127 F. Gholami, S. Zinadini, A. A. Zinatizadeh and A. R. Abbasi, *Sep. Purif. Technol.*, 2018, **194**, 272–280.
128 B. T. P. W. Huazhen Sun, *J. Membr. Sci.*, 2018, **551**, 283–293.
129 S. Wang and Y. Peng, *Chem. Eng. J.*, 2010, **156**, 11–24.
130 L. Lin, A. Wang, M. Dong, Y. Zhang, B. He and H. Li, *J. Hazard. Mater.*, 2012, **203**, 204–212.
131 R. N. Putra and Y. H. Lee, *Sep. Purif. Technol.*, 2020, **237**, 116351.
132 F. Ji, C. Li, B. Tang, J. Xu, G. Lu and P. Liu, *Chem. Eng. J.*, 2012, **209**, 325–333.
133 M. Sivakumar, D. R. Mohan and R. Rangarajan, *J. Membr. Sci.*, 2006, **268**, 208–219.
134 A. Filimon, A. M. Dobos and V. Musteata, *Carbohydr. Polym.*, 2019, **226**, 115300.
135 M. Sivakumar, D. R. Mohan, R. Rangarajan and Y. Tsujita, *Polym. Int.*, 2005, **54**, 956–962.
136 S. Vidya and D. Mohan, *Sep. Sci. Technol.*, 2010, **45**, 740–750.
137 G. Arthanareeswaran, C. S. Latha, D. Mohan, M. Raajenthiren and K. Srinivasan, *Sep. Sci. Technol.*, 2006, **41**, 2895–2912.
138 D. L. Arockiasamy and A. Nagendran, *Sep. Sci. Technol.*, 2009, **44**, 398–421.
139 P. Moradihamedani and A. H. Abdullah, *Water Sci. Technol.*, 2017, **75**, 2422–2433.
140 K. A. Gebru and C. Das, *J. Water Process Eng.*, 2017, **16**, 1–13.
141 C. Liu and R. Bai, *J. Membr. Sci.*, 2006, **284**, 313–322.
142 R. Al-wafi, M. K. Ahmed and S. F. Mansour, *J. Water Process Eng.*, 2020, **38**, 101543.
143 S. Yu, M. Liu, M. Ma, M. Qi, Z. Lü and C. Gao, *J. Membr. Sci.*, 2010, **350**, 83–91.
144 S. Yang, Q. Zou and T. Wang, *J. Membr. Sci.*, 2018, **569**, 48–59.
145 S. Rajesh, A. Jayalakshmi, S. Senthilkumar, H. S. H. Sankar and D. R. Mohan, *Ind. Eng. Chem. Res.*, 2011, **50**, 14016–14029.
146 D. Zamel, A. H. Hassanin, R. Ellethy, G. Singer and A. Abdelmoneim, *Sci. Rep.*, 2019, **9**, 1–11.
147 J. Zhou, J. Chen, M. He and J. Yao, *J. Appl. Polym. Sci.*, 2016, **133**, 1–7.
148 S. Shenvi, A. F. Ismail and A. M. Isloor, *Ind. Eng. Chem. Res.*, 2014, **53**, 13820–13827.
149 K. Wang, Q. Ma, S. D. Wang, H. Liu, S. Z. Zhang, W. Bao, K. Q. Zhang and L. Z. Ling, *Appl. Phys. A: Mater. Sci. Process.*, 2016, **122**, 1–10.

150 R. Abedini, S. M. Mousavi and R. Aminzadeh, *Desalination*, 2011, **277**, 40–45.
151 M. E. El-Naggar, A. Abdel-Karim, E. K. Radwan, W. Sharmoukh, A. R. Wassel, A. M. Bayoumy and M. Ibrahim, *J. Clean. Prod.*, 2021, **324**, 129288.
152 A. F. de Faria, A. C. M. de Moraes, P. F. Andrade, D. S. da Silva, M. do Carmo Gonçalves and O. L. Alves, *Cellulose*, 2017, **24**, 781–796.
153 C. A. Fuenmayor, S. M. Lemma, S. Mannino, T. Mimmo and M. Scampicchio, *J. Food Eng.*, 2014, **122**, 110–116.
154 A. Rajeswari, E. J. Christy, G. I. Mary, K. Jayaraj and A. Pius, *J. Environ. Chem. Eng.*, 2019, **7**, 103278.
155 M. M. H. El-sayed, R. E. Elsayed, A. Attia, H. H. Farghal, R. A. Azzam and T. M. Madkour, *Carbohydr. Polym. Technol. Appl.*, 2021, **2**, 100123.
156 W. Chen, H. Ma and B. Xing, *Int. J. Biol. Macromol.*, 2020, **158**, 1342–1351.
157 J. Cheng, C. Zhan, J. Wu, Z. Cui, J. Si, Q. Wang, X. Peng and L. Turng, *ACS Omega*, 2020, **5**, 5389–5400.
158 M. Kumar, A. M. Isloor, S. Rao, T. G. P. Syed and I. Inamuddin, *Environ. Chem. Lett.*, 2020, **18**, 881–887.
159 M. A. Silva, L. Hilliou and M. P. de Amorim, *Polym. Bull.*, 2020, **77**, 623–653.
160 S. Yu, Q. Cheng, C. Huang, J. Liu, X. Peng and M. Liu, *J. Membr. Sci.*, 2013, **434**, 44–54.
161 N. M. Aboamera, A. Mohamed and A. Khattab, *Cellulose*, 2018, **25**, 4155–4166.
162 A. Celebioglu, F. Topuz, Z. I. Yildiz and T. Uyar, *ACS Omega*, 2019, **4**, 7850–7860.
163 A. S. Tsibart and A. N. Gennadiev, *Eurasian Soil Sci.*, 2013, **46**, 728–741.
164 C. Sun, J. Zhang, Q. Ma, Y. Chen and H. Ju, *Environ. Geochem. Health*, 2017, **39**, 63–74.
165 L. H. Keith, *Polycyclic Aromat. Compd.*, 2015, **35**, 147–160.
166 A. Celebioglu, F. Topuz, Z. I. Yildiz and T. Uyar, *ACS Omega*, 2019, **4**, 7850–7860.
167 B. Nas, M. E. Argun, T. Dolu, H. Ateş, E. Yel, S. Koyuncu, S. Dinç and M. Kara, *J. Environ. Manage.*, 2020, **268**, 110580.
168 Z. U. Zango, N. S. Sambudi, K. Jumbri, A. Ramli, N. H. H. A. Bakar, B. Saad, M. N. H. Rozaini, H. A. Isiyaka, A. M. Osman and A. Sulieman, *Water*, 2020, **12**, 1–40.
169 A. A. Akinpelu, M. E. Ali, M. R. Johan, R. Saidur, M. A. Qurban and T. A. Saleh, *Process Saf. Environ. Prot.*, 2019, **122**, 68–82.
170 A. Mojiri, J. L. Zhou, A. Ohashi, N. Ozaki and T. Kindaichi, *Sci. Total Environ.*, 2019, **696**, 133971.
171 S. Lamichhane, K. C. B. Krishna and R. Sarukkalige, *Chemosphere*, 2016, **148**, 336–353.
172 I. Oller, S. Malato and J. A. Sánchez-Pérez, *Sci. Total Environ.*, 2011, **409**, 4141–4166.
173 X. Wang, C. Chen, J. Li and X. Wang, *Chem. Eng. J.*, 2015, **262**, 1303–1310.
174 H. I. Abdel-shafy, H. E. Sayour and M. S. M. Mansour, *Polym. Adv. Technol.*, 2016, **27**, 724–732.
175 A. Celebioglu, S. Demirci and T. Uyar, *Appl. Surf. Sci.*, 2014, **305**, 581–588.
176 X. Li, Y. Zhu, T. Wu, S. Zhang and P. Christie, *Environ. Sci. Technol.*, 2010, **44**, 297–301.
177 K. Tungala, P. Adhikary and S. Krishnamoorthi, *Carbohydr. Polym.*, 2013, **95**, 295–298.
178 F. Kayaci, Z. Aytac and T. Uyar, *J. Hazard. Mater.*, 2013, **261**, 286–294.
179 N. N. M. Yusof, E. Tanioka and T. Kobayashi, *Sep. Purif. Technol.*, 2014, **122**, 341–349.
180 L. Donato, F. Tasselli and E. Drioli, *Sep. Sci. Technol.*, 2010, **45**, 2273–2279.
181 H. E. Emam, M. El-shahat and R. M. Abdelhameed, *J. Hazard. Mater.*, 2021, **414**, 125509.
182 Y. Mameri, N. Debbache, M. E. M. Benacherine, N. Seraghni and T. Sehili, *J. Photochem. Photobiol., A*, 2016, **315**, 129–137.
183 B. Jun, Y. A. J. Al-hamadani, A. Son, C. M. Park, M. Jang, A. Jang, N. C. Kim and Y. Yoon, *Sep. Purif. Technol.*, 2020, **247**, 116947.
184 C. Su, Y. Cui, D. Liu, H. Zhang and Y. Baninla, *Sci. Total Environ.*, 2020, **720**, 137652.
185 L. J. Carter, B. Chefetz, Z. Abdeen and A. B. Boxall, *Environ. Sci.: Processes Impacts*, 2019, **21**, 605–622.
186 P. S. Nasirabadi, E. Saljoughi and S. M. Mousavi, *Desalin. Water Treat.*, 2016, **57**, 24146–24175.
187 F. J. Benitez, J. L. Acero, F. J. Real, G. Rold and E. Rodriguez, *J. Chem. Technol. Biotechnol.*, 2011, **86**, 858–866.
188 R. M. Narbaitz, D. Rana, H. T. Dang, J. Morrissette, T. Matsuura, S. Y. Jasim, S. Tabe and P. Yang, *Chem. Eng. J.*, 2013, **225**, 848–856.
189 L. Penabad-pen, J. Herrera-morales, M. Betancourt and E. Nicolau, *ACS Omega*, 2019, **4**, 22463.
190 S. Yüksel, N. Kabay and M. Yüksel, *J. Hazard. Mater.*, 2013, **263**, 307–310.
191 D. Rana, B. Scheier, R. M. Narbaitz, T. Matsuura, S. Tabe, S. Y. Jasim and K. C. Khulbe, *J. Membr. Sci.*, 2012, **409**, 346–354.
192 X. Jin, J. Shan, C. Wang, J. Wei and C. Y. Tang, *J. Hazard. Mater.*, 2012, **227–228**, 55–61.
193 N. K. Khanzada, M. U. Farid, J. A. Kharraz, C. Y. Tang, L. D. Nghiem, A. Jang and A. K. An, *J. Membr. Sci.*, 2019, **598**, 117672.
194 H. Etemadi and R. Yegani, *Biofouling*, 2019, **35**, 618–630.
195 E. Vasile and A. M. Pandele, *Carbohydr. Polym.*, 2019, **214**, 204–212.
196 H. Mahdavi and R. Bagherifar, *J. Iran. Chem. Soc.*, 2018, **15**, 2839–2849.
197 S. Das, A. Barui and A. Adak, *J. Water Process Eng.*, 2020, **37**, 101497.
198 K. Kimura, S. Toshima, G. Amy and Y. Watanabe, *J. Membr. Sci.*, 2004, **245**, 71–78.
199 A. El-gendi, H. Abdallah, A. Amin and S. K. Amin, *J. Mol. Struct.*, 2017, **1146**, 14–22.
200 A. S. Nor Munirah Abdullah, A. Mimi Mazira and M. T. Ramlah, *Key Eng. Mater.*, 2014, **594**, 281–285.
201 G. F. De Castro, J. A. Ferreira, D. Eulálio, A. Robledo, V. Regina, L. Constantino, F. G. Pinto, R. F. Novais and J. Tronto, *J. Agric. Sci. Technol. B*, 2018, **8**, 360–374.

202 K. Azzaoui, A. Lamhamdi, E. Miloud, M. Berrabah, B. Hammouti, A. Elidrissi, M. M. G. Fouda and S. S. Aldeyab, *Carbohydr. Polym.*, 2014, **111**, 41–46.
203 J. Herrera-Morales, T. A. Turley, M. Betancourt-Ponce and E. Nicolau, *Materials*, 2019, **12**, 230.
204 M. Chaudhary and A. Maiti, *J. Membr. Sci.*, 2020, **611**, 118372.
205 R. Mukherjee and S. De, *J. Hazard. Mater.*, 2014, **265**, 8–19.
206 X. Jin, J. Hu and S. L. Ong, *Water Res.*, 2010, **44**, 638–648.
207 World Health Organization, Guidelines on Public Health Pesticide Management Policy, 2010.
208 K. V. Plakas and A. J. Karabelas, *Desalination*, 2012, **287**, 255–265.
209 T. Sultana, C. Murray, S. Kleywegt and C. D. Metcalfe, *Chemosphere*, 2018, **202**, 506–513.
210 X. Jin, Y. Liu, X. Qiao, R. Guo, C. Liu, X. Wang and X. Zhao, *Ecotoxicol. Environ. Saf.*, 2019, **182**, 109390.
211 The European Parliament and the Council of the European Union, Directive (EU) 2020/2184, EU Drinking Water Directive., 2020, vol. 2019.
212 World Health Organisation (WHO), The Who recommended clasification of pesticides by hazard, 2009.
213 Environment Protection Authority, EPA Guidelines for: Responsible Pesticide Use, 2005.
214 H. Hinden, *Water Sewage Works*, 1969, **116**, 446–470.
215 E. S. K. Chian, W. N. Bruce and H. H. P. Fang, *Environ. Sci. Technol.*, 1975, **9**, 52–59.
216 C. Lv, Y. Su, Y. Wang, X. Ma, Q. Sun and Z. Jiang, *J. Membr. Sci.*, 2007, **294**, 68–74.
217 N. Ghaemi, S. S. Madaeni, A. Alizadeh, H. Rajabi, P. Daraei and M. Falsa, *Desalination*, 2012, **301**, 26–41.
218 E. Saljoughi, M. Amirilargani and T. Mohammadi, *Desalination*, 2010, **262**, 72–78.
219 G. Arthanareeswaran, P. Thanikaivelan, K. Srinivasn, D. Mohan and M. Rajendran, *Eur. Polym. J.*, 2004, **40**, 2153–2159.
220 E. Saljoughi and T. Mohammadi, *Desalination*, 2009, **249**, 850–854.
221 N. Ghaemi, S. S. Madaeni, A. Alizadeh, P. Daraei, V. Vatanpour and M. Falsa, *Desalination*, 2012, **290**, 99–106.
222 N. Ghaemi, S. S. Madaeni, A. Alizadeh, P. Daraei and A. Akbar, *Sep. Purif. Technol.*, 2012, **85**, 147–156.
223 G. Arthanareeswaran, T. K. S. Devi and D. Mohan, *Sep. Purif. Technol.*, 2009, **67**, 271–281.
224 Y. Medina-Gonzalez, P. Aimar, J.-F. Lahitte and J.-C. Remigy, *Int. J. Sustainable Eng.*, 2011, **4**, 75–83.
225 A. Wang and Z. Sun, *Adv. Graph. Packag.*, 2019, **543**, 873–881.
226 E. Yuliwati and A. F. Ismail, *Desalination*, 2011, **273**, 226–234.
227 D. Wang, K. Li and W. K. Teo, *J. Membr. Sci.*, 2000, **178**, 13–23.
228 E. Fontananova, J. C. Jansen, A. Cristiano, E. Curcio and E. Drioli, *Desalination*, 2006, **192**, 190–197.
229 L. Y. Yu, Z. L. Xu, H. M. Shen and H. Yang, *J. Membr. Sci.*, 2009, **337**, 257–265.
230 N. Rakhshan and M. Pakizeh, *J. Ind. Eng. Chem.*, 2016, **34**, 51–60.
231 J. Baniasadi, Z. Shabani, T. Mohammadi and S. Sahebi, *J. Chem. Technol. Biotechnol.*, 2021, **96**, 147–162.
232 Z. Alhalili, C. Romdhani, H. Chemingui and M. Smiri, *J. Saudi Chem. Soc.*, 2021, **25**, 101282.
233 M. Sha, A. Sabir, A. Islam and S. Maqsood, *Carbohydr. Polym.*, 2018, **186**, 367–376.
234 S. Jin, N. Kim and Y. Taek, *J. Membr. Sci.*, 2009, **345**, 13–20.
235 Y. Mansourpanah, S. S. Madaeni, A. Rahimpour, Z. Kheirollahi and M. Adeli, *Desalination*, 2010, **256**, 101–107.
236 G. Ciobanu and O. Ciobanu, *Desalin. Water Treat.*, 2015, **57**, 23257–23265.
237 R. M. Abdelhameed, H. Abdel-Gawad and H. E. Emam, *J. Environ. Chem. Eng.*, 2021, **9**, 105121.
238 J. F. Tang, Y. P. Xu, M. Ma and Z. J. Wang, *Chin. Sci. Bull.*, 2012, **57**, 1788–1795.
239 N. I. F. Aris, N. A. Rahman, M. H. Wahid, N. Yahaya, A. S. Abdul. Keyon and S. Kamaruzaman, *R. Soc. Open Sci.*, 2020, **7**, 192050.
240 R. M. Abdelhameed, A. A. Shaltout, M. H. H. Mahmoud and H. E. Emam, *Sustainable Mater. Technol.*, 2021, **29**, 1–8.
241 A. Nagendran, A. Vijayalakshmi, D. L. Arockiasamy, K. H. Shobana and D. Mohan, *J. Hazard. Mater.*, 2008, **155**, 477–485.
242 A. Salama, A. Mohamed, N. M. Aboamera and T. A. O. A. Khattab, *Appl. Nanosci.*, 2018, **8**, 155–161.
243 J. Li, A. Niu, C. J. Lu, J. H. Zhang, M. Junaid, P. R. Strauss, P. Xiao, X. Wang, Y. W. Ren and D. S. Pei, *Chemosphere*, 2017, **168**, 112–121.
244 H. M. Marwani, E. Y. Danish, M. A. Alhazmi, S. B. Khan, E. M. Bakhsh, A. M. Asiri, H. M. Marwani, E. Y. Danish, M. A. Alhazmi and S. B. Khan, *Sep. Sci. Technol.*, 2018, **53**, 887–895.
245 E. A. Bell, T. E. Poynor, B. Kathryn, J. Regnery, B. Coday and Y. Tzahi, *J. Membr. Sci.*, 2017, **525**, 77–88.
246 A. Yao, Y. Yan, L. Tan, Y. Shi, M. Zhou, Y. Zhang and P. Zhu, *J. Membr. Sci.*, 2021, **637**, 119621.
247 R. E. Khalifa, A. M. Omer, M. H. A. Elmageed and M. S. M. Eldin, *ACS Omega*, 2021, **6**, 17194–17202.
248 G. Z. Ramon and E. M. V. Hoek, *J. Membr. Sci.*, 2013, **425–426**, 141–148.
249 R. Dai, H. Guo, C. Y. Tang, M. Chen, J. Li and Z. Wang, *Environ. Sci. Technol.*, 2019, **53**, 13776–13783.
250 Y. Zhao, F. Kong, Z. Wang, H. Yang, X. Wang, Y. F. Xie and T. D. Waite, *Front. Environ. Sci. Eng.*, 2017, **11**, 1–13.
251 C. Lavanya, R. G. Balakrishna, K. Soontarapa and M. S. Padaki, *J. Environ. Manage.*, 2019, **232**, 372–381.
252 M. Padaki, R. S. Murali, M. S. Abdullah, N. Misdan, A. Moslehyani, M. A. Kassim, N. Hilal and A. F. Ismail, *Desalination*, 2015, **357**, 197–207.
253 B. Singh, V. Kochkodan, R. Hashaikeh and N. Hilal, *Desalination*, 2013, **326**, 77–95.
254 X. Lu, X. Feng, Y. Yang, J. Jiang, W. Cheng, C. Liu, M. Gopinadhan, C. O. Osuji, J. Ma and M. Elimelech, *Nat. Commun.*, 2019, **10**, 3–9.
255 M. Kumar, A. M. Isloor, S. Rao, H. S. Nagaraja, A. Fauzi and R. Susanti, *Chem. Eng. J.*, 2021, **405**, 126809.

256 M. El-sakhawy, S. Kamel, A. Salama and H. Sarhan, *J. Drug Delivery*, 2014, **2014**, 1–7.
257 S. F. A. Ali, L. A. William and E. A. Fadl, *Cellulose*, 2020, **27**, 9525–9543.
258 J. E. Bachman, Z. P. Smith, T. Li, T. Xu and J. R. Long, *Nat. Mater.*, 2016, **15**, 845–849.
259 H. B. Park, J. Kamcev, L. M. Robeson, M. Elimelech and B. D. Freeman, *Membranes*, 2017, **356**, eaab0530.
260 M. Minelli, M. G. Baschetti, F. Doghieri, M. Ankerfors, T. Lindström, I. Siró and D. Plackett, *J. Membr. Sci.*, 2010, **358**, 67–75.
261 S. Tahazadeh, H. Karimi and T. Mohammadi, *J. Solid State Chem.*, 2021, **299**, 122180.
262 C. Bellona, E. Drewes, P. Xu and G. Amy, *Water Res.*, 2004, **38**, 2795–2809.
263 P. Cartagena, M. El Kaddouri, V. Cases, A. Trapote and D. Prats, *Sep. Purif. Technol.*, 2013, **110**, 132–143.
264 Y. Zhang, B. Van der Bruggen, G. Chen, L. Braeken and C. Vandecasteele, *Sep. Purif. Technol.*, 2004, **38**, 163–172.
265 J. Su, Q. Yang, J. F. Teo and T. Chung, *J. Membr. Sci.*, 2010, **355**, 36–44.
266 C. Chiam and R. Sarbatly, *Sep. Purif. Rev.*, 2011, **40**, 126–160.
267 J. Waniewski, M. Pietribiasi and L. Pstras, *Sci. Rep.*, 2021, 1–13.
268 A. A. Hussain, S. K. Nataraj, M. E. E. Abashar, I. S. Al-mutaz and T. M. Aminabhavi, *J. Membr. Sci.*, 2008, **310**, 321–336.
269 D. L. Oatley, L. Llenas, R. Pérez, P. M. Williams, X. Martínez-lladó and M. Rovira, *Adv. Colloid Interface Sci.*, 2012, **173**, 1–11.
270 A. Szymczyk and P. Fievet, *J. Membr. Sci.*, 2005, **252**, 77–88.
271 Y. Lanteri, A. Szymczyk and P. Fievet, *Langmuir*, 2008, **24**, 7955–7962.
272 L. Yong, A. Wahab and C. Yin, *Adv. Colloid Interface Sci.*, 2013, **197–198**, 85–107.
273 M. Jun, R. Rolly, A. Abdel-wahab, S. Phuntsho and H. Kyong, *Desalination*, 2018, **426**, 50–59.
274 J. T. Jung, H. H. Wang, J. F. Kim, J. Lee, J. S. Kim and E. Drioli, *J. Membr. Sci.*, 2018, **559**, 117–126.
275 A. Abdel-Karim, J. M. Luque-Alled, S. Leaper, M. Alberto, X. Fan, A. Vijayaraghavan, T. A. Gad-Allah, A. S. El-Kalliny, G. Szekely, S. I. A. Ahmed, S. M. Holmes and P. Gorgojo, *Desalination*, 2019, **452**, 196–207.
276 M. Amirilargani, E. Saljoughi, T. Mohammadi and M. R. Moghbeli, *Polym. Eng. Sci.*, 2010, **50**, 885–893.
277 R. W. Baker, John Wiley Sons.
278 G. Li, J. Wang, D. Hou, Y. Bai and H. Liu, *J. Environ. Sci.*, 2016, **45**, 7–17.
279 P. Maheswari, P. Barghava and D. Mohan, *J. Polym. Res.*, 2013, **20**, 1–17.
280 G. Arthanareeswaran, D. Mohan and M. Raajenthiren, *J. Membr. Sci.*, 2010, **350**, 130–138.
281 B. Han, D. Zhang, Z. Shao, L. Kong and S. Lv, *Desalination*, 2013, **311**, 80–89.
282 J. Dasgupta, S. Chakraborty, J. Sikder, R. Kumar, D. Pal, S. Curcio and E. Drioli, *Sep. Purif. Technol.*, 2014, **133**, 55–68.
283 J. Y. Law and A. W. Mohammad, *Chin. J. Chem. Eng.*, 2018, **26**, 976–983.
284 B.-M. Jun, J. Cho, A. Jang, K. Chon, P. Westerhoff, Y. Yoon and H. Rho, *Sep. Purif. Technol*.
285 Z. Wang, K. Xiao and X. Wang, *Desalination*, 2018, **444**, 75–83.
286 J. Y. Hu, S. L. Ong, J. H. Shan, J. B. Kang and W. J. Ng, *Water Res.*, 2003, **37**, 4801–4809.
287 A. I. Schäfer, R. Mauch, T. D. Waite and A. G. Fane, *Environ. Sci. Technol.*, 2002, **36**, 2572–2580.
288 Y. Yoon, G. Amy, J. Chob, N. Her and J. Pellegrino, *Desalination*, 2002, **147**, 11–17.
289 G. Hurwitz, G. R. Guillen and E. M. V. Hoek, *J. Membr. Sci.*, 2010, **349**, 349–357.
290 C. X. Liu, D. R. Zhang, Y. He, X. S. Zhao and R. Bai, *J. Membr. Sci.*, 2010, **346**, 121–130.
291 A. Al-Amoudi and R. W. Lovitt, *J. Membr. Sci.*, 2007, **303**, 4–28.
292 S. Cheng, D. L. Oatley, P. M. Williams and C. J. Wright, *Adv. Colloid Interface Sci.*, 2011, **164**, 12–20.
293 Z. Mi, Z. Liu, S. Jin, D. Zhang and D. Wang, *Polym. Test.*, 2021, **93**, 107000.
294 K. Gu, S. Wang, Y. Li, X. Zhao, Y. Zhou and C. Gao, *J. Membr. Sci.*, 2019, **581**, 214–223.
295 T. S. Chung, J. J. Qin, A. Huan and K. C. Toh, *J. Membr. Sci.*, 2002, **196**, 251–266.
296 A. Rahimpour and S. S. Madaeni, *J. Membr. Sci.*, 2007, **305**, 299–312.
297 J. Baniasadi, S. Zarghami, F. S. Kamelian, T. Mohammadi and R. Nikbakht, *Polym. Bull.*, 2022, **79**, 569–586.
298 H. Lee, M. Nishino, D. Sohn and J. Soon, *Cellulose*, 2018, **25**, 2829–2837.
299 Y. Elkony, E.-S. Mansour, A. Elhusseiny, A. Elhusseiny and S. Ebrahim, *Polym. Eng. Sci.*, 2020, **60**, 2852–2863.
300 Y. Elkony, E. Mansour, A. Elhusseiny and H. Hassan, *Sci. Rep.*, 2020, **10**, 1–13.
301 S. Zinadini, A. A. Zinatizadeh, M. Rahimi, V. Vatanpour and H. Zangeneh, *J. Membr. Sci.*, 2014, **453**, 292–301.
302 S. M. Ghaseminezhad, M. Barikani and M. Salehirad, *Composites, Part B*, 2018, **161**, 320–327.
303 A. A. Alturki, J. A. McDonald, S. J. Khan, W. E. Price, L. D. Nghiem and M. Elimelech, *Sep. Purif. Technol.*, 2013, **103**, 258–266.
304 M. Xie, W. E. Price, L. D. Nghiem and M. Elimelech, *J. Membr. Sci.*, 2013, **438**, 57–64.
305 Y. Kiso, K. Muroshige, T. Oguchi, T. Yamada, M. Hhirose, T. Ohara and T. Shintani, *J. Membr. Sci.*, 2010, **358**, 101–113.
306 I. Musbah, D. Cicéron, A. Saboni and S. Alexandrova, *Desalination*, 2013, **313**, 51–56.
307 Y. Li, E. Wong, A. Volodine, C. Van Haesendonck, K. Zhang and B. Van Der Bruggen, *J. Mater. Chem. A*, 2019, **7**, 19269–19279.
308 Y. Kiso, K. Muroshige, T. Oguchi, M. Hirose, T. Ohara and T. Shintani, *J. Membr. Sci.*, 2011, **369**, 290–298.
309 K. Doederer, M. José, M. Pidou, H. S. Weinberg and W. Gernjak, *J. Membr. Sci.*, 2014, **467**, 195–205.

310 Y. Xu, Z. Wang, R. Ke and S. U. Khan, *Environ. Sci. Technol.*, 2005, **39**, 1152–1157.
311 Y. Ni, H. Nie, J. Wang, J. Lin, Q. Wang, J. Sun, W. Zhang and J. Wang, *Food Chem.*, 2022, **366**, 130539.
312 Y. Kiso, A. Mizuno, R. Atul, Y. Jungb, A. Kumanoc and A. Arijic, *Desalination*, 2002, **143**, 147–157.
313 Y. Jung, Y. Kiso, R. Atul, A. Ikeda, K. Nishimura, K. Min, A. Kumano and A. Ariji, *Desalination*, 2005, **180**, 63–71.
314 Y. Kiso, Y. Sugiura, T. Kitao and K. Nishimura, *J. Membr. Sci.*, 2001, **192**, 1–10.
315 Y. Kiso, Y. Nishimura, T. Kitao and K. Nishimura, *J. Memb. Sci.*, 2000, **171**, 229–237.
316 F. Yang and Y. Peng, *Macromol. Rapid Commun.*, 2022, **43**, 2100669.
317 A. J. Jose, J. Kappen and M. Alagar, Polymeric membranes: Classification, preparation, structure physiochemical, and transport mechanisms, 2018.
318 X. Chen, J. Fu, J. Shao, U. Nguyen, S. Zhou and Y. He, *Sep. Sci. Technol.*, 2017, **52**, 1913–1919.
319 E. Chang, Y. Chang, C. Liang, C. Huang and P. Chiang, *J. Hazard. Mater.*, 2012, **221–222**, 19–27.
320 A. G. Boricha and Z. V. P. Murthy, *Chem. Eng. J.*, 2010, **157**, 393–400.
321 P. Kanagaraj, A. Nagendran, D. Rana and T. Matsuura, *Int. J. Biol. Macromol.*, 2016, **89**, 81–88.
322 X. Wang, W. Fan, Z. Dong, D. Liang and T. Zhou, *Interactions of natural organic matter on the surface of PVP-capped silver nanoparticle under different aqueous environment*, Elsevier Ltd, 2018, vol. 138.
323 A. E. Contreras, A. Kim and Q. Li, *J. Membr. Sci.*, 2009, **327**, 87–95.
324 C. Jarusutthirak and G. Amy, *Water Res.*, 2007, **41**, 2787–2793.
325 A. S. Al-Amoudi, *Desalination*, 2010, **259**, 1–10.
326 S. Hong and M. Elimelech, *J. Membr. Sci.*, 1997, **132**, 159–181.
327 M. T. Rose, A. F. Patti, K. R. Little, A. L. Brown, W. R. Jackson and T. R. Cavagnaro, *Adv. Agron.*, 2014, **124**, 37–89.
328 K. V. Plakas and A. J. Karabelas, *J. Membr. Sci.*, 2009, **336**, 86–100.
329 M. Mänttäri, L. Puro, J. Nuortila-Jokinen and M. Nyström, *J. Membr. Sci.*, 2000, **165**, 1–17.
330 W. S. Ang and M. Elimelech, *J. Membr. Sci.*, 2007, **296**, 83–92.
331 H. Mo, K. G. Tay and H. Y. Ng, *J. Membr. Sci.*, 2008, **315**, 28–35.
332 S. Chen, J. S. Taylo, L. A. Mulford and C. D. Norris, *Desalination*, 2004, **160**, 103–111.
333 X. Jin, C. Y. Tang, Y. Gu, Q. She and S. Qi, *Environ. Sci. Technol.*, 2011, **45**, 2323–2330.
334 A. L. Ahmad, L. S. Tan and S. R. A. Shukor, *J. Hazard. Mater.*, 2008, **151**, 71–77.
335 S. Phuntsho, S. Vigneswaran, J. Kandasamy and S. Hong, *J. Membr. Sci.*, 2012, **415–416**, 734–744.
336 F. Zhou, C. Wang and J. Wei, *J. Membr. Sci.*, 2013, **429**, 243–251.
337 M. Shibuya, M. Yasukawa, T. Takahashi and T. Miyoshi, *Desalination*, 2015, **362**, 34–42.
338 R. Xu, M. Zhou, H. Wang, X. Wang and X. Wen, *J. Membr. Sci.*, 2020, **599**, 117817.
339 A. H. Hawari, N. Kamal and A. Altaee, *Desalination*, 2016, **398**, 98–105.
340 A. Kajau, M. Motsa, B. B. Mamba and O. Mahlangu, *ACS Omega*, 2021, **6**, 31797–31809.
341 M. M. Mahlambi, O. T. Mahlangu, G. D. Vilakati and B. B. Mamba, *Ind. Eng. Chem. Res.*, 2014, **53**, 5709–5717.
342 O. T. Mahlangu, R. Nackaerts, J. M. Thwala, B. B. Mamba and A. R. D. Verliefde, *J. Membr. Sci.*, 2017, **524**, 43–55.
343 M. Peyravi, M. Jahanshahi and S. Khalili, *Chin. J. Chem. Eng.*, 2017, **25**, 741–751.
344 A. Pasricha, S. L. Jangra, N. Singh, N. Dilbaghi, K. N. Sood, K. Arora and R. Pasricha, *J. Environ. Sci.*, 2012, **24**, 852–859.
345 M. M. Hasan, M. S. Hossain, M. D. Islam, M. M. Rahman, A. S. Ratna and S. Mukhopadhyay, *ACS Appl. Mater. Interfaces*, 2023, **15**, 32011–32023.